Supramolecular Self-Assembly: Models for Speciation in Solution and Ion Channels in Lipid Bilayer Membranes

by

Christine Chia Lin Tong
B.Sc., University of Waterloo, 2000

A Dissertation Submitted in Partial Fulfillment of the Requirements for the Degree of

Doctor of Philosophy

in the Department of Chemistry

© Christine Chia Lin Tong, 2006
University of Victoria

All rights reserved. This dissertation may not be reproduced in whole or in part, by photocopying or other means, without the permission of the author.

Supramolecular Self-Assembly: Models for Speciation in Solution and Ion Channels in Lipid Bilayer Membranes

by

Christine Chia Lin Tong
B.Sc., University of Waterloo, 2000

Supervisory Committee

Dr. Tom Fyles (Department of Chemistry)
Supervisor

Dr. Robin Hicks (Department of Chemistry)
Departmental Member

Dr. Matt Moffitt (Department of Chemistry)
Departmental Member

Dr. Paul Romaniuk (Department of Biochemistry and Microbiology)
Outside Member

Dr. Hanadi Sleiman (Department of Chemistry, McGill University)
External Examiner

Abstract

The self-assembled complex $(Pden)_4(bipy)_4^{+8}$ is potentially suited as a portal for synthetic ion channels (Pden = (1, 2-ethylenediamine) Pd(II), bipy = 4, 4'-bipyridine). This thesis examines the solution speciation of mixtures of Pden and bipy and the ion channel activity of the proposed channel.

A model which describes the concentration of the species in solution as a function of pH and Pden:bipy ratio was developed. The method determines the solution speciation by solving the mass balance equation for each species using the total concentration of Pden, bipy and H^+ and the cumulative formations constants for species in solution. This model is general and can be applied to other systems provided that the cumulative macroscopic formation constants ($\log\beta_{pbh}$) of the species are either known or can be estimated.

The cumulative macroscopic formation constant for a species is determined by an additive free energy process as the sum of the logarithms of a microscopic formation constant ($\log\beta'_{pbh}$) and a statistical factor ($\log Y$). Values for $\log\beta'_{pbh}$ were estimated using stepwise formation constants ($\log K$) for model systems which were determined by potentiometric titration. Values for $\log Y$ were calculated from the symmetries of the species. The model calculates the concentration of each species as a function of pH and Pden:bipy ratio to give a map of the species and their relative concentrations.

The model shows that $(Pden)_4(bipy)_4$ is the single most abundant species between pH = 4 and 7 and a Pden:bipy ratio of 1:0.4 to 1:6. Under optimum conditions, $(Pden)_4(bipy)_4$ holds a maximum of ~80 % of the total Pd in solution

when the total [Pd] = 1 x 10^{-5} M. The apparent equilibrium constants for $2\cdot(Pden)(bipy)_2 \leftrightarrows (Pden)_2(bipy)_3+bipy$ and $4\cdot(Pden)(bipy) \leftrightarrows (Pden)_4(bipy)_4$ were ~0.6 and ~10^6, respectively, at Pden:bipy = 1:1 and pH = 7. The model also permits analysis of the relative rates of formation of $(Pden)_4(bipy)_4$ from a number of different precursors. The dominant stepwise processes for the formation of $(Pden)_4(bipy)_4$ are dimerization of $(Pden)_2(bipy)_2$, addition of Pden to $(Pden)_3(bipy)_4$ and addition of $(Pden)_2(bipy)$ to $(Pden)_2(bipy)_3$. Other possible pathways to $(Pden)_4(bipy)_4$ involve less abundant species so are disfavored.

Lipophilic derivatives of Pden (PdenR) were synthesized from 1-bromodecane or 1-bromohexadecane and solketal in 30 % and 23 % overall yield, respectively. The complex PdenR was reacted with bipy in acetonitrile and the resultant solution was then tested for ion channel activity using the bilayer clamp experiment. The decyl derivative (R = $C_{10}H_{21}$) was inactive but a range of activity which include erratic behaviors, short openings and long openings were observed for the hexadecyl derivative (R = $C_{16}H_{33}$) using the bilayer clamp technique. Erratic openings were observed before all short and long openings, but were also observed independently. Hille pore radii, calculated from the observed conductances, were between ~ 1 and 6.5 Å for the rare short openings. The Hille radii for long opening pores were between ~ 1 and 14 Å and these pores did not show any ion selectivity. Channels that exhibit long opening activity were also observed in the absence of bipy. The large Hille radii and activity in the absence of bipy indicate that the proposed $(PdenR)_4(bipy)_4$ channel did not form possibly because the local concentration of bipy was not high enough to compete with the lipid for coordination sites on PdenR. The implications of these findings for self-assembly of ion channels in lipid bilayer membranes are discussed.

Table of Contents

List of Tables

List of Figures

List of Schemes

List of Abbreviations

3-ppy	3-phenylpyridine
4-ppy	4-phenylpyridine
Å	Ångströms = 1 x 10^{-10} m
β	macroscopic cumulative formation constant
β'	microscopic cumulative formation constant
σ	symmetry number
aap	*N*-(pyridyl-2-methyl)-1,2-diamino-ethane
ACN	acetonitrile
aq	aqueous
bipy	4, 4'-bipyridine
br	broad (in reference to the shape of a peak in IR or NMR spectrum)
Bu	butyl
Bz	benzyl
d	doublet
dd	doublet of doublets
dien	diethylenetriamine
diphyPC	1, 2-Diphytanoyl-*sn*-Glycero-3-Phosphocholine
dt	doublet of triplet
EI	electron ionization (with reference to MS)
en	1, 2-ethylene diamine
eq	equivalents
E_{rev}	reversal potential
Et	ethyl
EtOH	ethanol
FAB	fast atom bombardment (with reference to MS)
FT-IR	Fourier transform infrared spectroscopy
h	hours
i-PrOH	*iso*-propanol
K	stepwise formation constant
k	rate constant
K_a	acid dissociation constant
K_w	water dissociation constant
l_c	critical chain length
m	multiplet (in reference to peaks in NMR spectra)
m/z	mass to charge ratio
Me	methyl
MeOH	methanol
min	minutes

MS	mass spectrum
MsCl	methanesulfonyl chloride
NMR	nuclear magnetic resonance
OTf	trifluoromethanesulfonate (or triflate)
pbh e.g. **21-1**	$(enPd^{2+})_p(bipy)_b(H^+ \text{ or } OH^-)_h$; h < 0 denotes OH^- and h > 0 denotes H^+
PC	1, 2-diacyl-*sn*-glycero-3-phosphocholine
P_{Cl}	membrane permeability of Cl^-
PG	1, 2-diacyl-*sn*-glycero-3-[phospho-*rac*-(1-glycerol)]
Ph	phenyl
P_K	membrane permeability of K^+
P_{Na}	membrane permeability of Na^+
POPC	1-palmitoyl-2-oleoyl phosphatidylcholine
ppm	chemical shift with reference to TMS (in the context of NMR spectra)
psi	pounds per square inch
py	pyridine or pyridyl if used as a prefix
R	ideal gas constant
S	Siemens
s	seconds
s	singlet (in the context of NMR spectroscopy)
s	strong (in reference to peaks in IR spectra)
sh	shoulder (in reference to peaks in IR spectra)
T	temperature
t	triplet (in the context of NMR spectroscopy)
THF	tetrahydrofuran
w	weak (in reference to peaks in IR spectra)

Acknowledgements

Completing a thesis is certainly a milestone in my life and there are a lot of people who have contributed to getting me here, some belong to my science life and others to my personal life; in either case, thanks!

Thanks Tom! for a google of things, but mostly for giving me the latitude and support which allowed me to get smarter and for access to your brilliantly varied expertise.

Thanks Kelli and Dave! for your continued dedication to teaching/learning and mentoring. I think it's rubbed off a little.

Thanks Bryan! my bestest bud, for making the journey with me, helpful chemistry discussions and promising to buy me a dog.

Thanks Fyles and Hicks groups past and present members! for being neighborly.

Thanks Joe! for being a pal and for your chemical and gastronomical insights.

Thanks Horace! for being yourself and for helpful chemistry discussions. It is true that you "survive dammed near everything".

Thanks Jane! for playing sticks+words and being a fellow miscreant.

Thanks to everyone in the UVic chemistry community! for making this a super and unique place to learn.

Thanks to Garry Hanan! for giving me the summer job that got me started.

Thanks Autay! for sending good vibes and being the bestest friend ever!

Thanks Alwin! for being your own dude and a whole load of other things you probably don't even know about. You're a constant reminder that the most interesting things happen when we travel the road less taken.

Thanks Mom and Dad! for instilling us with a love of learning and giving us every opportunity to do so.

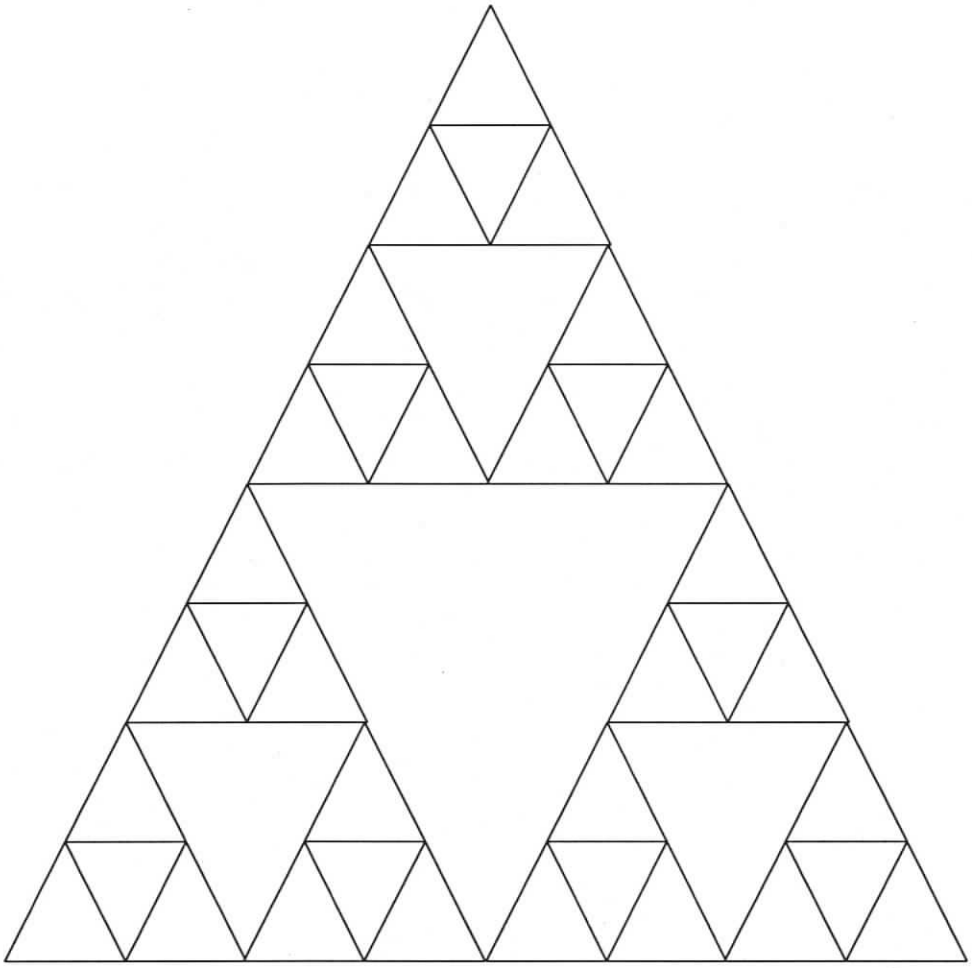

For my teachers and mentors,
(Especially my parents)
Who taught me to climb The Trees
So that I may see the forest
From the highest boughs

1 Introduction

Lipid bilayers, such as those found in cell membranes, are impermeable to ions and other small polar molecules such as glucose. Ion channels are structures that span a lipid bilayer and allow ions to pass from one side of the membrane to the other along a chemical or potential gradient[1]. Ion channels enable ions to traverse the hydrophobic region of the bilayer thereby providing a mechanism by which cells can regulate their contents. Channels are found in all types of cells and are known to play key roles in physiological processes, for example signal transduction in nerves[2], muscle contraction[3] and cell signalling[4]. The malfunction of ion channels have also been implicated in genetic diseases such as cystic fibrosis[5] and hypertension[6].

Ion channels in cell membranes have just two elements of control: ion selectivity and gating[7]. Ion selective channels allow only specific ions through the channel. Gating is the ability to turn channel function 'on' and 'off' in response to external stimuli such as changes in voltage, complexation of ligands or excitation by light or touch[8]. Voltage gated channels are found in nerve cells and respond to changes in electrical potential[9]. In animals, sodium channels found in nerve cells open/close when acetylcholine is bound. Channels gated by light are found in the retina[10] and those gated by touch are found in the skin[11, 12]. Not all ion channels are ion selective or gated but simply regulate the ionic composition on either side of a cell membrane[2].

The underpinning theme in ion channel study is to understand the mechanism by which channels function and the structural features necessary to form a channel[2]. Ion channels found in cell membranes are proteins. The most common method of studying the structure-function relationship in these channels is to

alter the structure by site specific mutation then study the effect on the structure by X-ray crystallography[13] and function by whole cell electrophysiological techniques.

Synthetic ion channels offer an alternative to the bioscience approach. The structure-function relationship is explored in synthetic channels by an iterative approach which involves three steps: design, synthesis and evaluation of the function[14]. Every new ion channel design challenges existing tenets so that each iteration gives new insight. The ultimate goal is to create synthetic channels that can exhibit the control and selectivity observed in biological channels. Synthetic channels that mimic the function of natural channels would be beneficial considering their utility in living systems. Some possible applications are in sensors[15, 16], catalysts[17-19] and antimicrobial agents[20, 21]. The potential applications are unrealized at present and research in synthetic ion channels is largely focused on fundamental questions of synthesis and mechanism.

Many synthetic channels have been reported in the literature. They are structurally simpler than their natural counterparts but still exhibit interesting function. Synthetic channel designs that are structurally well defined yields function that can be thoroughly studied which is useful in advancing our understanding of ion channels. Design principles for well defined synthetic ion channels have relied on covalent synthesis of molecules with strictly regimented functionality[22]. These molecules are usually obtained after long and difficult syntheses[23-25].

A supermolecule is a discrete, ordered structure that uses non-covalent interactions to organize the molecular components[26]. Hydrogen bonding and metal-ligand coordination are commonly used for non-covalent interactions in supermolecules. Dipole-dipole or dipole-cation interactions are sometimes used

as well[27]. The subunits that make up a supermolecule are called components, techtons or synthons[26, 27]. Supermolecules self-assemble from synthons under equilibrium conditions. Examples of synthetic ion channels that utilize the principles of self-assembly have been reported in the literature[17, 18, 28-30]. These ion channels represent an alternative and, in principle, simpler synthetic route towards structurally discrete ion channels. However, current designs for self-assembled ion channels require extensive covalent synthesis and/or pre-assembly and purification. Examples of unimolecular and self-assembled synthetic ion channels are described later in this chapter.

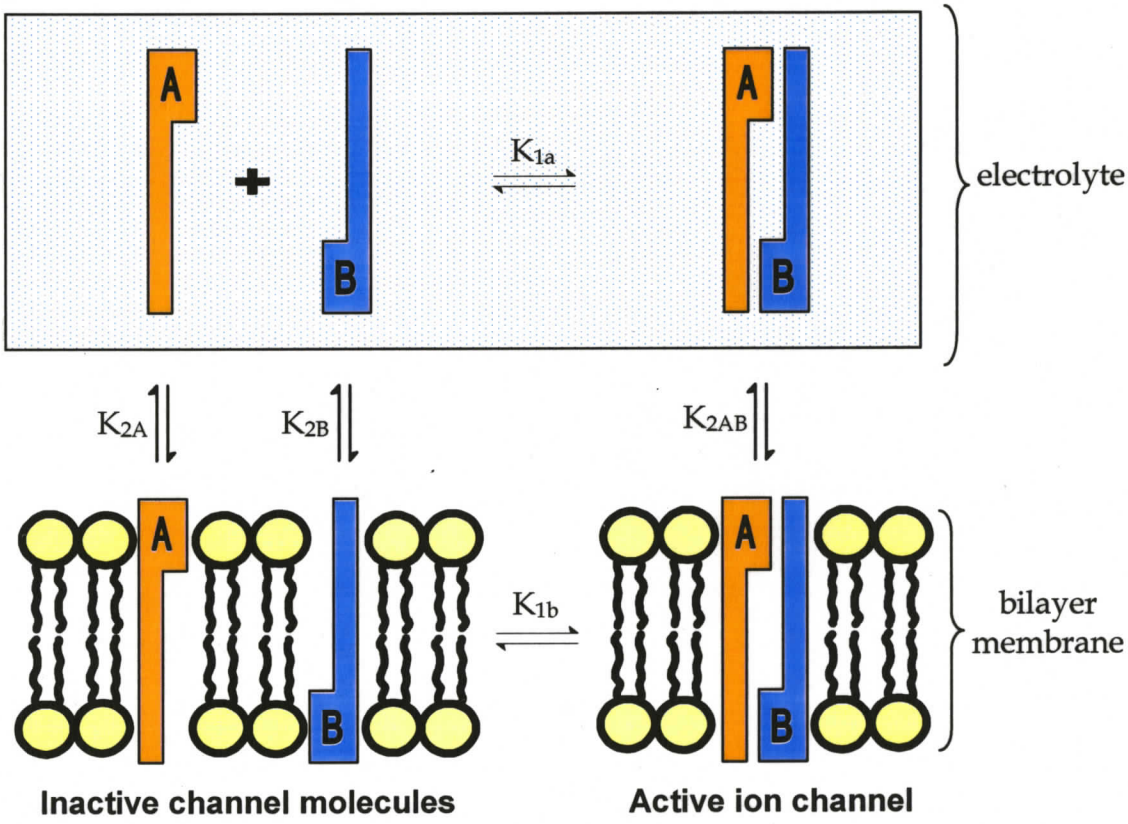

Figure 1 Equilibria leading to the formation of synthetic ion channels by self-assembly in a bilayer membrane

Synthetic ion channel molecules within a bilayer membrane are in equilibrium with free channel molecules in the electrolyte surrounding the bilayer. The relative amounts of ion channel in the bilayer and electrolyte depends on the

partition coefficient of the ion channel into the bilayer. For ion channels that are self-assembled, the supermolecule and synthons are also in equilibrium both in the electrolyte and in the bilayer membrane[18]. Figure 1 is an illustration of the equilibria that are possible for two synthons (**A** and **B**) and a self-assembled ion channel (**AB**). The equilibria described by K_{2A}, K_{2B} and K_{2AB} in Figure 1 define the partition equilibrium for the synthons and channel, respectively. The equilibrium between **A**, **B** and **AB** is described by K_{1a} when the synthons are in solution and by K_{1b} when the synthons are in the bilayer. The equilibrium constants, K_{1a}, K_{1b}, K_{2A}, K_{2B}, and K_{2AB} are expected to be different.

While there are several examples[17] of ion channels that self-assemble by the route described by K_{1a} followed by K_{2AB}, the route towards ion channels described by K_{2A} and K_{2B} followed by K_{1b} remains relatively unexplored, although some examples that lack specific intermolecular interactions apparently act in this manner[29]. However, there are no clear examples that involve specific and directed self-assembly of an ion channel within a bilayer (K_{1b}). Ion channels self-assembled in the bilayer under equilibrium conditions would reduce the synthetic effort and bypass the necessity of purification after the channel has been formed. Many examples of self-assembled systems in aqueous solution (K_{1a}) have been reported. This thesis will explore how these systems can be adapted to make ion channels and identify design parameters that influence self-assembly in the bilayer by evaluating a channel design which depends on equilibrium self-assembly.

1.1 Equilibrium self-assembly of palladium pyridyl structures

Equilibrium self-assembly is driven by the energetics of the species involved[31, 32]. In order to get a complete understanding of the self-assembled product, it must

be considered within the context of the entire reaction mixture instead of an isolated species. Metallosupermolecules are a class of supermolecules that are self-assembled from metals and organic ligands[27]. Palladium is an integral feature of the proposed self-assembled channel discussed in this thesis so this section will focus on palladium based metallosupermolecules. Palladium self-assembled supermolecules[27, 33, 34] have been extensively reviewed in the literature.

Numerous examples of self-assembled compounds based on Pd and organic ligands have been reported in the literature[27]. Palladium (II) has square planar geometry and is usually used as a synthon to connect two neutral ligands so that they are 90° or 180° to each other in metallosupramolecular complex. In order to make 90° linkages, capping ligand(s) must be bound in a *cis* fashion. Normally, bidentate diphosphine, dithiol or diamine ligands such as 1, 2-diaminoethane (en) are used because they form strong bonds with the Pd^{2+} centre. It is important that these capping ligands are strongly associated to the metal under the self-assembly conditions so that the coordination with other synthons will proceed with the expected geometry at the Pd^{2+} center. Bonds between Pd and en are very strong so Pden can be considered as a single component for self-assemblies conducted at room temperature and atmospheric pressure*.

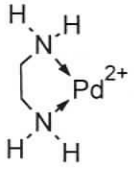

Pden

Equilibrium controlled self-assembly has been used to create complex structures. Different organic ligands are used to achieve unique structures such as **1** and **2**.

---

* Changes in oxidation state are not expected in these reactions so the charges will be dropped from notation that refers to Pd^{2+}, H^+ and OH^- for simplicity. It should be assumed that the charge for Pd is always 2+ throughout this thesis unless otherwise noted. The charge on H and OH are +1 and -1, respectively.

Compound **1** is based on the cuboctahedral framework and consists of 12 Pden centers and 24 pyridyl terminated organic bridges. The metal centres occupy the vertices of the cuboctahedron and the pyridyl terminal organic bridges form the edges. The cuboctahedron is self-assembled by mixing the components in dimethylsulfoxide at 70 °C for 4 hours[35]. This supermolecule is a great example of the complexity that can be achieved using self-assembly. Compound **2** is based on a simple design consisting of 4 tridentate bridging ligand and 5 Pden centers which self-assemble in water to form a tetrahedral supermolecule. The interior cavity is hydrophobic and can host up to 4 adamantane guest molecules. Electron rich guests are preferred because the ligand is electron deficient. Colour changes have been observed due to the formation of charge transfer complexes between **2** and an internal guest. The Fujita group has also demonstrated that the rates for Diels-Alder and [2+2] photodimerization reactions are enhanced within the cavity of **2**. Compound **2** illustrates that ligands can be designed to impart structure as well as function[36-40]. The simplicity of the synthesis described for **1** and **2** is typical of supramolecular synthesis and serve as good examples of the synthetic appeal of equilibrium self-assembly[27].

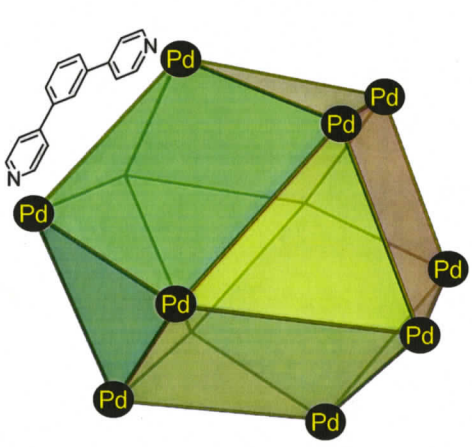

1

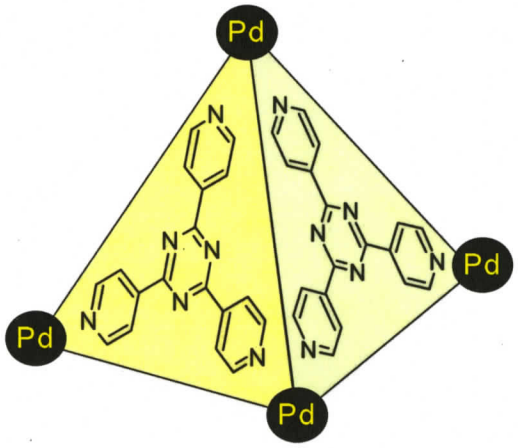

2

Little is known about the effect of changes in pH or Pden:ligand ratio or the kinetics of equilibrium self-assembly reactions because the researchers who

synthesize these molecules are usually more interested in their structure, ideally determined by X-ray crystallography, and possible encapsulation functions rather than the mechanics of the self-assembly process itself. Consequently, they focus on defined stoichiometric mixtures and conditions under which the desired product is dominant or the sole product detected.

1.2 Synthetic ion channels

1.2.1 The bilayer membrane

A planar lipid monolayer is a single sheet of lipid molecules arranged so that all the molecules are aligned with the headgroups pointing in the same direction. Each monolayer has a headgroup region which is hydrophilic and a tail group region which is hydrophobic. A bilayer is two monolayers stacked so that a hydrophobic region which is roughly twice the thickness of the hydrophobic region in a monolayer separates the headgroup regions (Figure 2)[41, 42]. The formation of bilayers from lipids in aqueous media is driven by the reduction of free energy that results from minimizing hydrocarbon-water contacts[42]. Small polar molecules and ions can only traverse the hydrophobic region of the bilayer when facilitated by channels or other transport molecules[2].

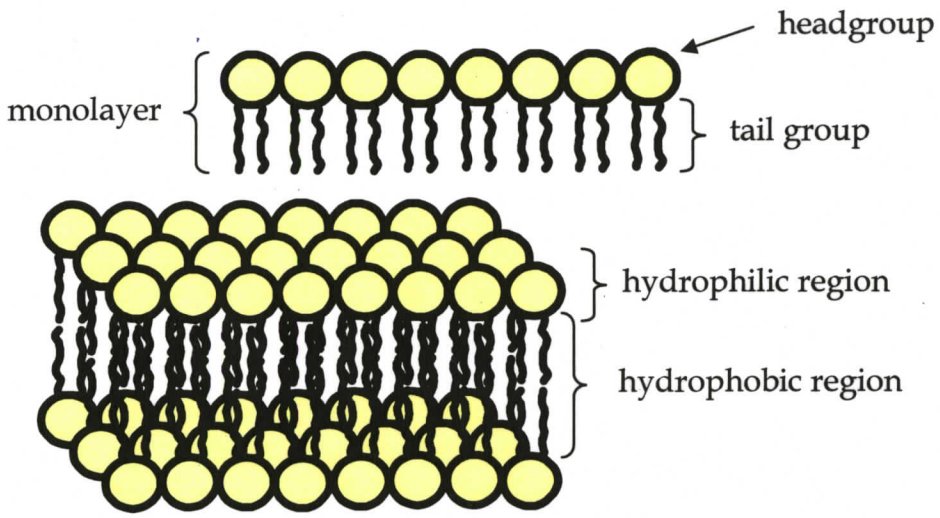

Figure 2 Schematic drawing of a bilayer membrane

Amphiphilic compounds can form a wide range of morphologies such as planar bilayers or vesicles in an aqueous environment. The type of morphology found depends on the molecular shape of the amphiphile which determines how the molecules pack with respect to another. The overall morphology can be estimated using the critical packing parameter, P, which is defined by (1-1)[42].

$$P = \frac{v}{a_0 l_c} \qquad \textbf{(1-1)}$$

where, v is the volume occupied by the lipid chain, a_o is the optimal surface area occupied by the headgroup and l_c is the critical chain length. Values for v, a_o and l_c are determined empirically. Planar bilayers are obtained when the lipid has P = 1 and vesicles are obtained when $0.5 < P < 1$. Typically, planar bilayers are formed with double chain amphiphiles such as naturally occurring esters of glycerol found in phosphate headgroups[42].

Ion channels must partition into the bilayer before they can show activity. Although most discussion about ion channels consider the bilayer as an inert slab, it should be noted that some channel structures (hence function) depend strongly on the energetics of the bilayer[43-45].

1.2.2 A survey of synthetic ion channels

The function of an ion channel can be defined by four main characteristics: selectivity, conductance, lifetime and probability of opening. A channel is said to be selective if it transports a particular ion preferentially. Conductance is the ionic current passed through the channel per unit potential and is related to the dimensions of the channel. The lifetime of a channel is defined by the average duration of an open channel and is related to the stability of the open state of the channel relative to the closed or dissociated states. The probability of opening is a measure of how often a channel is open during an experiment and also relates to channel stability.

The variation in molecules that have been reported as synthetic channels is enormous. Channel forming molecules can be divided into two broad categories based on their design, as suggested by Matile[22]. Type 1 channels are those designed to function as a single molecule and Type 2 channels include those designed to function as supermolecules or aggregates. The exact structure of the active channel aggregates is usually unknown, although it is sometimes possible to determine the number of components involved in a supramolecular channel by experiment. Channel function is characterized by experiment in planar bilayers or vesicles, discussed later in the thesis.

Type 1 designs all consist of "hoop" moieties linked together by organic components. They are also designed so that a single molecule will span the thickness of a lipid bilayer. Macrocycles are the most common hoop moiety used [46, 47]; however, helices and polyethers have also been used[14, 48]. Joining hoop structures with an organic moiety pre-organizes the pore forming molecules. An example of a type of synthetic channel made using this strategy is shown in

Figure 3. The structure-function relationship has been explored for the molecules shown in Figure 3 by changing the length of the "hydrophobic spacer" between the macrocycles, changing the ring sizes of the "central relay" macrocycle and replacing the "pendant sidearm" with other moieties. These molecules, studied extensively by Gokel and co-workers, have been coined "hydraphile" channels. The general construction consists of two macrocyclic headgroups appended with a pendant sidearm and a hydrophobic spacer which is bridged by a central relay moiety. The activities of hydraphile channels described in the following section were measured using dynamic ^{23}Na NMR in PC/PG vesicles or an ion selective electrode. The former method observes the transport of Na^+ across the bilayer membrane. Ions on the inside and outside of the vesicle are differentiated using a ^{23}Na NMR shift reagent. Rate constants are determined by analyzing the changes in line shape over time[49, 50]. The activity reported by Gokel and co-workers on gramicidin is reported with respect to the rate constant observed for gramicidin ($k = \sim 175\ s^{-1}$)[51]. The later method observes Na^+ efflux from inside the vesicles by use of an ion selective electrode. The relative transport rates are normalized using the total amount of Na^+ in the vesicles. Although this method provides only the relative transport rates, it is more amenable to survey work[52]. (PC = 1, 2-diacyl-*sn*-glycero-3-phosphocholine and PG = 1, 2-diacyl-*sn*-glycero-3-[phospho-*rac*-(1-glycerol)])

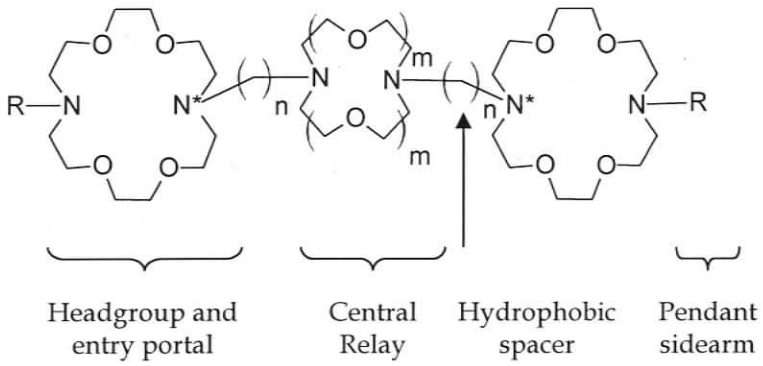

Figure 3 Structure of a hydraphile

Studies on the length of the "hydrophobic spacer" groups showed that the maximum activity was obtained when the hydrophobic spacers were 12 and 14 methylene units long which corresponds to a length of 38 and 43Å measured from N* on the terminal macrocycles using CPK models (Table 1). The hydrophobic spacers in **3e** have 16 methylene units which increases the overall length of the molecule by 5 Å compared to **3d**. This modification is accompanied by a 2-fold decrease in activity. A 2-fold decrease in activity was also observed for **3b** which has hydrophobic spacers with ten methylene units. These observations are consistent with the view that small changes in the length (< 5Å) are compensated by the flexibility of the molecule which will have modest effect on the activity. Activity was not detectable for the derivatives with hydrophobic spacers that contained 8 methylene units, presumably because the molecule was too small to span the length of the lipid bilayer and hence could not form a channel[53].

Table 1 Effect of changing the length of hydrophobic spacers in hydraphiles in which R = benzyl and m = 4

Compound	n	Length,	% Activity relative to maximum observed
3a	8	28	0
3b	10	33	25
3c	12	38	100
3d	14	43	100
3e	16	48	25

Changes in the "central relay" showed that polar groups between the terminal macrocycles are important to the function of the channel. Increases in the size of the central relay was accompanied by an increase in the activity (Table 2)[54]. The greatest activity was observed for m = 3 and was roughly double the activity observed for m = 2 and triple the activity for m = 1. Molecules with two macrocycles in the middle of the molecule, for example **5**, showed greater activity than those with only one macrocycle[55].

Table 2 Effect of changes in the size of the central relay macrocycle on hydraphiles in which R = benzyl and n = 14

Compound	m	% Activity relative to maximum observed
4a	1	30
4b	2	50
4c	3	100

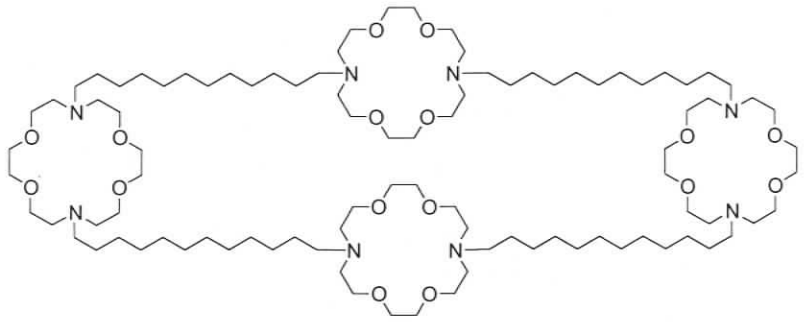

5

Greater activity was observed for molecules in which the pendant sidearm groups are electron rich (Table 3). The relative activity was determined for **6** in vesicles made with DOPC which is a zwitterionic lipid (DOPC = 1, 2-dioleoyl-*sn*-glycero-3-phosphocholine)[56]. The activity was diminished for **6** when the vesicles were prepared with 30% w/w of negatively charged DOPA lipids (DOPA = 1, 2-dioleoyl-*sn*-glycero-phosphate). The authors infer that the lipid headgroup and the pendant sidearm interact with a transported cation in π-cation fashion that stabilizes the channel, thus enhances transport activity. This interpretation is corroborated by fluorescence quenching experiments using **6f**[56]. The effect of changing the ring size of the terminal crowns has not been reported.

Type 1 channels are usually obtained after lengthy synthetic procedures that require significant investments of time and materials. Compounds **3**, **4**, **5** and **6** were prepared after three steps in ~4% overall yield. Dissymmetric species require additional steps[54-57].

Table 3 Effect of changing the pendant sidearm moiety in hydraphiles in which n = 14 and m = 4

Compound	R	% Activity relative to the total observed[a]
6a		100
6b	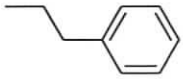	95
6c	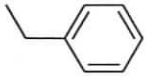	75
6d	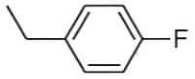	45
6e	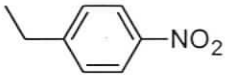	15
6f	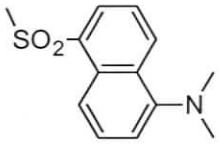	10

[a] measured in DOPC vesicles

Molecules that fall under the Type 2 category vary greatly in their molecular and supramolecular structures. In these structures the supermolecule may be formed in the bilayer or before bilayer insertion (Figure 1). Type 2 channels can be divided into two categories based on their design: (2a) channels that have functional groups designed to stabilize the supramolecular structure (2b) channels that are designed with a particular shape parameter (or critical packing parameter) that may affect the bilayer so that a channel may be formed by changing the curvature of the bilayer, thereby opening a pore.

Some examples of Type 2a molecules include bolaamphiphiles, steroidal staves and rigid-rod β-barrels. Bolaamphiphiles, such as compound **7**, are two-headed amphiphilic structures with a hydrophobic core and two hydrophilic terminal groups. These structures form channels that conduct ions under applied potentials. Although the actual structure of the channel is unknown, there is

evidence that the active structures are dimers which include water molecules that hold the channel together[29].

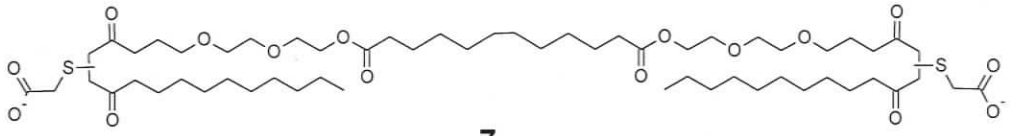

7

Steroidal channels such as **8** are believed to intercalate into the bilayer and form a 'half channel' that spans one leaflet of the bilayer. Experimental evidence from ^{23}Na NMR kinetics indicates that the channel formed is a dimer. The channel is thought to form when two half channels align to make a pore that opens from one side of the bilayer to the other thereby allowing ions to pass through the bilayer (Figure 4); gramicidin A, a naturally sourced peptide channel, functions by way of a similar mechanism. An increase in the number of steroidal groups in larger oligomers of **8** shows an exponential increase in the rate of Li^+/Na^+ exchange measured in spherical POPC bilayers (POPC = 1-palmitoyl-2-oleoyl phosphatidylcholine). An increase in the rate of Li/Na exchange implies that the pores increase in diameter, assuming that the supramolecular structure of the channel remains the same[58].

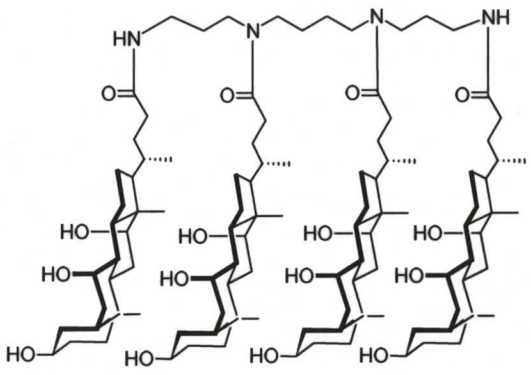

8

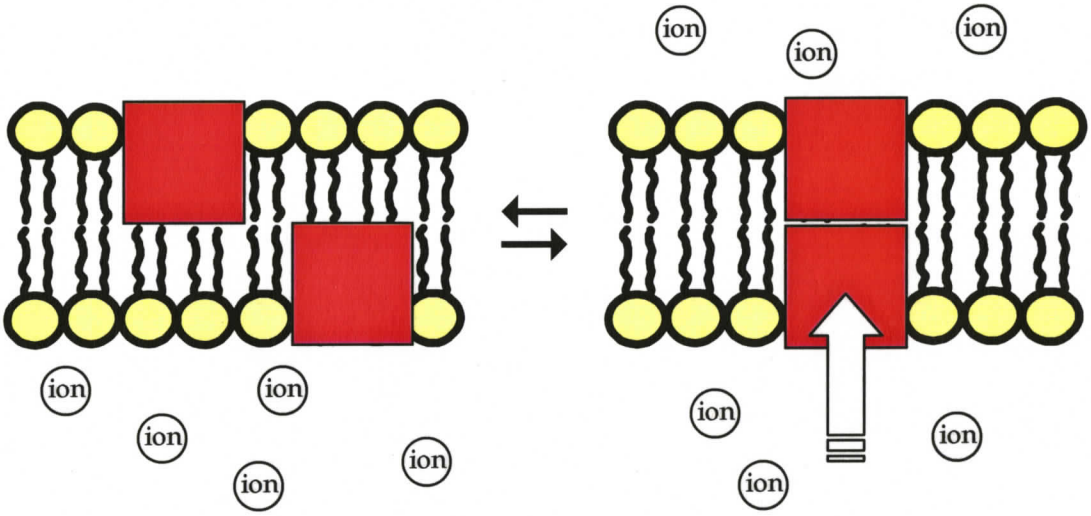

Figure 4 Mechanism for channel opening observed for 8

The rigid rod barrel design reported by the Matile group is an example of a type 2a design that is particularly well studied. The synthons used to form the supramolecular ion channel have an oligophenyl backbone appended with short peptide chains, **9** and **10**. The phenyl groups are oriented orthogonally with respect to each other as a result of steric interactions. The peptide moieties are designed so that the hydrogen bonding complements the peptide chain from an adjacent molecule in a structure related to an anti-parallel β-sheet. The length of the peptide chain dictates the stoichiometry of the channel. The channels are hexamers for peptide chains with three amino acid residues (β^3) such as **9** and tetramers for peptide chains with five residues (β^5) such as **10**. The channel is formed by interdigitating the peptide side chains to form the channel walls. The

interior and exterior surfaces of the channel can be functionalized by changing the amino acid. Large conductances, 0.7 nS for **9** and 1.2 nS for **10**, were reported. These conductances correspond to interior diameters of about 5.2 and 7Å, respectively. The lifetime of these channels were on the order of seconds for **9** and milliseconds for **10** [18].

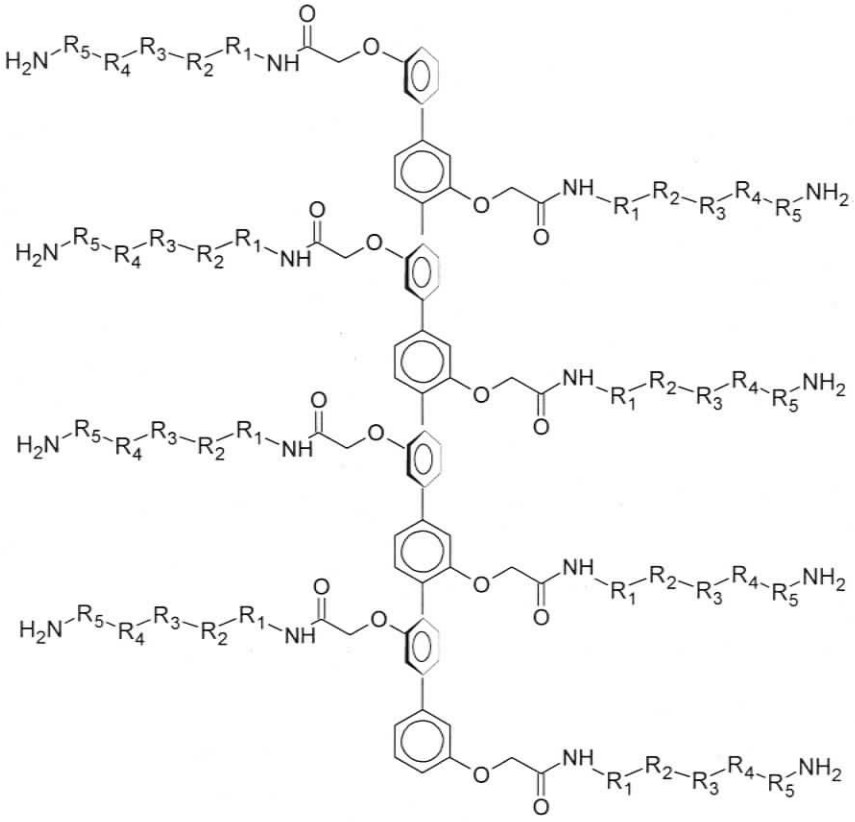

L = Leucine =

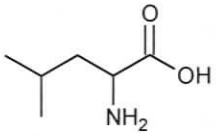

H = Histidine =

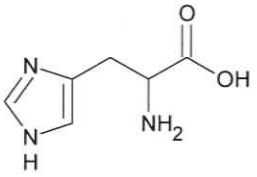

K = Lysine =

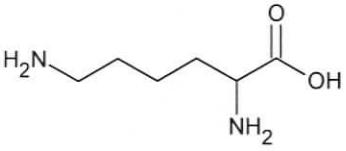

monomer	R_1	R_2	R_3	R_4	R_5
9	L	K	L	---	---
10	L	H	L	H	L

The synthetic ion channel designs that belong in the type 2b category are made from simple molecules such as **11**. Type 2b channels are perhaps the most enigmatic of the channels discussed thus far. The components are designed to

function as a supramolecular structure yet they contain very few functional groups that will stabilize the supramolecular assembly. Channels made from **11** have lifetimes on the order of seconds. The current passed varies linearly with the potential applied. The conductance of these channels is 15.4 pS in a planar bilayer with 1M KCl. The selectivity of the channel is as follows: Cs > K > Na. Variations based on **11** in which the length of the alkyl chain is increased or decreased by 2 methylene units show no activity under the same experimental conditions[59]. The channel is proposed to function as an aggregate of between 2 and 10 molecules with the alkyl chains situated perpendicular to the plane of the bilayer. One possible model that has been proposed would have the phenyl headgroup sitting below the bilayer headgroups in both leaflets and the alkyl groups in **11** would be associated in a face to face fashion[59].

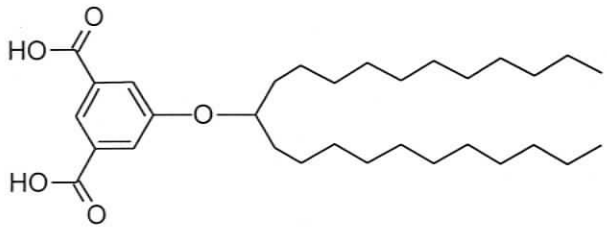

11

In general, type 2b channels have low conductances compared to other synthetic channels because their structures are tenuous so they do not form large pores. Channel radii are usually small because channels that enforce large pores require well defined and robust structures which are difficult to synthesize.

The mechanism for channel formation in type 1 or type 2a channels rely on supporting a tunnel with defined dimensions that spans the bilayer. The tunnel has water or other polar groups that stabilize the charge on the ions as they flow through the pore. Synthetic channel designs based on this mechanism are common probably because the structure-function relationship is intuitive.

1.2.3 Natural ion channels that form from 'small' components

Other mechanisms for channel formation are also possible. Ceramide and melittin are examples of channels that use other mechanism to make pores. They have been included in this survey of ion channels, even though they are naturally sourced, because they have interesting mechanisms for channel formation. Ceramide, **12**, is a neutral lipid known to form very large pores in diphyPC planar bilayers (diphyPC = 1, 2-Diphytanoyl-*sn*-Glycero-3-Phosphocholine). Ceramide is a simple molecule and would be classified as a type 2b channel if it was of synthetic origin. The structure proposed for ceramide channels consists of several stacks of 7- 8 ceramide molecules arranged radially around a central pore. In this structure, the hydroxyl groups line the interior of the pore. The stability of ceramide pores is attributed to hydrogen bonding between the hydroxyl groups. Hydrogen bonding between amide groups in adjacent molecules is thought to stabilize the stacks[60].

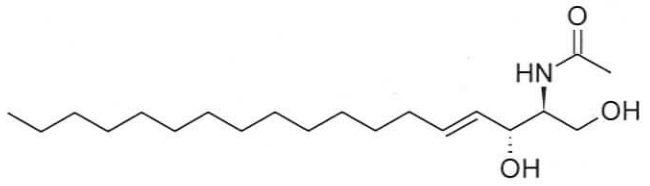

12

Conductance measurements on ceramide channels in planar bilayers show that pore radii vary from 0.4 to 110 nm[60]. Changes in pore size are rationalized by differences in the number of stacks involved in the channel. Pores grow into larger pores over time because smaller pores are incorporated into larger assemblies thus the largest pores are observed at longer times. The channels can grow so large that changes in pore size due to the addition or loss of a small number of stacks results in an insignificant increase in conductance. The lack of selectivity observed for ceramide channels is reasonable considering the large size of the pore.

Ceramide channel formation progresses through three phases[60]. Ceramide stacks are thought to form during the first phase, which lasts for 2-45 min, and is characterized by sparse activity. In the second phase, a period of random step behaviour along with an increase in total conductance is observed. In last the phase, the conductance increases in large steps and appears to reach a steady state. The large opening will continue to remain open for several minutes. At the end of this period the channel will close in a single step.

Melittin is a 26 residue helical peptide that is isolated from bee venom and has a +6 charge at physiological pH. Melittin forms channels by stabilizing curvature in the bilayer membrane[61]. The channels formed are toroidal and the exact structure is still speculative although experimental data confirms that the peptide helix is oriented perpendicular to the plane of the bilayer. The dimensions of the pore vary with changes in the type of bilayer used and the protein to lipid ratio. The pore was characterized using orientated circular dichroism (OCD) and neutron scattering. Pore formation by melittin has been rationalized using a biophysical approach to membrane energetics[43]. Modeling shows that the channel might include a small number helices positioned equidistant from each other but not touching around a toroidal cavity[61]. The helices stabilize curvature in the membrane so that the top and bottom leaves blend into one continuous surface around the pore. Some synthetic channels may also operate using mechanisms similar to ceramide or melittin channels but these have not yet been identified.

The bilayer activity observed for ion channels is a continuum that ranges from consistent uniform activity for ion channels that have defined radii to erratic random activity for bilayer disrupting agents. There are also channels that may change their size between or even during a single opening but enforce a pore

with a defined radius for an extended period of time. In all of these cases, the channel structure will define the activity observed.

1.3 Proposal for a metallosupramolecular ion channel

The study of synthetic ion channels presents an opportunity to learn more about ion channel function and to make channels which can be tailored for a specific application. Equilibrium self-assembly is an effective synthetic strategy for building complex structures with a high degree of control over the structure. This strategy has so far been unexploited in synthetic ion channel synthesis.

Products synthesized by self-assembly are in equilibrium with other species in solution. Equilibrium systems are sensitive to the ratio of starting reagents and pH at a fixed temperature and pressure. Ion channels that self-assemble under equilibrium conditions in the bilayer will also be sensitive to these factors therefore channel activity will be affected as well. This response may be useful in some applications. For example, a channel that was inactive may become active with a change in pH and may find application as a sensor[62]. Consider a scenario in which two different channels, with distinct activity are in equilibrium with each other. If the system is controlled in such a way that only one channel is active at any given time then this system would display OR logic. Of course more complex scenarios for digital logic and even analog logic are possible. These channels may be useful in the development of nanofluidic devices[63].

There are a plethora of self-assembled structures reported in the literature which can be modified to make an ion channel[27]. An ideal supermolecule would consist of no more than two components that are commercially available or simple to synthesize in good yield. Ion channel designs that include a cyclic moiety which

can enforce a hole in the bilayer have been successful so a supermolecule with these characteristics would be desirable[64]. Selectivity in ion channels has been correlated with pore size thus a design in which the interior of the cyclic moiety can be easily changed would also be benificial[65].

This thesis will explore equilibrium self-assembly of ion channels in the bilayer through a model design based on a metallosupramolecular "square", **13**. The complex **13** was first reported by Fujita in 1990 and consists of three main components: 4, 4'-bipyridine (bipy), Pd, and 1, 2-ethylenediamine (en). The literature reports that these synthons self-assemble into the square, **13**, for [Pd] ≈ 0.1 M and Pden:bipy molar ratio of about 1:1 in a water or water/methanol mixture at room temperature (Figure 5). Under these conditions, the self-assembly process is complete within a few minutes[66]. The crystal structure shows that the square encloses a space ~7.8 Å in width which is large enough for large hydrated anions to pass through the center[67]. The square was originally reported as a host for organic molecules, such as 1,3,5-trimethoxybenzene, in aqueous media[68]. Derivatives in which the bridging bipy ligands are substituted for other linear or bent bridging components have been reported[69]. There are also structures in which the en ligand is replaced by other bidentate ligands, for example 2,2'-bipyridine and 1,3-diaminopropane. Cyclic trimetallic species (triangles) are observed in addition to squares for some of these derivatives. The en ligand is the only capping ligand that has consistently shown the formation of squares with no triangular species in competition[33].

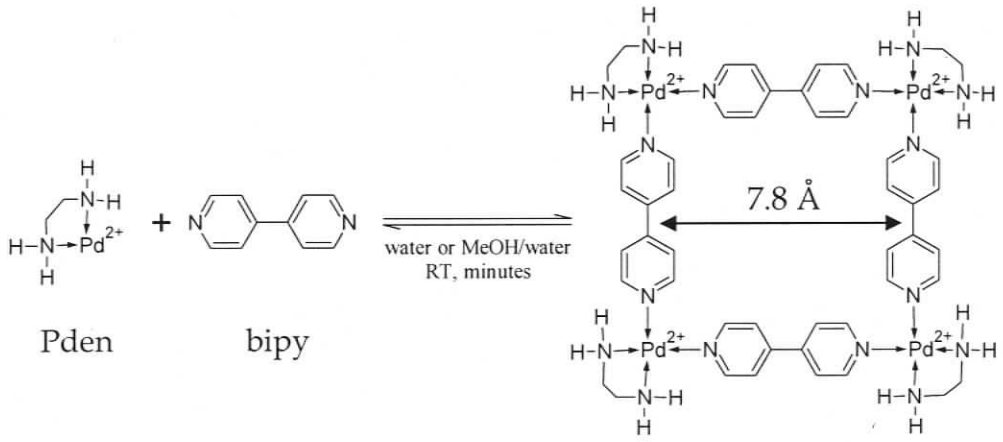

$(Pden)_4(bipy)_4$

13

Figure 5 Equilibrium used to synthesize a square $(Pden)_4(bipy)_4$ complex from Pden and bipy

In order to use **13** to form a portal in an ion channel, it needs to be derivatized so that it will partition into the bilayer from the surrounding electrolyte. Bipy and en could be derivatized with alkyl groups to anchor **13** in the bilayer. It would be better to modify the en group because the size of the portal could potentially be changed by substituting bipy with longer bridging ligands. If the square was anchored to the bilayer through the bridging ligand, then synthetically challenging modifications would be required for each derivative of the square.

The design proposed for the ion channel that will be used to explore equilibrium self-assembly in the bilayer membrane is shown in Figure 6. The design has a strong resemblance to **13**, the difference being the decyl or hexadecyl groups appended to each en chelated to Pd. The bridging bipy are used without derivatization.

The channel is expected to self-assemble so that the square is in the hydrophilic headgroup region of the bilayer. On the basis of reports on ion channels that have macrocyclic components, it is reasonable to assume that ions will pass

through the center of the square. Because the square is highly charged (+8), we expect the portal to be anion selective due to electrostatic repulsion between the portal and cations. The conductance calculated based on the internal radius of **13** should be approximately 100 nS in 1M KNO_3 at 22 °C. It should also be of constant value because the size of the portal defined by $Pd_4en_4bipy_4$ is fixed. The lifetime of the openings should be related to the kinetics of the self-assembly process. The activity of the proposed channel will be surveyed using the bilayer clamp technique which will directly report on the activity, selectivity and lifetimes of channels that form.

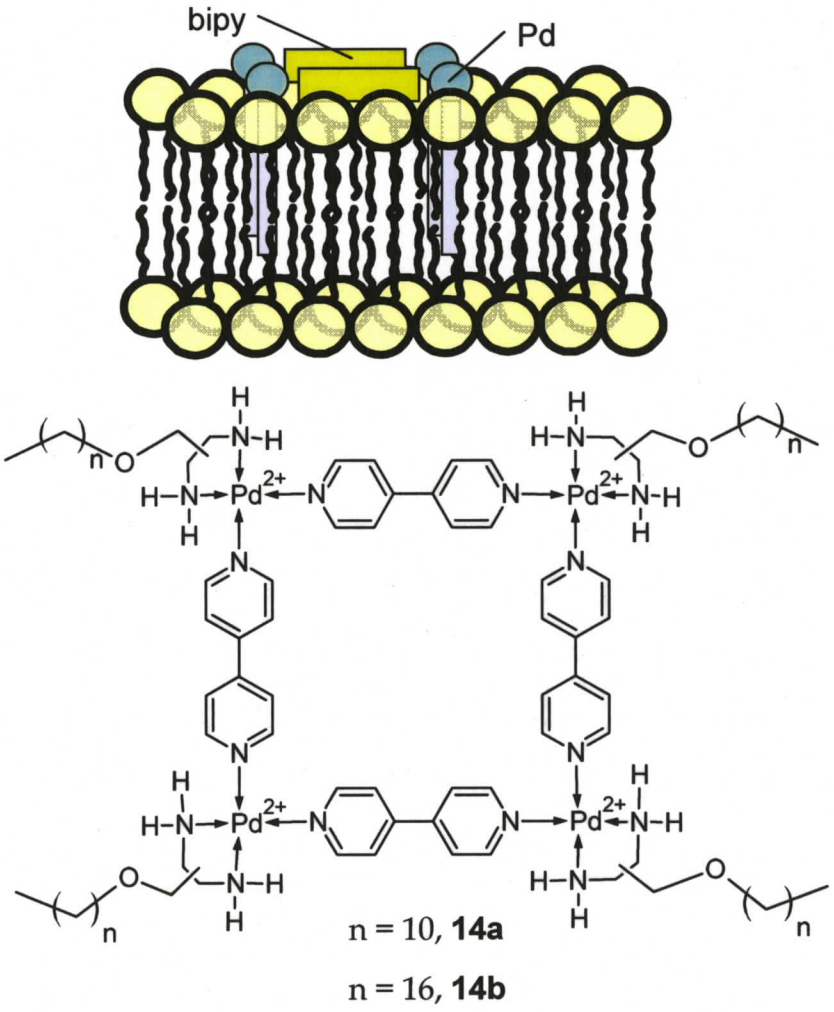

Figure 6 Proposed design for a self-assembled ion channel

Figure 1 shows that two different self-assembly processes are expected, one in water and the other in the bilayer. These will be influenced by the partition equilibria of the components. It is unreasonable to assume that the Pden portion of **14** will partition into the bilayer to the same extent as bipy. Thus control over the stoichiometry in the bilayer will be difficult. It is therefore important to examine how changes in stoichiometry affect self-assembly. The relative concentrations of species in equilibrium are known as the speciation. The speciation for the Pden+bipy equilibrium reaction in solution can be modeled by solving the mass balance equations for Pden and bipy. The parameters that are required to solve the equations are the formation constants, β, for each species in the solution and the total concentration of Pden and bipy in order to determine the speciation. The values for the total concentration are arbitrary and can be chosen to reflect any Pden:bipy molar ratio. A model that can simulate the speciation would be useful because it allows us to estimate the speciation as a result of changes in the ratios of starting reagents and pH, assuming that the volume, pressure and temperature are constant. If we could determine the speciation for any pH and Pden:bipy ratio, then we could answer the questions: what other species are major species in the solution? What pH and Pden:bipy ratio would give maximum yield? What is the effect of changes in pH and Pden:bipy ratio on the concentration of square or any other species in the solution? Although the model is for the solution equilibrium, we expect that the information provided by the model will be transferable, at least on a qualitative level, to self-assembly in the bilayer.

2 A model for the self-assembly of Pden-bipy macrocycles

2.1 Introduction

Supramolecular self-assembly at equilibrium is a thermodynamically driven process in which the products observed are the result of a complex interplay between competing equilibria. Insight into the fundamental processes which drive equilibrium self-assembly is garnered by considering self-assembly in the context of thermodynamics. This type of exploration not only allows us to rationalize empirical observations but to predict the outcomes of self-assembly as well. Work on modeling the self-assembly process has been reported in the literature but has been limited to two component systems[70-73]. The general approach presented in this thesis includes more than two components and allows for variations in the ratio of components in the solution. The model proposed is presented through the self-assembly of **13** from Pden and bipy in water.

The models proposed in the literature and the model proposed by us relies on knowing values for the cumulative formation constants for all the species in equilibrium. In most cases these values are not readily available in the literature so they must be measured or estimated. In the present work, the cumulative formation constants for **13** were estimated using an additive process in which stepwise equilibrium constants from model equilibria are summed. This chapter describes how the model for the self-assembly of **13** was constructed.

2.2 Self-assembly – a thermodynamic view

2.2.1 Describing self-assembly using cumulative and stepwise formation constants

The composition of solutions in equilibrium will shift to accommodate changes in the total amount of reactants in solution as well as pH. This phenomenon, which is described more generally by Le Châtelier's principle[74], applies to equilibrium self-assembled systems provided that the volume, temperature and pressure are constant. Under these conditions, the equilibrium constant, K, for a system will be a fixed value. The equation (2-1) relates standard molar reaction Gibbs free energy, ΔG°, and K.

$$\Delta G^\circ = -RT \ln K \qquad \textbf{(2-1)}$$

where R is the gas constant, T is temperature and K is the stepwise formation constant[75]. When a multi-equilibrium system is considered the expression for ΔG° must include K for all the equilibria in the system. Equation (2-2) is an expression for a system consisting of n equilibria.

$$\Delta G^\circ = -RT \ln K_1 - RT \ln K_2 - RT \ln K_3 - \ldots - RT \ln K_n \qquad \textbf{(2-2)}$$

It is convenient to express the thermodynamics of equilibrium processes in terms of K rather than ΔG° because K can be related directly to chemical structure. The formation constants are expressed as logarithmic values for computational simplicity.

Consider the general equilibrium (2-4) which consists of components A, B, and A_aB_b. In order to fully describe the equilibrating system, equation (2-2) must include (a+b) log$K$ terms. The stepwise chemical equilibria and corresponding

expressions for K_{ab} are shown in equations (2-5) to (2-10). The subscripts a and b are used to indicate the stoichiometry of the product.

$$a\,A + b\,B \rightleftharpoons A_aB_b \qquad \beta_{ab} = \frac{[A_aB_b]}{[A]^a[B]^b} \qquad (2\text{-}4)$$

$$A + B \rightleftharpoons AB \qquad K_{11} = \frac{[AB]}{[A][B]} \qquad (2\text{-}5)$$

$$AB + B \rightleftharpoons AB_2 \qquad K_{12} = \frac{[AB_2]}{[AB][B]} \qquad (2\text{-}6)$$

$$AB_2 + B \rightleftharpoons AB_3 \qquad K_{13} = \frac{[AB_3]}{[AB_2][B]} \qquad (2\text{-}7)$$

$$\vdots \qquad \vdots \qquad \vdots \qquad \vdots$$

$$AB_{(b-1)} + B \rightleftharpoons AB_b \qquad K_{1b} = \frac{[AB_b]}{[AB_{b-1}][B]} \qquad (2\text{-}8)$$

$$AB_b + A \rightleftharpoons A_2B_b \qquad K_{2b} = \frac{[A_2B_b]}{[AB_b][A]} \qquad (2\text{-}9)$$

$$\vdots \qquad \vdots \qquad \vdots \qquad \vdots$$

$$A_{(a-1)}B_b + A \rightleftharpoons A_aB_b \qquad K_{ab} = \frac{[A_aB_b]}{[A_{(a-1)}B_b][A]} \qquad (2\text{-}10)$$

The cumulative formation constant, β, describes the equilibrium between initial reagents and final products regardless of the number of intermediate species involved. The cumulative formation constant is defined in general terms for (2-4) by (2-11). Because $\log\beta$ describes the cumulative equilibrium between species, it can be defined in terms of $\log K$. Equations (2-11) to (2-13) derive the relationship between $\log\beta$ and $\log K$ for (2-4) using K defined by (2-4) to (2-10). The $\ln K$ terms in (2-2) can be substituted with $\log\beta$ terms which results in a more serviceable

form because logβ values can be determined experimentally. This relationship is used to find log$K$ for species involved in complex equilibria in this thesis.

$$\beta_{ab} = \prod_{\substack{i=0 \\ j=0}}^{\substack{i=a \\ j=b}} \frac{[A_iB_j]}{[A]^i[B]^j} \qquad \textbf{(2-11)}$$

$$= \frac{[A_aB_b]}{[A_{a-1}B_b][A]} \bullet \frac{[A_{a-1}B_b]}{[A_{a-2}B_b][A]} \bullet \ldots \bullet \frac{[A_2B_b]}{[AB_b][A]} \bullet \frac{[AB_b]}{[AB_{b-1}][B]} \bullet \frac{[AB_{b-1}]}{[AB_{b-2}][B]} \bullet \ldots \bullet \frac{[AB_2]}{[AB][B]} \bullet \frac{[AB]}{[A][B]}$$

$$= K_{ab} \bullet K_{(a-1)b} \bullet \ldots \bullet K_{2b} \bullet K_{1b} \bullet K_{1(b-1)} \bullet \ldots \bullet K_{12} \bullet K_{11} \qquad \textbf{(2-12)}$$

$$\therefore \log\beta_{ab} = \log K_{ab} + \log K_{(a-1)b} + \ldots + \log K_{2b} + \log K_{1b} + \log K_{1(b-1)} + \ldots + \log K_{12} + \log K_{11} \qquad \textbf{(2-13)}$$

To be strictly correct species activities should be used instead of species concentrations; however, we have followed the convention established in the coordination chemistry literature which expresses equilibrium and formation constants in terms of concentration[76]. The need to estimate unknown activity coefficients is eliminated by making the assumption that activities and concentrations are approximately the same. Approximating the activity by concentration is a reasonable assumption because the solutions involved in this thesis are in the 10^{-6} to 10^{-5} M range.

2.2.2 Structural isomers and the statistical factor

The relationship between log$K$ and logβ has so far been discussed without regard to the specific structure of the species involved. If specific structures are considered, then the need to differentiate between microscopic and macroscopic formation constants becomes necessary. So far the discussion has revolved around macroscopic formation constants K and β only, the microscopic analogues are denoted as K' and β'. The macroscopic formation constants are

observed directly in an experiment. The macroscopic and microscopic cumulative formation constants are related in (2-14) by a statistical factor, *Y*; the more convenient logarithmic form is shown in (2-15). The statistical factor corrects the cumulative formation constant for the effect of structural isomers that can be interconverted by symmetry operations or bond rotation [77].

$$\beta_{xy} = Y\beta_{xy}' \qquad \textbf{(2-14)}$$

$$\log \beta_{xy} = \log Y + \log \beta_{xy}' \qquad \textbf{(2-15)}$$

Consider the example in (2-16) where Pden and bipy react to form Pden(bipy) (Figure 7). The ligand en is a bidentate ligand and coordinates to the square planar Pd centre at adjacent sites. The ligand bipy coordinates to open sites on Pden through the pyridyl nitrogen. The complex Pden(bipy) has an overall charge of +2 and one free coordination site at Pd. Statistically, bipy can coordinate to either site which gives two different structures; however, these structures are related by rotation along the axis drawn and the two structures are identical, hence should only be considered once (Figure 7).

$$\text{Pden} + \text{bipy} \rightleftharpoons \text{Pden(bipy)} \qquad \textbf{(2-16)}$$

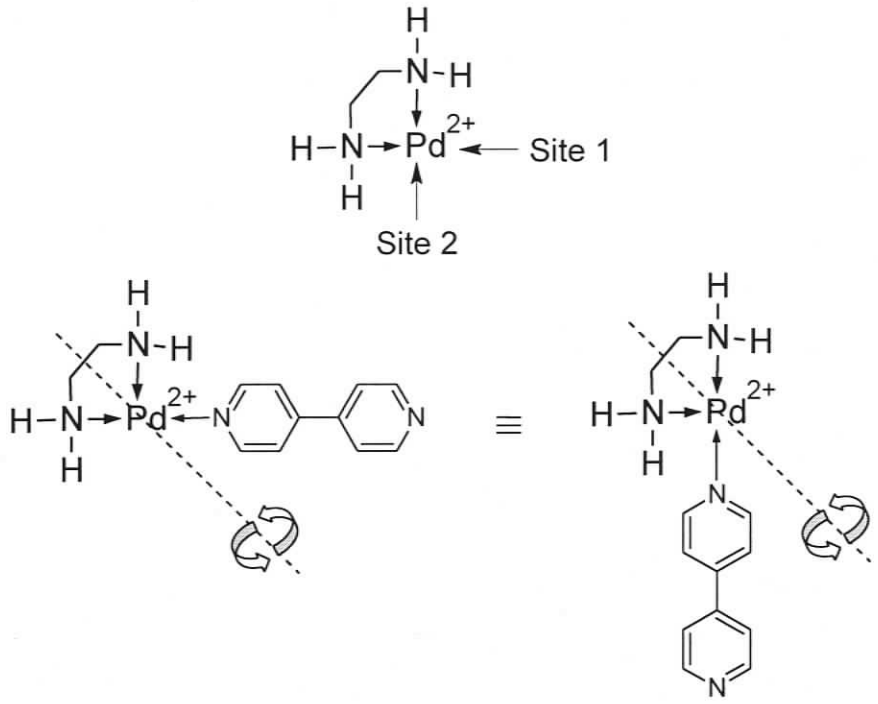

Figure 7 Example of equivalent molecules formed by reacting at different sites on a Pden centre

The general expression for Y is shown in (2-17). The statistical factor for a reaction that involves two reactants and one product, for example equation (2-4), is shown in (2-18) where σ_A, σ_B and σ_{AaBb} are the symmetry numbers for A, B and A_aB_b, respectively, and a, b and n are the stoichiometric coefficients for A, B and A_aB_b from the chemical equation. The symmetry number is equivalent to the order for the principle axis of rotation[77].

$$Y_{ab\ldots yz} = \frac{\sigma_A^a \sigma_B^b \ldots \sigma_y^y \sigma_Z^z}{\sigma_{A_aB_b\ldots Y_yZ_z}^n} \qquad \textbf{(2-17)}$$

$$Y_{ab} = \frac{\sigma_A^a \sigma_B^b}{\sigma_{A_aB_b}^n} \qquad \textbf{(2-18)}$$

An example for the calculation of log$Y$ for $(Pden)_3(bipy)_2$ is shown in Figure 8. The symmetry number for Pden, bipy and $(Pden)_3(bipy)_2$ is 2 because each has a

C_2 principle axis of rotation. The $\log\beta$ observed experimentally does not distinguish between the two different isomers. In this example, $\log\beta$ is 1.2 log units greater than the microscopic $\log\beta'$ as a direct consequence of the symmetries of the reactants and products.

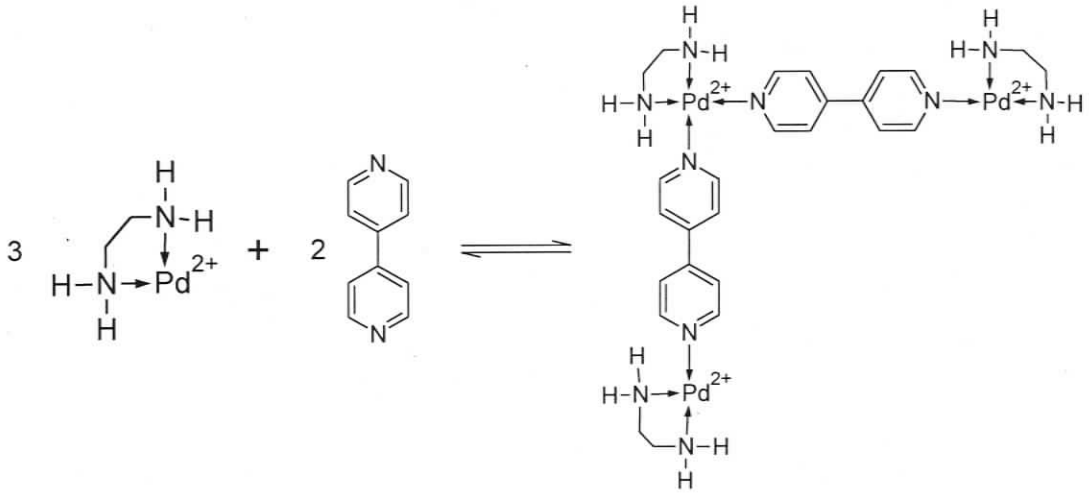

$\sigma_{100} = 2$ $\quad$ $\sigma_{010} = 2$ $\quad$ $\sigma_{320} = 2$

$$Y_{pb} = \frac{\sigma_{100}^{p}\sigma_{010}^{b}}{\sigma_{320}^{n}}$$

$$\log Y_{320} = \log \frac{2^3 2^2}{2^1} = 1.2$$

$$\log \beta_{320} = \log \sigma + \log \beta'_{320}$$

$$\log \beta_{320} = 1.2 + \log \beta'_{320}$$

Figure 8 Calculation of $\log Y_{pbh}$ for $(Pden)_p(bipy)_b(OH)_h$ where p = 3, b = 2, h = 0

2.2.3 Models for equilibrium self-assembly

There was little interest in describing equilibrium self-assembly using concrete terms until the mid 1990s, despite its fundamental nature[78]. Since then, several groups reported models for thermodynamic self-assembly however it was a description advanced by Ercolani that has emerged as the commonly accepted model[70]. The model is based on concepts used to rationalize ring closing and

polymerization reactions. It also emphasizes the fact that thermodynamic self-assembly is an equilibrium process and can be described using β and K.

In the initial report Ercolani describes the self-assembly of 2D macrocycles comprised of only bifunctional monomers. It was followed by a more general description of polycyclic supramolecular assemblies (S) consisting of two monomers, L and M. The species in solution have the general formula L_lM_m where $l = zs$ and $m = zr$. The variable z accounts for the stoichiometry of the monomers in S and r and s are the number of binding sites on monomers L and M, respectively (2-19). The values for m and l are limited by r and s, for example if $r = 3$, $s = 2$ and $m = 1$ then $l \leq 3$ (Figure 9). The model is constrained by considering M-L interactions only (that is, bonding interactions between M-M and L-L are not allowed) and assumes that S is the only cyclic or polycyclic species that can be formed. Figure 9 shows an example where S has the formula L_8M_{12} with $z = 4$, $r = 3$ and $s = 2$.

$$m\,M + l\,L \rightleftharpoons L_lM_m \qquad (2\text{-}19)$$

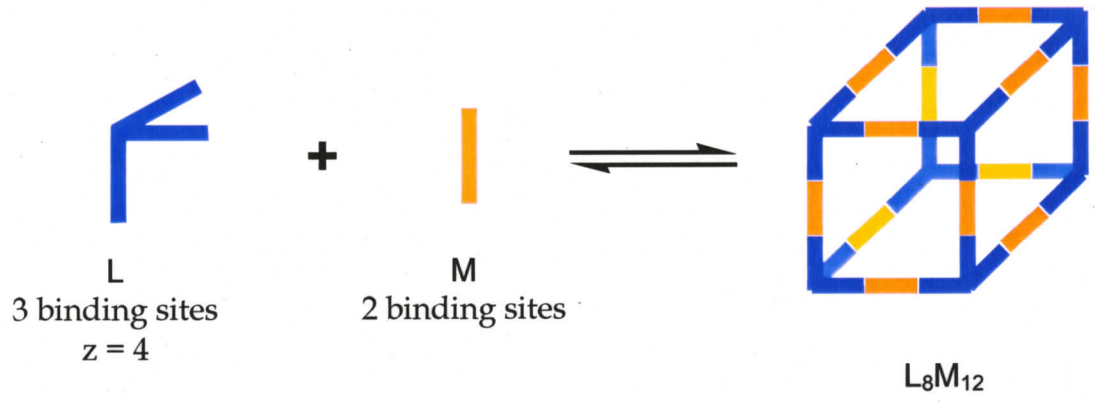

Figure 9 Equilibrium self-assembled system which consists of components L and M. Component L has three binding sites and component M has two bindings.

$$\beta_{lm} = Y_{lm}\beta'_{\text{inter}}\,\beta'_{\text{intra}} \qquad \textbf{(2-20)}$$

$$\beta_{lm} = Y_{lm}K_{\text{inter}}^{\text{N-1}}K_{\text{intra}}^{\text{B-N+1}} \qquad \textbf{(2-21)}$$

The Ercolani model describes S using formation constants calculated by (2-21). The microscopic formation constant, β'_{inter}, is $(K_{\text{inter}})^{\text{N-1}}$ where, K_{inter} is the stepwise formation constant for each M-L interaction and β'_{intra} is $(K_{\text{intra}})^{\text{B-N+1}}$ where, K_{intra} is the statistically corrected formation constant for a ring closing interaction. The variable N is the total number of components in the species and is given by (m + l). The variable B is the total number of bonds between all the components in the product L_lM_m and is given by ml/z. Y is the statistical factor for the species L_lM_m. The exponent (N-1) accounts for the number of intermolecular interactions in species S and (B-N+1) accounts for the number of intramolecular interactions in species S.

One of the main assumptions in the Ercolani model is that all binding interactions are equal. This can only apply in an ideal case. Steric and electrostatic interactions between monomers in real molecules may affect the value of K_{inter}, hence a single value for K_{inter} is not an accurate estimate for all M-L interactions in a supermolecule. For example two positively charged metals bound by a ligand in close proximity may repel each other, this would destabilize the species, making the free energy more positive and hence decrease the magnitude of the stepwise formation constant associated with binding the second metal centre. Solutions to (2-21) depend heavily on being able to determine K_{inter} and K_{intra} values which is not always possible[70].

The Ercolani model is a theoretical construct that provides a method for examining self-assembled systems. Reinhoudt *et al.* have applied the principles proposed by Ercolani in order to rationalize the self-assembly of hydrogen bonded assemblies[73]. The system consists of two monomers, melamine and

cyanurate, that self-assemble in chloroform to form linear tapes, crinkled tapes and rosettes (Figure 10)[79, 80].

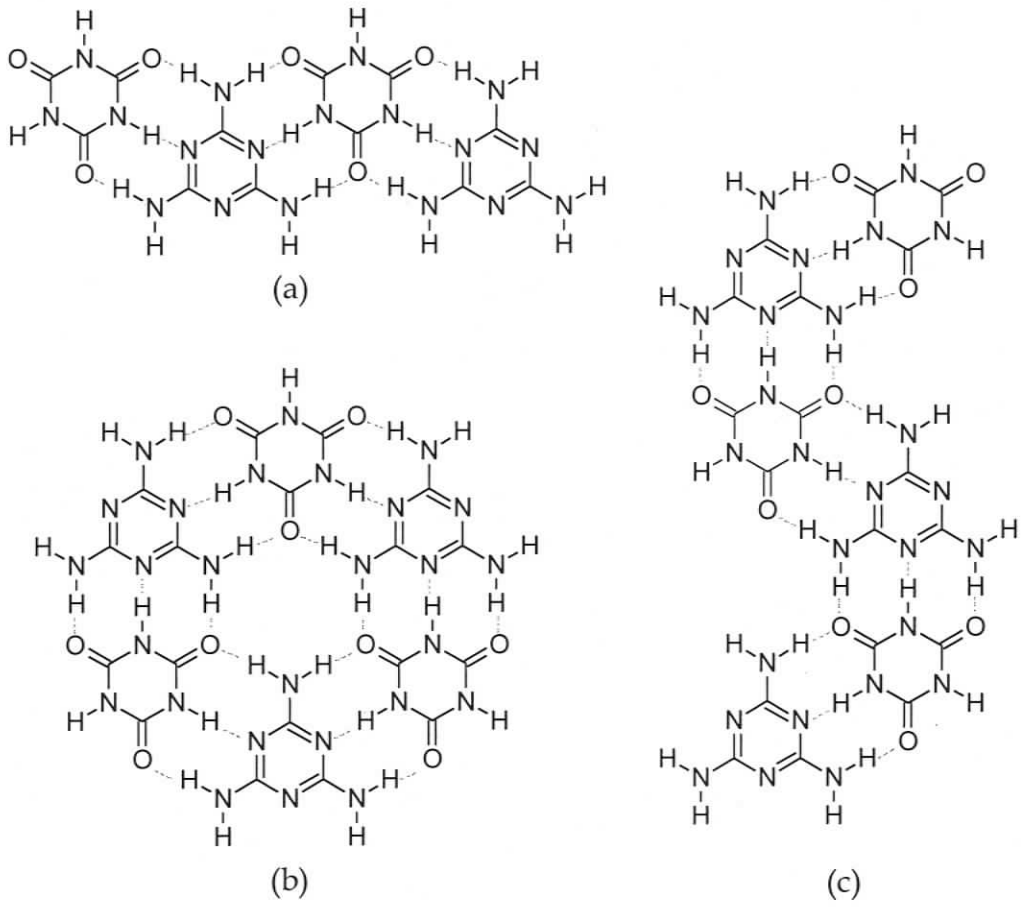

Figure 10 Self-assembled complexes of (a) linear tapes (b) rosettes and (c) crinkle tapes using cyanuric acid and melamine

The Reinhoudt group extends the Ercolani model by including a steric repulsion term, R, that accounts for steric interactions between components of the supermolecule. The augmented expression for β is given in (2-22), where R is $K_{repulsion}/K_{inter}$ and Y, K_{inter}, K_{intra}, N and B are as defined earlier. The Reinhoudt model was able to show that the impact of steric repulsion on the product distribution was minimal compared to the effect of changes in K_{inter} and K_{intra} values for melamine/cyanuric acid systems[73]. The important theme that remains consistent between the Ercolani and Reinhoudt models is that β can be directly

correlated to chemical species through analysis of the contributing stepwise equilibria.

$$\beta = RYK_{inter}^{N-1} K_{intra}^{B-N+1} \qquad (2\text{-}22)$$

The Ercolani and Reinhoudt models are limited to two component systems in which the ratio of the components is the same as the stoichiometry of the product. A more recent approach by Piguet *et al.* which utilizes a statistical mechanical approach to derive the expression for the cumulative formation constants is able to accommodate more than one product, but is still restricted to two component systems[71]. Piguet and co-workers have shown that this approach can be applied effectively to rationalizing trimetallic helicate systems in which the product can have either the same or different (as well as missing) metal ions. These models are important because they provide a rational means of looking at self-assembling systems in a semi-quantitative manner. The method proposed by Ercolani, Reinhoudt and Piguet focus on an additive free energy relationship to derive cumulative formation constants from stepwise formation constants. The work by Ercolani and Reinhoudt applies strictly to systems in which the stoichiometry of the product is fixed and can accommodate only two starting reagents. The scope of the model proposed by Piguet is slightly larger because it can incorporate products with different stoichiometries but is still restricted to two reagent systems[81]. The model proposed in this thesis is able to accommodate multiple products with varying stoichiometries and can incorporate more than two starting reagents. This general model is illustrated by application to the self-assembly of **13**.

2.3 Speciation model for 13

The design of our ion channel, which was discussed in Chapter 1, is dependent on the self-assembly of the supramolecular square first reported by Fujita in 1990 [66]. The equilibrium can be simulated and the speciation calculated by solving the overall mass balance equations for the component species in solution.

2.3.1 Using mass balance to simulate the speciation

Mass balance equations are solved using a program called HySS[82]. In principle the solution contains 5 reactants: Pd^{2+}, en, bipy, H^+ and HO^-. The 1:1 Pden formation constant is very large ($\log\beta$ = 23.6)[83]. For simplicity, we assume a system in which Pd and en are pre-mixed in a 1:1 ratio thus Pden can be considered a single species in the self-assembly equilibrium. Similarly, $[H^+]$ and $[OH^-]$ are interrelated by K_w. The program HySS and other speciation programs regard hydroxide as a stoichiometric sink of H^+, hence H^+ and OH^- can be described by a single term h that can take either positive (H^+) or negative(OH^-) values.

The general mass balance equations for Pden, bipy and OH^- are shown in (2-23), (2-24) and (2-25). The term **[pbh]** is the concentration of the species where the stoichiometric coefficients for Pden, bipy and H or OH are **p**, **b** and **h**, respectively. The number of terms in each equation will vary depending on the species included in the model solution. In order to solve the mass balance equations, expressions and values for $\log\beta$ are necessary for each species included in the model solution. The general expression for β is given by (2-27) for the equilibrium (2-26). Values for $\log\beta$ will be calculated using stepwise formation constants, which were determined by experiments on model systems.

The details regarding the theory and method used to determine stepwise formation constants will be presented later in the chapter.

$$[\text{Pden}]_{\text{Total}} = \sum p[\mathbf{pbh}] \quad \text{(2-23)}$$

$$[\text{bipy}]_{\text{Total}} = \sum b[\mathbf{pbh}] \quad \text{(2-24)}$$

$$[\text{H}]_{\text{Total}} = \sum h[\mathbf{pbh}] \quad \text{(2-25)}$$

$$p\ \text{Pden} + b\ \text{bipy} + h\ \text{H} \rightleftharpoons (\text{Pden})_p(\text{bipy})_b(\text{H})_h \quad \text{(2-26)}$$

$$\beta_{pbh} = \frac{[(\text{Pden})_p(\text{bipy})_b(\text{H})_h]}{[\text{Pden}]^p[\text{bipy}]^b[\text{H}]^h} \quad \text{(2-27)}$$

2.3.2 Selecting the species in the model

Any chemically sensible combination of Pden, bipy, H^+ and OH^- can be included in the model however species with $p > 6$ are excluded in order to keep the model manageable. Higher oligomers are disfavored by mass action so will be present in low concentrations; consequently their effect on speciation will be small. This rationale is also experimentally supported by the observation that the square is the dominant species. At high concentrations, significant proportions of the species are oligomeric which results in a gel[70]. The present model accommodates only solutions speciation.

The number of species included in the simulation was further constrained by assuming that Pden would be fully associated under the conditions of the simulation. The high formation constant for Pd + en ($\log\beta = 23.6$) makes this reasonable in simulations where the Pd:en ratio was fixed at 1:1. The starting reagents included in the simulation are Pden, bipy and OH^- (or H^+).

Species with more than two Pd centres are described using the chemical formula:

$$(Pden)_p(bipy)_b(H)_h$$

where, p is the number of Pden centres, b is the number of bipy and h is the number of H^+ when $h > 0$ and h is the number of OH^- when $h < 0$. The variables p, b and h are not independent as there are a limited number of binding sites on each component. In species where $6 \geq p \geq 2$ and $h = 0$, each Pden must be joined by one bipy ligand so the minimum value for b is p-1. The component Pden can bind to a maximum of 2 bipy so the maximum value for b is p+1. Each terminal bipy can bind to one H^+ so values for h range from 0 to b-p+1. Because OH^- must bind directly to Pden, the maximum number of OH^- in a species is defined by h = p-b+1. Species in the model will be referred to using the stoichiometric coefficients, **pbh**, throughout the thesis. For example **342** refers to the species $(Pden)_3(bipy)_4(H)_2$.

One of the primary goals of the model is to determine the effect of pH on the speciation. The terms for H+ and OH- are included in the formula to allow $(Pden)_p(bipy)_b$ species to respond to changes in pH. There are 45 species with $p > 2$ that are described using the general formula above.

Eight species that include Pden cannot be described using the general formula above have also been included in the model. They are **110**, **120**, **111**, **121**, **122**, **11-1**, **10-2**, and **20-2**. The most elementary Pden+bipy species are **110** and **120**. These species are protonated at acidic pH to make **111**, **121** and **122**. Studies show that **10-2** and **20-2** complexes form in significant quantities as pH increases but only a small amount of **10-1** is observed, probably because it dimerizes to make **20-2**[84]. The **10-1** species has not been included in the model because it has not been detected in Pden mixtures therefore it can be safely ignored in the model[83]. The species **11-1** will be included because hydroxo species are observed

in model reactions. Protonated bipy, species **011** and **012**, are also included in the model.

2.3.3 Linear and cyclized species in the model

For species with the same stoichiometry in equilibrium with each other, the species with the greater logβ value will be preferred[75]. A cyclized species is stabilized with respect to the linear species with the same stoichiometry by a factor of logβ_{intra} because it contains one additional intramolecular bond. The cyclized species will always be favoured in an equilibrium between species with the same stoichiometry given that logβ_{intra} is positive. Therefore, linear structures with the chemical formula $(Pden)_4(bipy)_4$, have been excluded from the model even though cyclized and linear structures with the general formula $(Pden)_n(bipy)_n$ where $n \geq 3$ are possible.

Palladium(II) normally coordinates in a square planar fashion however there is evidence that it can be distorted from this geometry to form cyclic trimetallic coordination compounds with linear bridging ligands[69, 85]. The Pden moiety has been used to form 90° corners in a number of coordination compounds and significant deviation from the expected square planar geometry has never been observed[27, 33]. For this reason, cyclic trimetallic species have not been included in the model.

2.4 Estimating logβ

The details regarding the calculation of logβ values needed to simulate the solution are examined in this section. Equation (2-15) is used as the general formula to calculate logβ_{pbh}.

2.4.1 Log*Y*

This section focuses on log*Y* in the context of estimating logβ and modeling the self-assembly of **13**. Values for log*Y* for any species in a solution containing Pden and bipy is calculated using (2-28)[86]. The symmetry numbers for Pden, bipy and H^+ (or OH^-) are 2, 2, and 1, respectively. The variables p, b and h are the stoichiometric coefficients in the product. Calculating the numerator for log*Y* is simple because the starting reagents are always the same, so the symmetry numbers are constant. For product species in which h = 1 or -1, $\sigma = 1$ and species in which p = b will also have $\sigma = 1$. All other species will have $\sigma = 2$, except for the species **440** for which $\sigma = 4$.

$$\log Y_{pbh} = \log \frac{2^p 2^b 1^h}{\sigma_{pbh}} \qquad \textbf{(2-28)}$$

Values for $\log Y_{pbh}$ increase in magnitude as p increases in a species (Figure 11). For our model which includes species containing up to six Pden centres, the highest value calculated for log*Y* was 3.9 for **671**. Larger log*Y* values are found when Pd:en ratios were allowed to vary from 1:1. In these cases, log*Y* could contribute as much as five log units to logβ, which is almost as much as one Pden + bipy bond.

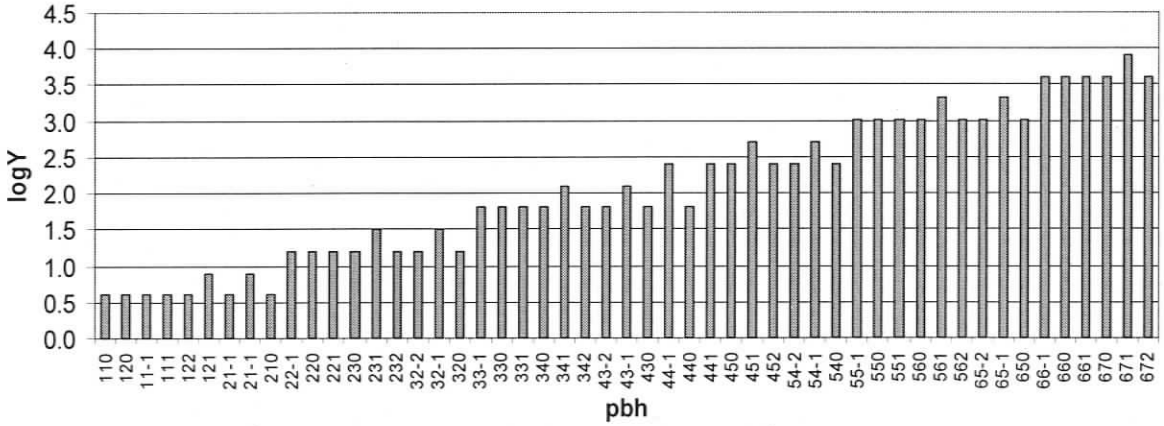

Figure 11 Variation in log*Y* for the species included in the model

2.4.2 Estimating $\log\beta'$ for the species included in the simulation

The microscopic formation constants, $\log\beta'$, need to be estimated from microscopic stepwise interactions between Pden and bipy, OH^- and H^+. Pden has two free binding sites that are orthogonal to each other. All five possible stepwise interactions between Pden and bipy, OH^- and H^+ are shown in (2-29) to (2-33).

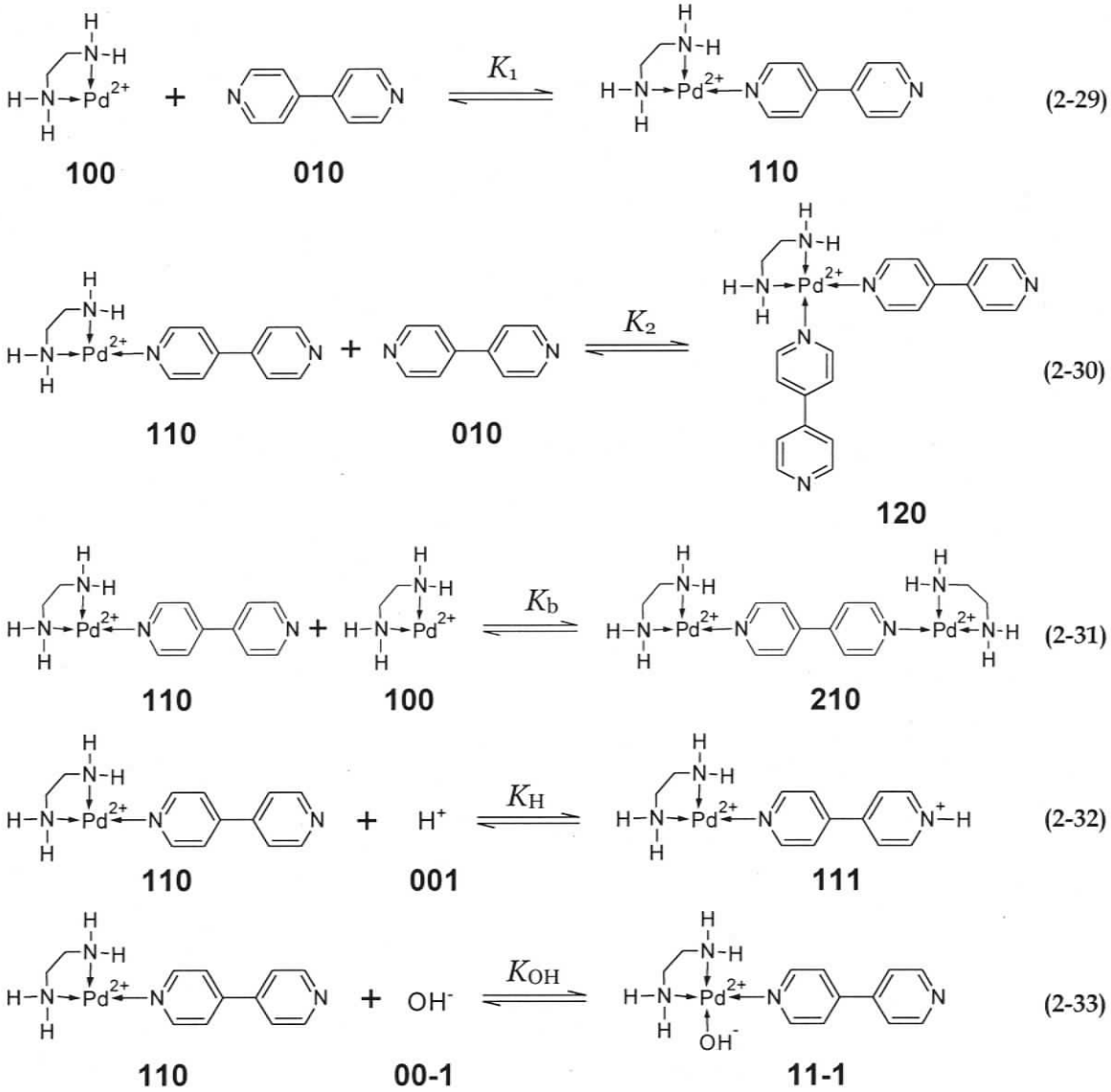

The stepwise equilibrium that corresponds to $\log K_1$ ((2-29)) is for the interaction between Pden and bipy when no other ligands are present on Pden. The

formation of a Pden+bipy bond with one of the sites on the Pden centre already occupied by another bipy is represented by $\log K_2$ ((2-30)). There may be a slight difference in the values between $\log K_1$ and $\log K_2$ due to steric interferences or a slight change in acidity of the Pd centre. The formation constant between Pden and bipy such that the bipy forms a bridge between two Pd centres is represented by $\log K_b$ ((2-31)). This situation is different from K_1 and K_2 because two Pd centres are bonded to the same bipy. This puts the two Pd ions in close proximity which may have a destabilizing effect on the overall structure due to the electrostatic repulsion between the two Pd. In other words, binding to one end of the bipy lowers the basicity of N at the other end. This electrostatic destabilization was observed as a significant effect in lanthanide helices by Piguet[81]. Further support for the separate treatment of bonding described by K_b comes from the differences in acid dissociation constants for bipy ($\log K_{a1}$ = 4.7 and $\log K_{a2}$ = 2.8)[76]. Although the statistical factor accounts for 0.3 log units, the bulk of the difference arises from the influence of coordination on one end with binding at the other.

The species **110** has one basic site on the unbound pyridyl nitrogen. Under acidic conditions this site could react with H^+ as shown in (2-32). The stepwise formation constant for this process is given by $\log K_H$. The species **110** also has one open site on the Pd centre which can bind to OH^- under neutral or basic conditions. The stepwise formation constant for this process is given by $\log K_{OH}$ in (2-33).

The general equation needed to calculate $\log \beta'_{pbh}$ for the species in solution is given in (2-34) where, B_1 is the number of Pden+bipy bonds in the species, B_2 is the number of Pdenbipy+bipy bonds formed in the species, and B_b is number Pdenbipy+Pden bonds formed in the species. B_H is the number of Pdenbipy+H bonds in the species and B_{OH} is the number of Pden+OH bonds in the species.

The microscopic stepwise formation constants ($\log K_1'$, $\log K_2'$, $\log K_b'$, $\log K_H'$ and $\log K_{OH}'$) corresponding to (2-29) to (2-33) are used to calculate $\log \beta'_{pbh}$ for all 55 species included in the model using (2-34).

$$\log \beta'_{pbh} = B_1 \log K_1' + B_2 \log K_2' + B_b \log K_b' + B_H \log K_H' + B_{OH} \log K_{OH}' \qquad \textbf{(2-34)}$$

Values for $\log K_1$, $\log K_2$, $\log K_b$, $\log K_H$ and $\log K_H$ cannot be determined directly from the components (Pden, bipy and H^+ or OH^-) because a solution of these components would yield the complicated solution we are aiming to understand. Therefore model compounds have to be used to estimate the $\log K$ values. The model systems used to the approximate formation constants for $\log K_1$, $\log K_2$, and $\log K_{OH}$ are shown in Figure 12. Substituted pyridines (pyR) with similar pKa are chosen as monodentate analogues of bipy.

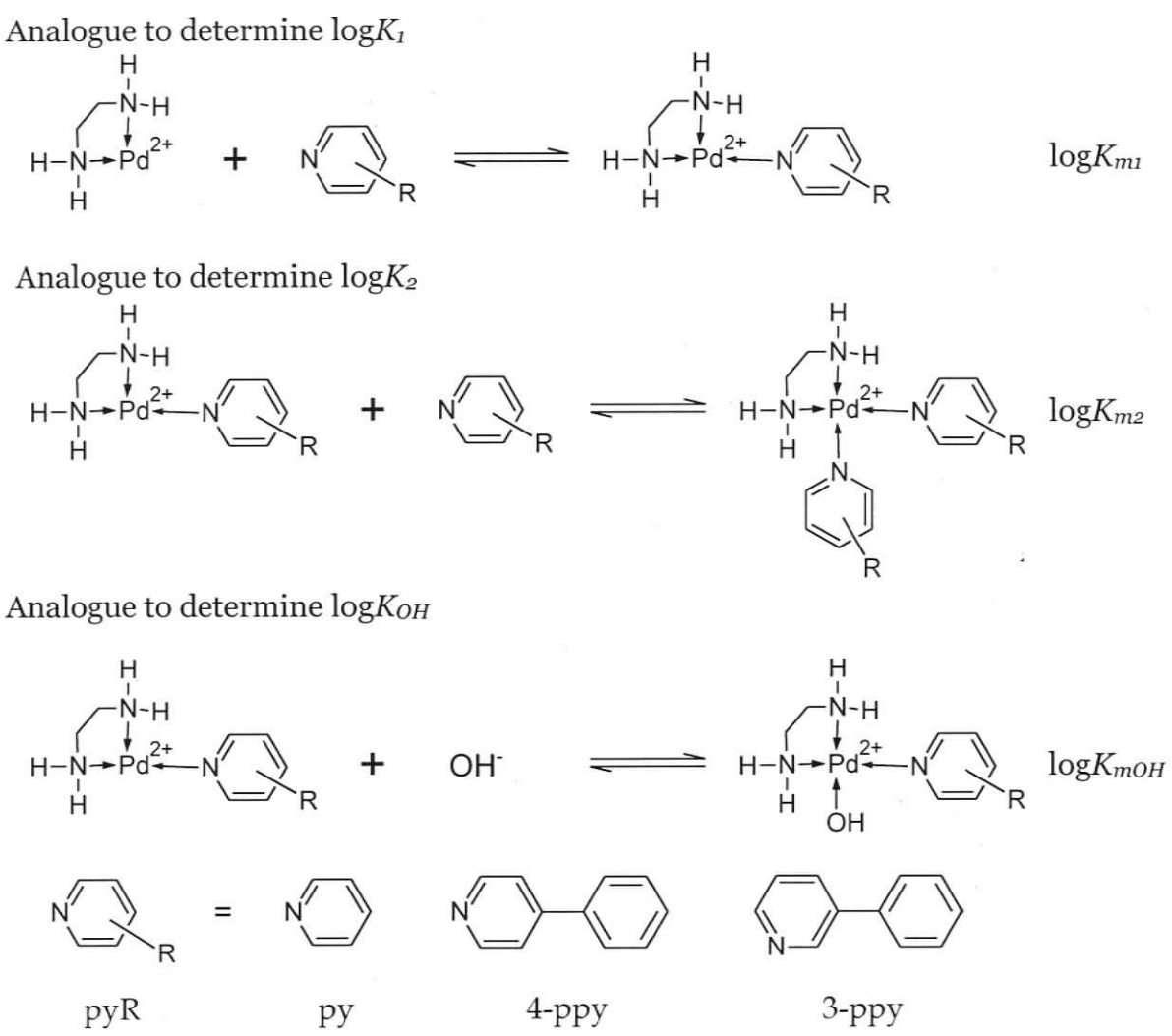

Figure 12 Model systems used to obtain values for $\log K_1$, $\log K_2$ and $\log K_{OH}$

Diethylenetriamine (dien) is a tridentate ligand that will coordinate to three adjacent sites on a Pd, which leaves one free site for binding with an incoming ligand thereby limiting the number of possible species. Values for $\log K_b$ and $\log K_H$ were determined using the model equilibria shown in Figure 13. The determination of $\log K_1$, $\log K_2$, $\log K_b$, $\log K_H$ and $\log K_{OH}$ is described in detail in the following section.

Analogue to determine logK_b

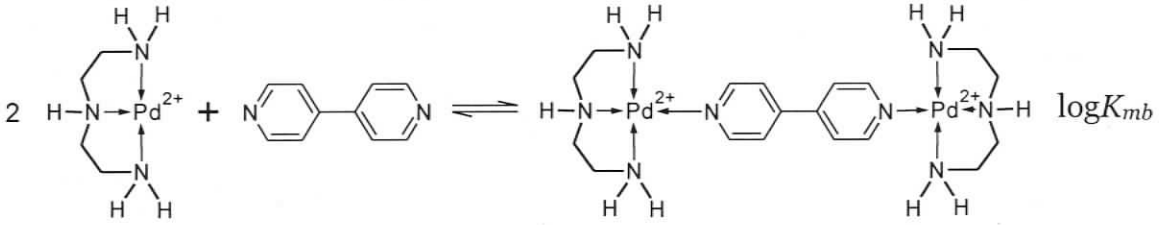

Pd(dien)

Analogue to determine logK_H

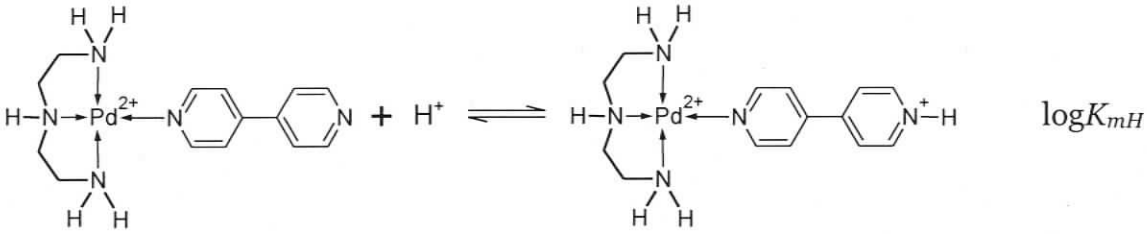

Figure 13 Model equilibria that use Pddien as an analog for 110

2.4.2.1 Finding log$K$' for model systems

A search through the literature for the stepwise formation constants required to estimate logβ' was unsuccessful so were determined by potentiometric titration. Values for log$K$ of (pyR)H, **011**, **012**, **102** and **202** were available in the literature[76, 83]. All other values for log$K$' were determined from potentiometric acid-base titration on the model systems summarized in Figure 12 and Figure 13.

Acid-base titrations can be used to determine the formation constants of metal ligand complexes if the total concentrations of acid, metal, and ligand are known[87]. The normal strong acid-strong base titration curve will be perturbed by competing equilibria that involve components of the model systems. Values for cumulative formation constants, from which stepwise formation constants are calculated, can be extracted by fitting the experimental titration curve to a model

described by the analytical concentrations of the reactants and a set of β values that describe the system. The concentration of H^+ is monitored using a proton selective electrode. Typically, only one or two unknown β values are sought by the fitting procedure. The following is a simple example in which $\log\beta_{o11}$ and $\log\beta_{o12}$ are determined using the process described.

The strong acid-strong base titration curve is perturbed because bipy competes with OH^- for H^+. The equilibrium between **010**, **011**, and **012** yields the strong acid-weak base curve observed in Figure 14 (dots). The titration curve was fit using a model that included logβ values for the following equilibria:

010 + **001** ⇆ **011**	$\log\beta_{o11}$
011 + **001** ⇆ **012**	$\log\beta_{o12}$
H_2O ⇆ H^++OH^-	$\log\beta_w$

as well as the concentrations of bipy and H^+. The values for $\log\beta_{o11}$ and $\log\beta_{o12}$ obtained by this method are 4.73 and 7.62, respectively. The formation constants of py, 3-ppy and 4-ppy were determined in the same manner.

The $\log\beta$ values obtained using this method are converted into $\log\beta'$ values for the model equilibria using (2-35a). The values for the microscopic stepwise formation constants ($\log K'$), which are used to estimate $\log\beta'_{pbh}$, are calculated using the relationship between stepwise and overall formation constants. In this case, values for $\log Y_{o11}$ and $\log Y_{o12}$ are 0.3 and 0, respectively; therefore values for $\log\beta'_{o11}$ and $\log\beta'_{o12}$ are 4.43 and 7.62, respectively. Because **011** is formed directly from the reactants, $\log\beta'_1$ and $\log K'_1$ are the same. The value for $\log K'_{o12}$ which was obtained by subtracting $\log\beta'_{o11}$ from $\log\beta'_{o12}$ is 3.19.

$$\log\beta' = \log\beta - \log Y \qquad \textbf{(2-35a)}$$

This method can be extended to more complex solutions which contain palladium complexes as well as pyridyl species. The addition of palladium complexes will perturb the strong acid-weak base titration curve observed for

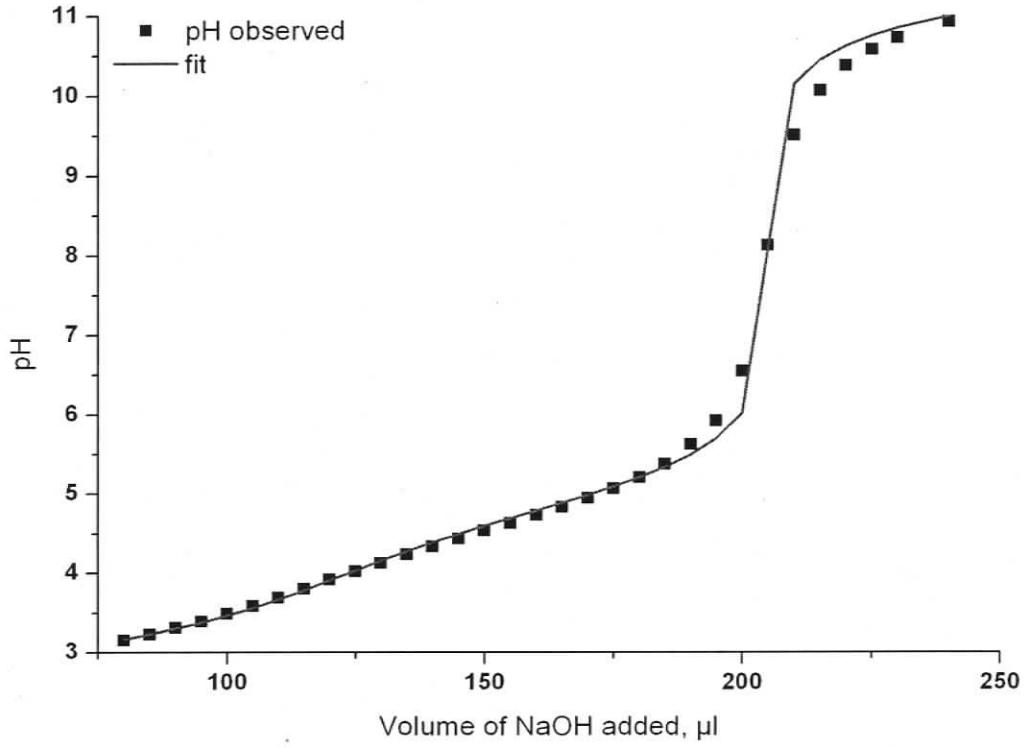

Figure 14 Titration curve for bipy ([bipy] = 4.1 mM) titrated using ~0.2 M NaOH and corresponding fit

solutions that contain only pyridyl species because palladium will complex to pyridyl species. This titration method uses H^+ as the reporting species, therefore any species in equilibrium with H^+ will be observed.

Consider an example in which a solution with Pddien+bipy is titrated. The number of equilibria involved includes the three simple equilibria from the previous case as well as the following:

$$\text{Pddien+OH} \leftrightarrows \text{(Pddien)OH} \qquad \log\beta_{m10\text{-}1}$$

$$\text{Pddien+bipy} \leftrightarrows \text{(Pddien)(bipy)} \qquad \log\beta_{m110}$$

$$\text{Pddien(bipy)+H} \leftrightarrows \text{(Pddien)(bipy)H} \qquad \log\beta_{m111}$$

$$\text{Pddien(bipy)+Pddien} \leftrightarrows \text{(Pddien)}_2\text{(bipy)} \qquad \log\beta_{m120}$$

Models that treat Pddien as a single species fit the data with the same precision as models that treat Pd and dien as separate species so Pddien is treated a single species. The model that is used to fit the titration curve observed includes seven different logβ values and the total concentrations of Pddien, bipy and H^+. Because only a few logβ values can be extracted from the fitting model, all other values for logβ must be "known". These values were determined separately by titration of simpler solutions or obtained from the literature. In this case, the values for $\log\beta_{o11}$, $\log\beta_{o12}$, $\log\beta_{Pddien+OH}$ and $\log\beta_w$ were treated as constant in the fitting model for the titration of solutions containing Pddien and bipy. The values obtained for logβ from this model is shown in Table 4.

Table 4 Values for logβ, logβ' and log$K$' obtained by titration of model species

Species	logβ	log$Y$	logβ'	log$K$'
(Pddien)(bipy)	6.35	0.3	6.05	6.05
(Pddien)(bipy)H	10.70	0.3	10.40	4.35
$(Pddien)_2(bipy)$	11.42	0.6	10.82	4.77

The log$K$' values for other model systems were determined in a similar fashion. Each model system was titrated in duplicate for at least three different concentrations. The fit between the calculated curve and the experimental data points was acceptable at the 95% confidence limit in all cases. The standard deviation for logβ values determined for equilibria that contained Pden or Pddien and a pyridyl containing ligand was ±0.2. For equilibria with only the pyridyl ligand, the standard deviation for logβ was ±0.04. Values determined for $\log K_{m1}$ and $\log K_{m2}$, that were used to estimate $\log\beta'_{pbh}$, were averaged over three different bipy analogs (py, 3ppy, 4ppy). A complete list of the logβ values and log$K$' values determined by experiment are given in Appendix 1. Values for log$K$'

that are pertinent to the model are highlighted in Table 5. Details regarding the procedure used for the titrations are described in the experimental section of this chapter.

Table 5 Model systems for determination of $\log\beta'_{pbh}$ [a]

Actual reaction	Model Reaction	K for model reaction	log K' for model titrations
Pden+bipy ⇆ (Pden)(bipy)	Pden+pyR ⇆ (Pden)(pyR)	$K_{m1} = \frac{[(Pden)(PyR)]}{[Pden][PyR]}$	5.1[b]
(Pden)(bipy)+bipy ⇆ (Pden)(bipy)$_2$	(Pden)(pyR)+pyR ⇆ (Pden)(pyR)$_2$	$K_{m2} = \frac{[(Pden)(PyR)_2]}{[(Pden)(PyR)][PyR]}$	5.8[b]
(Pden)(bipy)+Pden ⇆ (Pden)$_2$(bipy)	(Pddien)(bipy)+Pddien ⇆ (Pddien)$_2$(bipy)	$K_{mb} = \frac{[(Pddien)_2(bipy)]}{[(Pddien)(bipy)][bipy]}$	4.9
(Pden)(bipy)+H ⇆ (Pden)(bipy)(H)	(Pddien)(bipy)+H ⇆ (Pddien)(bipy)(H)	$K_{mH} = \frac{[(Pddien)(bipy)(H)]}{[(Pddien)(bipy)][H]}$	4.6
(Pden)(bipy)+OH ⇆ (Pden)(bipy)(OH)	(Pden)(pyR)+OH ⇆ (Pden)(pyR)(OH)	$K_{mOH} = \frac{[(Pden)(PyR)(OH)]}{[(Pden)(PyR)][OH]}$	-6.4

[a] A complete list of the $\log\beta$ determined is given in

[b] These values are averaged over reactions where pyR = py, 3-ppy and 4-ppy systems.

2.4.3 Pdaap as a possible model for Pden corners in 13

A model for **110** was required to determine $\log K_H'$ and $\log K_b'$. A tridentate ligand that would block three of the four coordination sites on Pd was necessary. A palladium complex with a tridentate ligand would also be more thermodynamically stable as a result of the chelate effect; therefore the palladium complex could be assumed to be one species under the reaction conditions. This is advantageous because it simplifies the curve fitting analysis required to extract the $\log K_b$ and $\log K_H$ values.

Some ligands, when coordinated to Pd, are known to increase the lability of the adjacent ligands[88]. This phenomenon is known as the *cis* influence in situations

where the ligand is coordinated *cis* to the site of substitution. A ligand with a high *cis* influence makes the bonding at the site *cis* to the ligand weaker. The *cis* influence of selected ligands increase according to the following order for Pd[89]: PhCN < EtCN < *n*-Bu_3P < py < piperidine.

The ligand aap (aap = 2-pyridylmethyl-2'-aminoethylamine) is tridentate with a terminal pyridyl group and was considered as a model for **110**. The pyridyl group should also have electronic effects that are similar to bipy so $\log K_b$ and $\log K_H$ determined using Pdaap would also include electronic phenomena such as the *cis* influence. The synthesis of $PdaapCl_2$ and the preparation of Pdaap(ClO_4) solutions is reported in the experimental section.

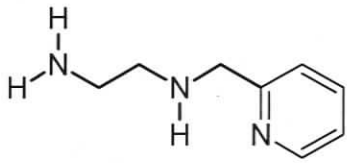

aap

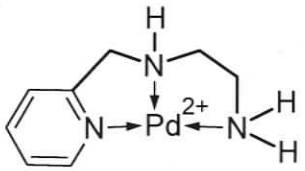

Pdaap

Solutions of Pdaap(ClO_4) were titrated according to the method used for the other model systems. The analysis of the data for Pdaap, Pdaap-bipy and Pdaap-pyR was eventually abandoned because it could not be adequately fitted (greater than 95% confidence level). A variety of different models were used, including one that is analogous to the model used to fit Pddien titration curves. Modifications to the model which include partially associated Pdaap species were also unsuccessful.

During the course of the titration experiments, we noticed that the amount of time required for Pdaap and Pddien solutions to equilibrate was at least 3 times longer than the amount of time required for Pden solution. Although the reason for the discrepancy is unknown, the observations suggest that slower kinetics is

an attribute of tridentate coordinated Pd despite the structural differences between app and dien.

2.5 Results of the simulation

The $\log\beta'_{pbh}$ values for the species discussed earlier were calculated according to (2-34) using values for $\log K_1$, $\log K_2$, $\log K_b$, $\log K_H$ and $\log K_{OH}$ estimated using model systems. The macroscopic formation constant required in the model was calculated from $\log\beta'_{pbh}$ and $\log Y$ using (2-35b). A table for the values calculated for $\log\beta_{pbh}$ is shown in Appendix 2. The speciation is obtained by calculating the concentration of each species using the method described in section 2.3.1.

$$\log\beta_{pbh} = \log\beta'_{pbh} + \log Y \qquad \textbf{(2-35b)}$$

Calculated $\log\beta_{pbh}$ values were used as inputs in the solution simulation program HySS to determine the speciation for various Pden:bipy molar ratios between pH 3 to 10. The results of the simulation for a fixed Pden:bipy molar ratio is represented as a two dimensional plot with pH as the independent axis and the % of total Pd held in the species as the dependant axis. The plot for [Pd] = 1×10^{-5} M at Pden:bipy ratio of 1:1 is shown in Figure 15. The predominant species are **100**, **440**, **11-1** and **10-2**. Note that at the maximum **440** accounts for ~85% of the total Pd in the solution. The amount of **10-2** formed as a % of total Pd surpasses **440** but only at high pH. All other species account for no more than 50% of the total Pd content in solution. The simulations for a range of other Pden:bipy molar ratios are shown in Figure 16, Figure 17 and Figure 18. These figures indicate that **100**, **10-2**, **20-2**, **11-1**, **120**, **121**, **122**, and **440** are the dominant Pd containing species in the solution over the pH range and Pden:bipy molar ratio range simulated. It is also evident that the **440** species is unstable with respect to **120** in the presence of excess bipy. Species that constitute less than 5% of the total Pd have been omitted from Figure 15 through Figure 19 for clarity.

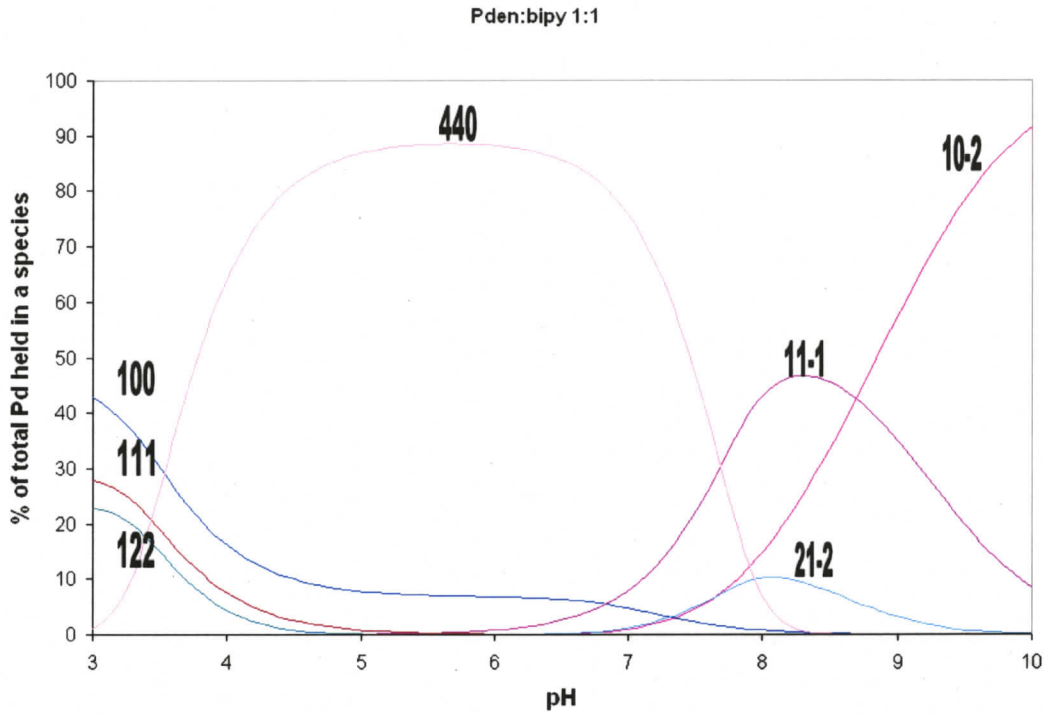

Figure 15 Speciation at [Pd] = 1 x 10^{-5} M for Pden:bipy ratio = 1:1

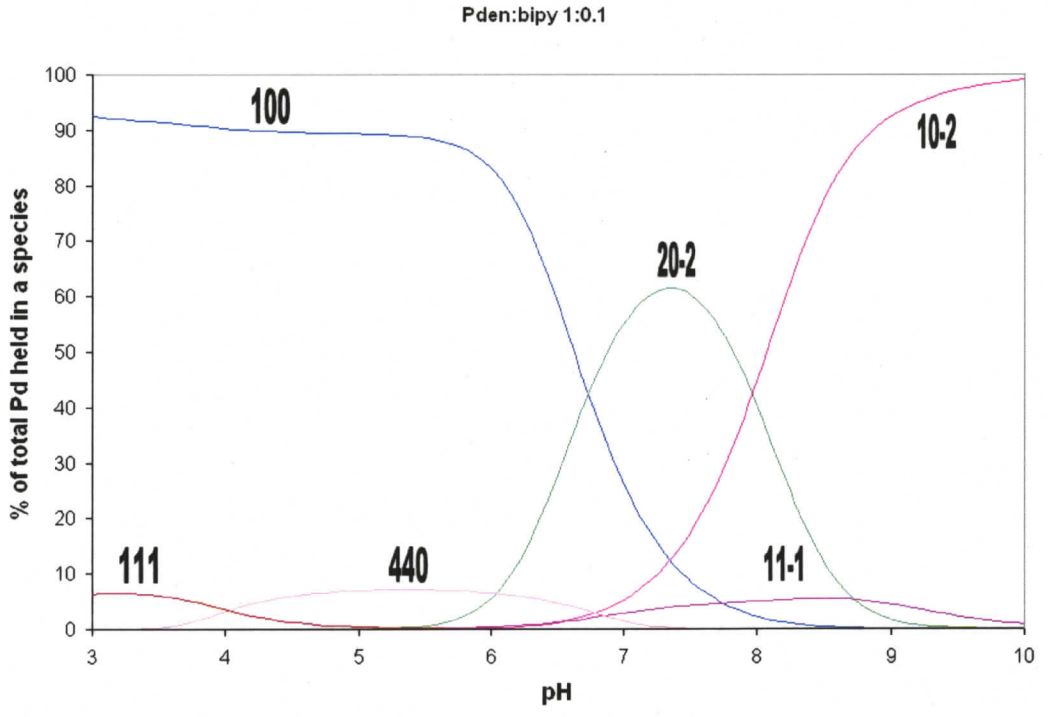

Figure 16 Speciation at [Pd] = 1 x 10^{-5} M for Pden:bipy ratio = 1:0.1

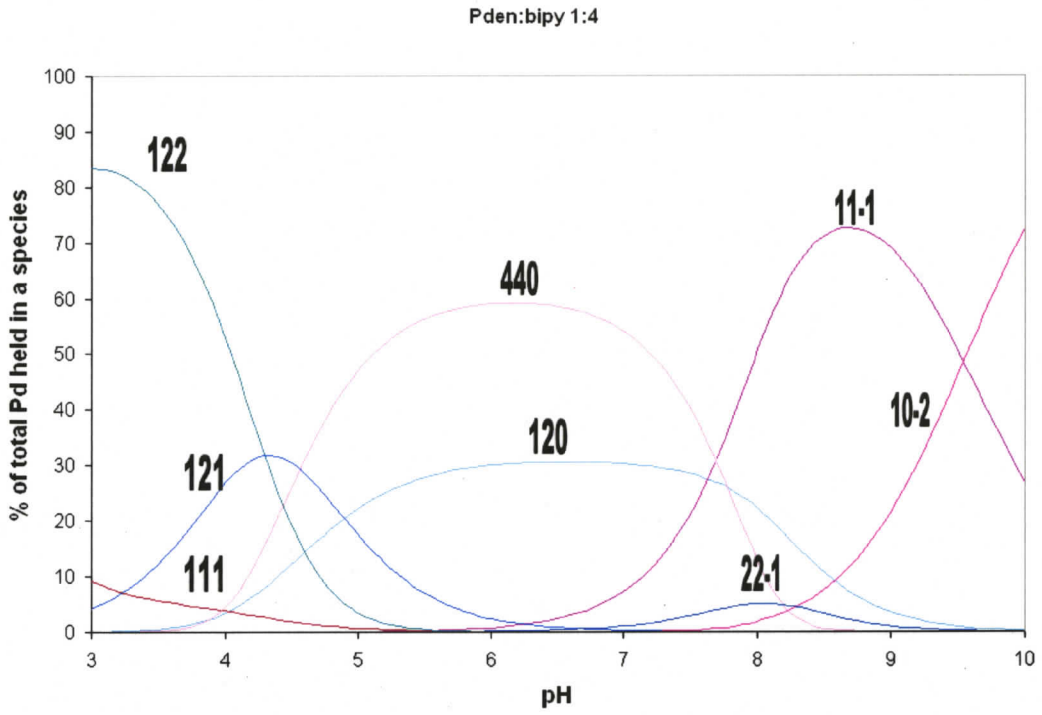

Figure 17 Speciation at [Pd] = 1 x 10^{-5} M for Pden:bipy ratio = 1:4

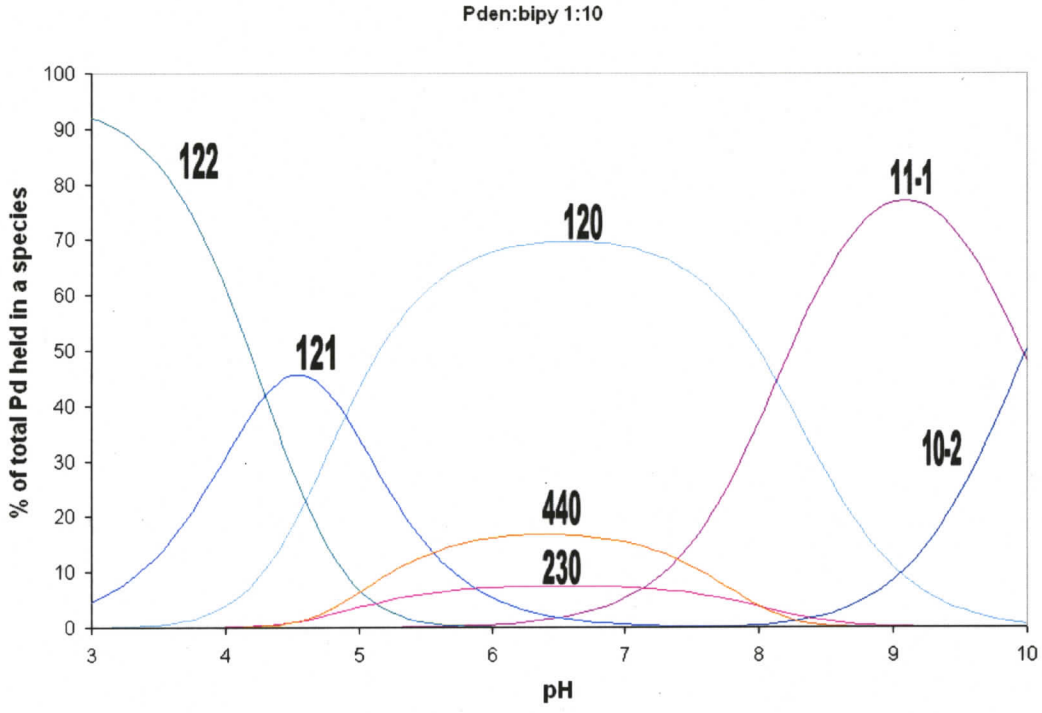

Figure 18 Speciation at [Pd] = 1 x 10^{-5} M for Pden:bipy ratio = 1:10

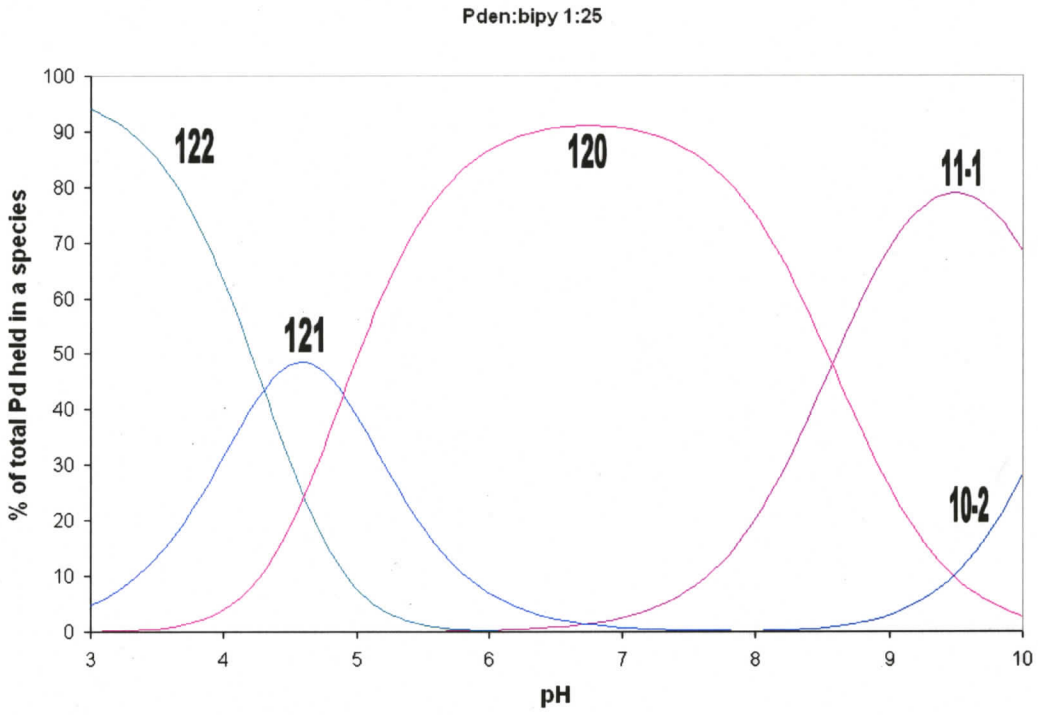

Figure 19 Speciation at [Pd] = 1 x 10^{-5} M for Pden:bipy ratio = 1:25

Figure 15 through Figure 19 vary in two dimensions (% of total Pd held in a species and pH) while the Pden:bipy ratio is fixed. The Pden:bipy ratios can be varied systematically to give a series of plots like those shown in Figure 15 to Figure 19. A series of plots can be combined to give a three dimensional plot with pH and Pden:bipy ratio as axes. The % of total Pd held in a species constitutes the dependent third dimension. A plot that shows the % of total Pd held in **440** is shown in Figure 20. The contours show the % of total Pd held in **440** as a function of pH and Pden:bipy molar ratio. Similar contour plots can be generated for other species as well. The contour plots for the dominant species in solution are amalgamated into one plot to show the change in dominant species as a function of pH and Pden:bipy ratio (Figure 21).

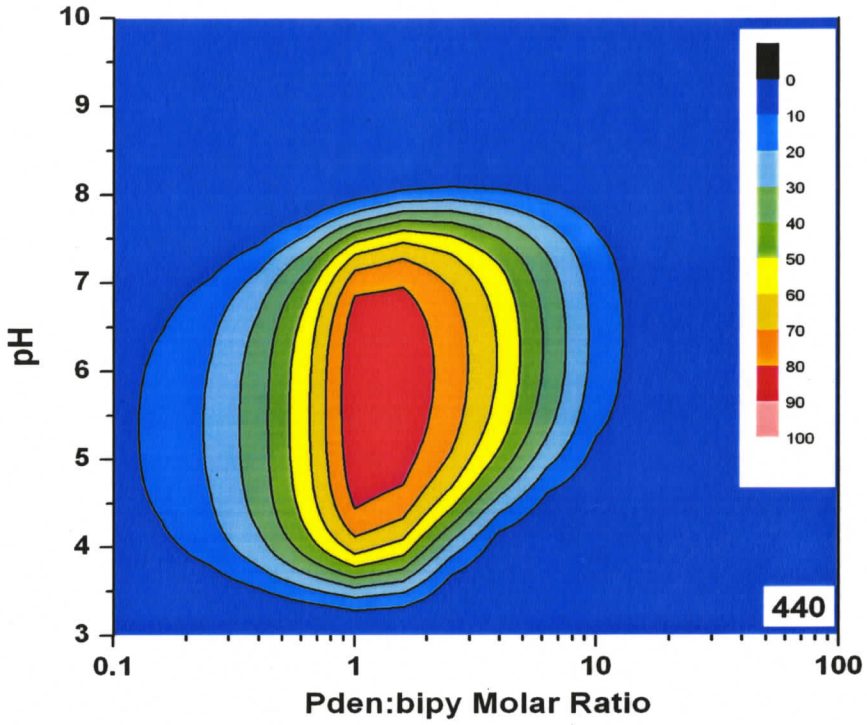

Figure 20 Contour plot for 440

Figure 21 shows that **440** is only dominant when the pH is between approximately 4 to 7 and the Pden:bipy molar ratio is between approximately 0.6 to 6 molar equivalents. Within the composition region where **440** is the dominant species, the square accounts for up to 80% of total Pd in solution. The remaining Pd is distributed among a large number of other species.

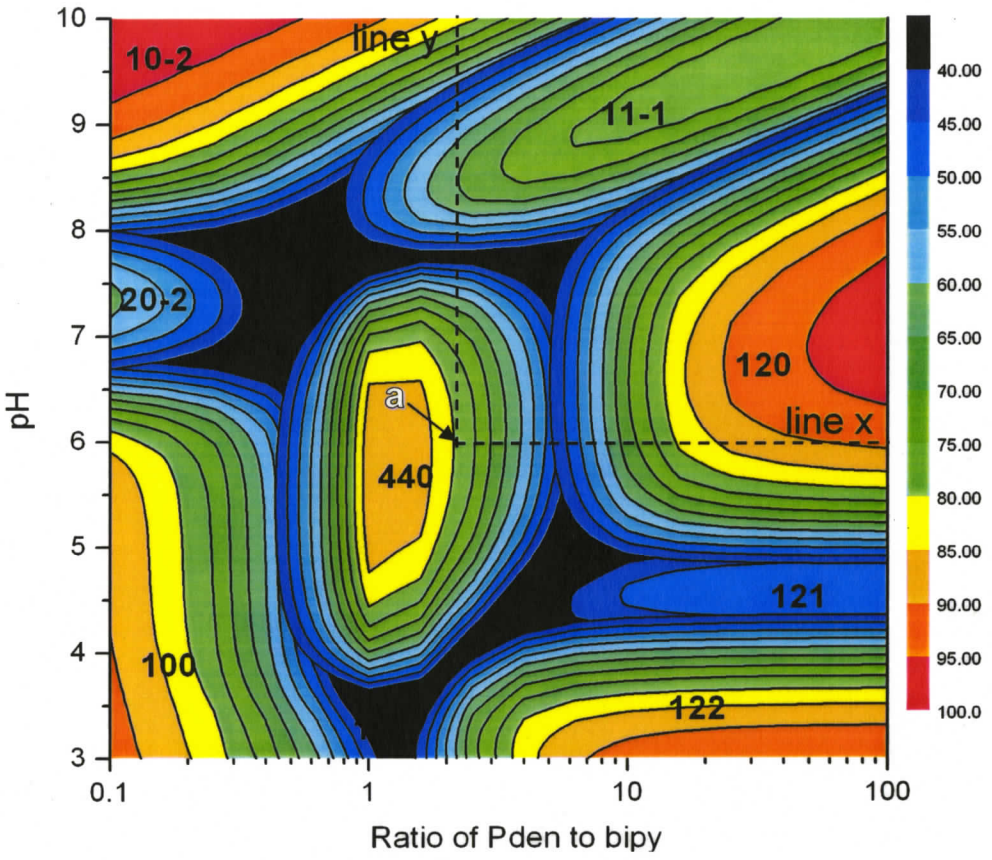

Figure 21 Amalgamated contour plots of the dominant species

This contour map can also be used to predict the changes in speciation as a function of pH and Pden:bipy molar ratio. At point **a** in Figure 21, where the pH = 6 and Pden:bipy is 1:2, the dominant species is **440**. The amount of bipy increases along **line x** and the % of total Pd held by **440** declines. At the point where Pden:bipy ratio = 1:5 the dominant species becomes **120.** The effect of adding OH^- to a solution in which the Pden:bipy ratio is held at 1:2 can be tracked along **line y**. In this case, the % of total Pd held by **440** declines until pH ≈ 7.5 when **11-1** begins to emerge as the dominant species. A second transition to another dominant species is observed at pH ≈ 9.3 where the % of total Pd consumed by **10-2** supersedes **11-1**.

The contour plots are also useful in identifying species that share a common region of the pH-Pden:bipy molar ratio landscape. All species in solution are interrelated by equilibria; however, the ways in which they are related are not always clear. Species that share the same region are correlated so their relationship is more obvious. Concentrations are computed by the simulation program for each species therefore the apparent equilibrium constant between the species can be estimated for a given pH and Pden:bipy ratio.

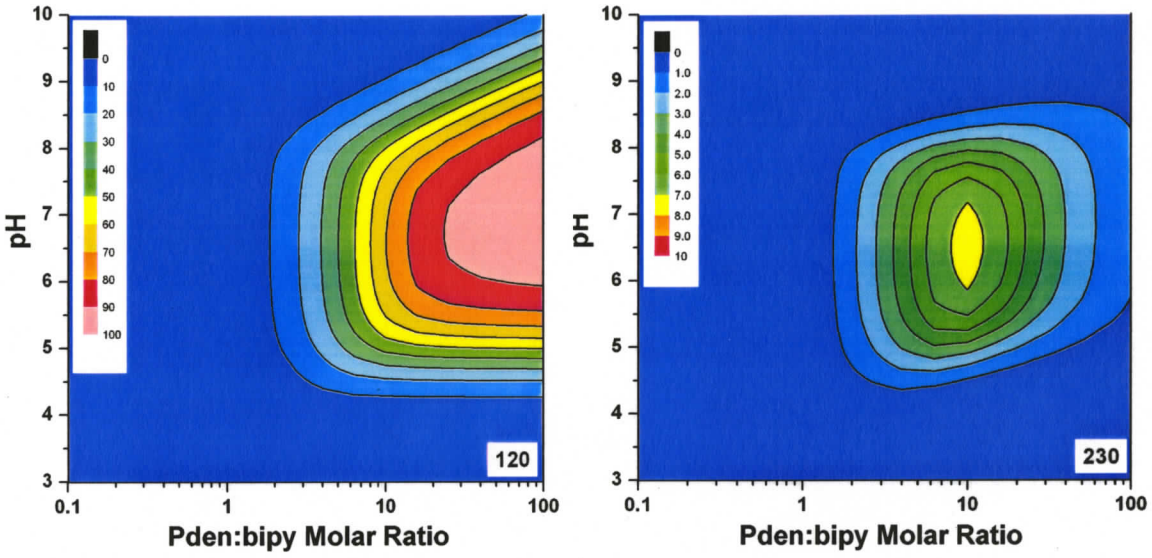

Figure 22 Contour plots for 120 and 230 for [Pd] = 1 x 10^{-5} M. Note the difference in the scale on the z-axis between the two contour plots.

$$2 \cdot \mathbf{120} \leftrightarrows \mathbf{230} + \mathbf{010} \qquad K_{eq} \approx 0.5 \qquad \textbf{(2-36)}$$

The contour plots for **120** and **230** are shown in Figure 22. The equilibrium inferred by these plots is shown in (2-36). The species **010** is abundant in this region of the pH-Pd:bipy molar ratio landscape hence is a reasonable species to use to balance the chemical equation. The concentrations simulated for **120, 230** and **010** at pH = 7 and Pden:bipy=1:1 were 1.1 x 10^{-7} M, 8.4 x 10^{-9} M and 7.4 x 10^{-7} M, respectively. The equilibrium constant, K_{eq}, for the equilibrium (2-36) was calculated from simulated concentrations is 0.5. This value agrees with expectations for energetically similar species in equilibrium.

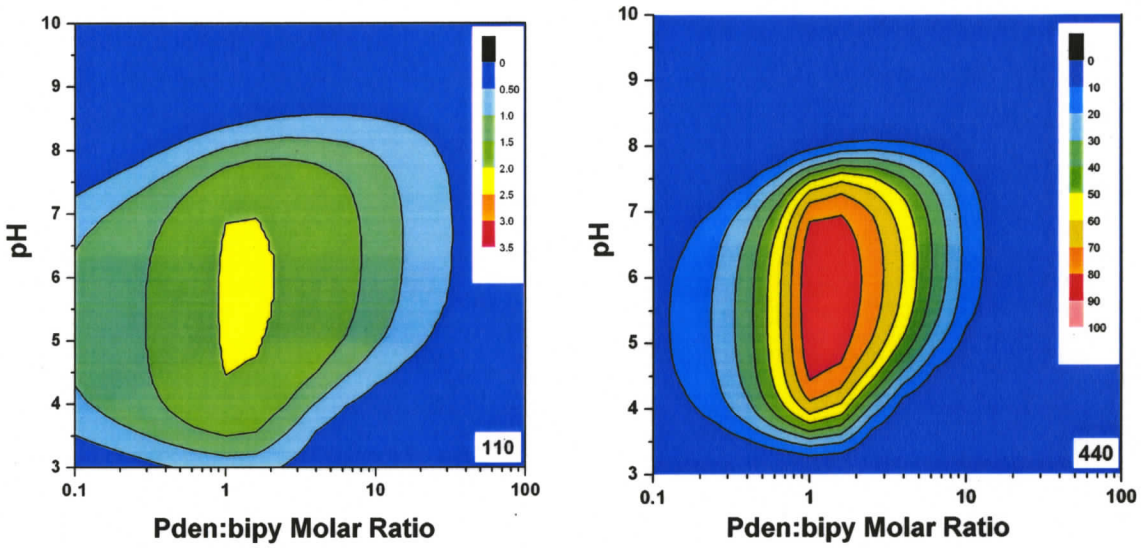

Figure 23 Contour plots for 110 and 440 at [Pd] = 1 x 10^{-5} M. Note the difference in the scale on the z-axis between the two contour plots.

$$4 \cdot \mathbf{110} \leftrightarrows \mathbf{440} \qquad K_{eq} \approx 10^{21} \qquad \textbf{(2-37)}$$

The contour plots overlap for species **110** and **440** in the region in which **440** is dominant (Figure 23). Equation (2-37) describes the equilibrium implied by the overlap. The concentrations calculated by the simulation program for **110** and **440** at Pden:bipy = 1:1 and pH = 7 are 1.9 x 10^{-7} M and 1.8 x 10^{-6} M, respectively. The calculated apparent equilibrium constant is 10^{21} for these conditions which agrees with the observation that **440** is the dominant species in solution as detected by ^{1}H NMR spectroscopy[66]. This implies that **440** lies in a deep energetic well relative to other species in the mixture for the pH and Pden:bipy ratio considered.

2.6 Parametric study

2.6.1 The effect of including cyclic **330** species in the model

The model depends on the species included and the logβ of these species. Subtle variations may have significant effects on the speciation calculated from the model. This section focuses on the impact of including the cyclized **330** species rather than the linear species in the model and the variation in speciation that results from the uncertainty of the experimental log$K$ values used to calculate logβ for species included in the model.

Dimers are the first species to form in a linear polymerization reaction. They are followed by the trimers, then tetramers and so forth. Higher order oligomers can only be formed when the concentration of the lower order species are sufficient. If all the interaction energies are indeed the same, the triangular species will be dominant over the square within the concentration ranges used for the self-assembly of Pden-bipy squares simply as a result of having a lower number of reactants within itself. The values of logβ corresponding to the linear species (logβ_{330L}) and cyclic species (logβ_{330C}) can be estimated as described previously. The value for logβ_{330L} was estimated at 27.6. If the Pden coordination geometry allows the hypothetical cyclic 330 species to form without energetic penalties due to bond strain then logβ_{330C} = 32.6. The solution simulation that includes cyclized **330** for [Pd] = 1 x 10^{-5} M at Pden:bipy molar ratio of 1:1 shows that cyclized **330** would be the predominant product observed, holding ~90% of the total Pd (Figure 24). If **330** formed cyclic species rather than linear species then it would certainly have been observed experimentally[66, 68]. This result in conjunction with the experimental evidence supports a model that includes **330** as a linear species rather than as a cyclic species.

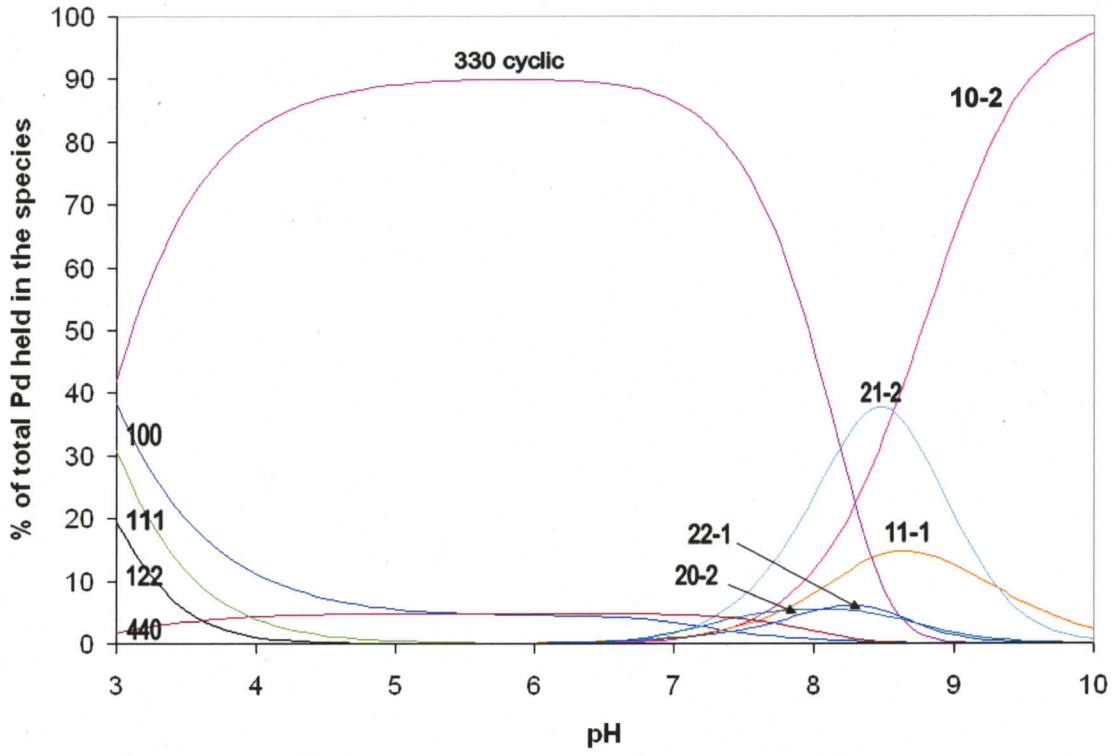

Figure 24 Speciation at [Pd] = 1 x 10^{-5} and Pden:bipy = 1:1 for a model that includes cyclized 330 unstrained species instead of linear 330 species

2.6.2 The impact of errors in logK on the speciation

The error for log*K* determined in a single species titration, such as py+H, was determined to be ± 0.04 and the error for log*K* determined for a two species reaction, such as Pden + py, was determined to be ± 0.2. In order to explore the impact that these errors might have on the speciation modeled, logβ for the species in solution were recalculated using log*K* values that reflect the upper and lower limits of these measurements (Table 6). The speciation simulated using the maximum and minimum log*K* values for Pden:bipy ratios of 1:1 and 1:4 at [Pd] = 1 x 10^{-5} M are shown in Figure 25 through Figure 28.

Table 6 Minimum and maximum log*K* values used to calculate log*β* in parametric studies

Model Reaction	Minimum LogK	Maximum LogK
Pden+pyR ⇆ (Pden)(pyR)	4.94	5.34
(Pden)(pyR)+pyR ⇆ $(Pden)(pyR)_2$	5.38	5.78
(Pden)(pyR)+OH ⇆ (Pden)(pyR)(OH)	-6.64	-6.24
(Pddien)(bipy)+H ⇆ (Pddien)(bipy)(H)	4.44	4.84
(Pddien)(bipy)+Pden ⇆ $(Pddien)_2(bipy)$	4.69	5.09

A visual inspection of Figure 25 through Figure 28 confirms the similarity in the speciation between the maximum and minimum log*K* values at both Pden:bipy ratios. At pH = 7 and Pden:bipy molar ratio of 1:1, the amount of **440** in the solution increases from ~75 to 90 % of total Pd held in **440** over the range for log*K* defined by the error in the measurements. A similar trend is observed when Pden:bipy is 1:4 although the change is less pronounced.

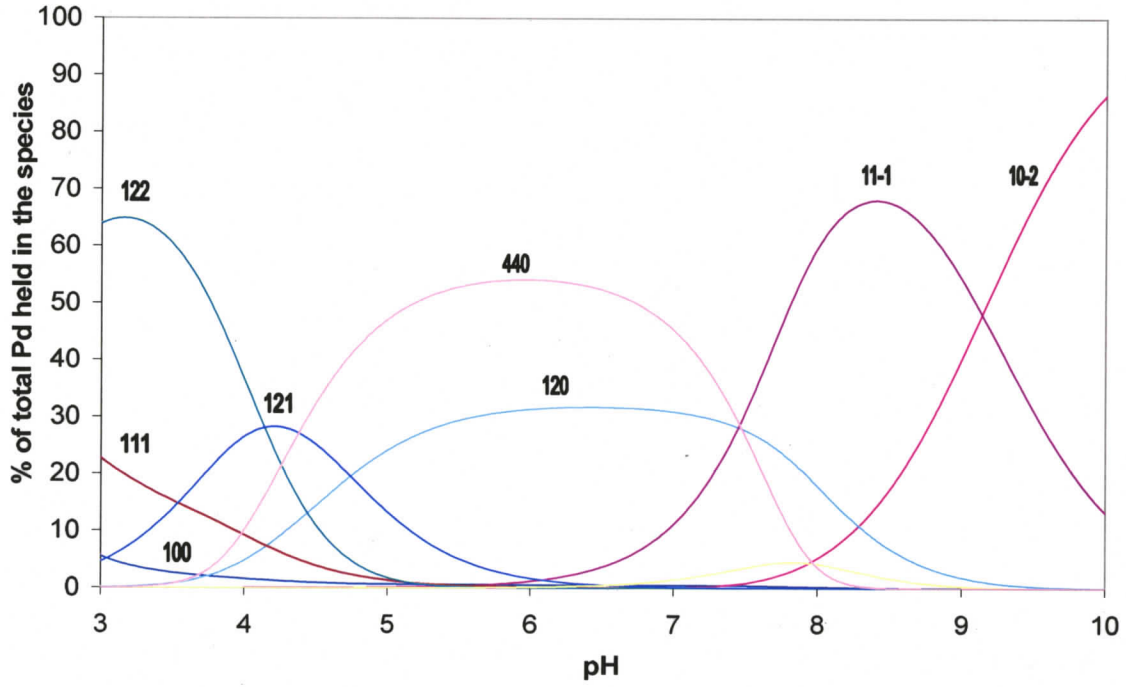

Figure 25 Speciation for Pden:bipy = 1:4 and [Pd] = 1 x 10^{-5} M calculated using log*β* values estimated from minimum log*K* values determined by titration of model systems

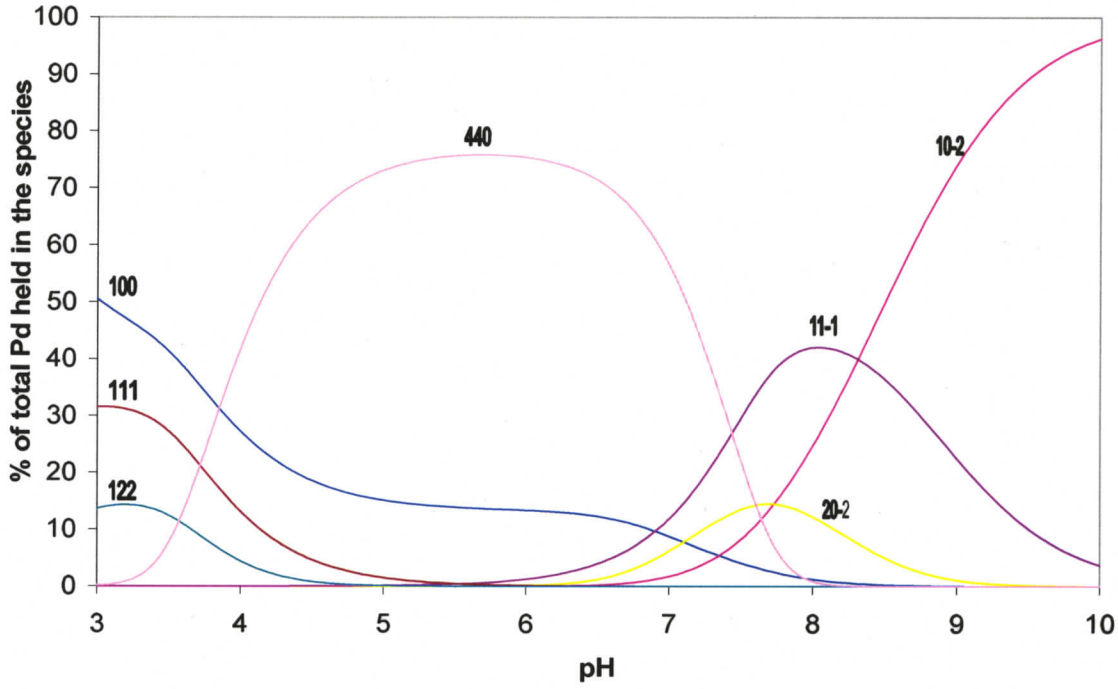

Figure 26 Speciation for Pden:bipy = 1:1 and [Pd] = 1 x 10^{-5} M calculated using logβ values estimated from minimum log$K$ values determined by titration of model systems

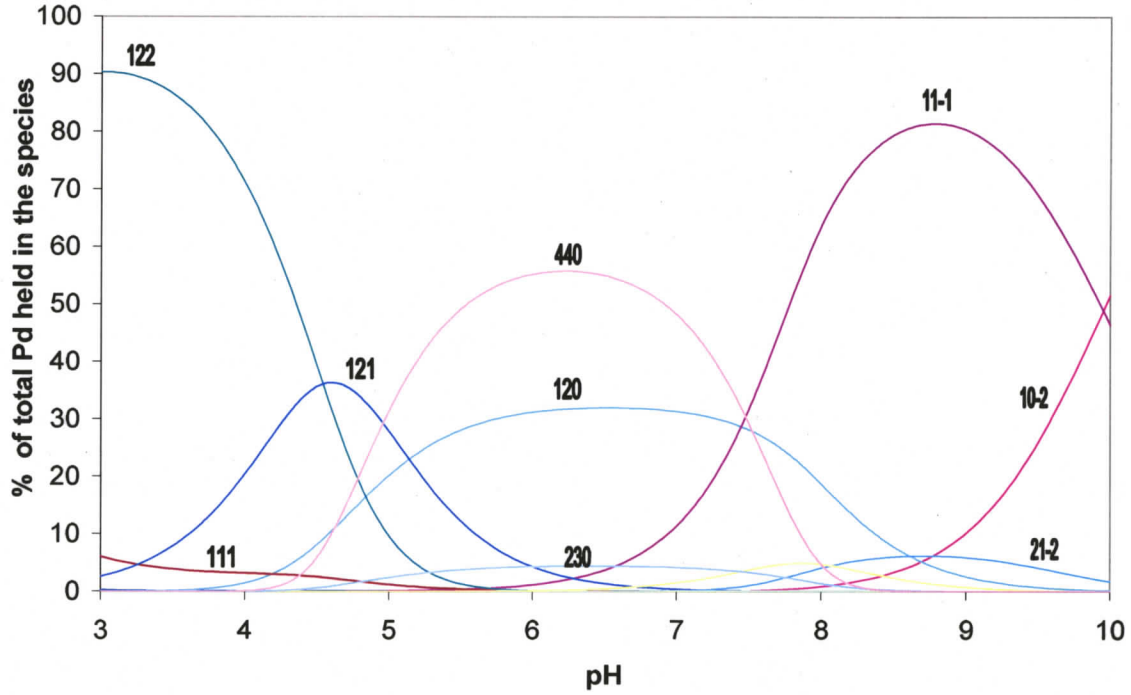

Figure 27 Speciation for Pden:bipy = 1:4 and [Pd] = 1 x 10^{-5} M calculated using logβ values estimated from maximum log$K$ values determined by titration of model systems

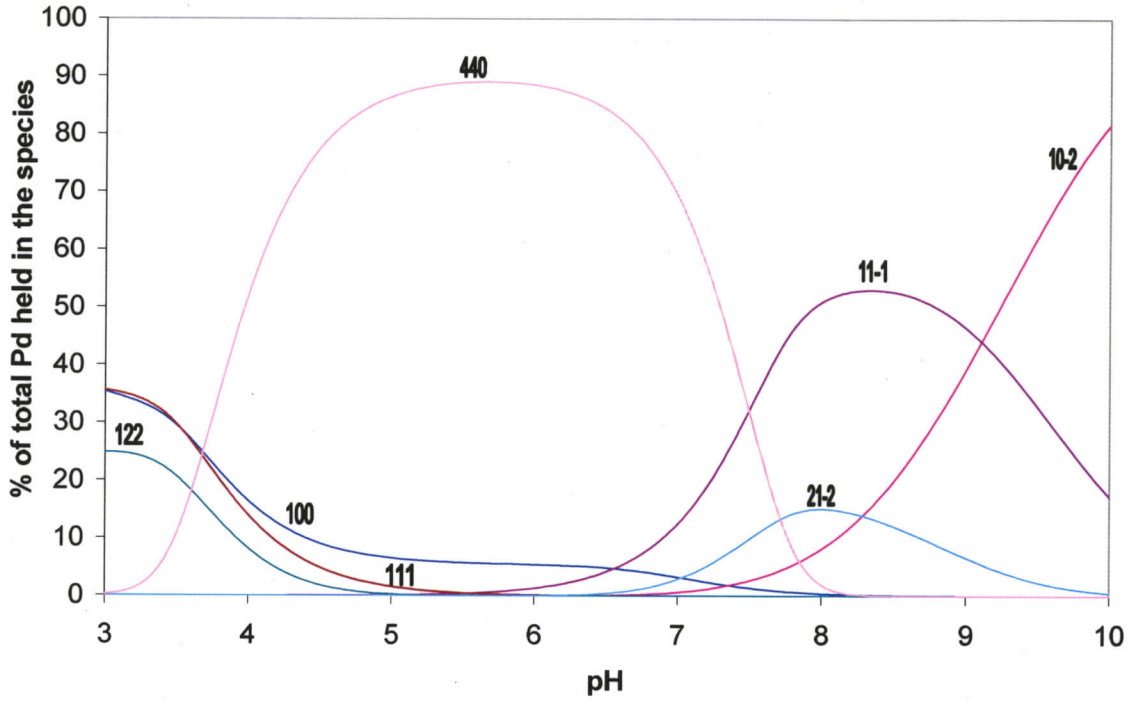

Figure 28 Speciation for Pden:bipy = 1:1 and [Pd] = 1 x 10^{-5} M calculated using logβ values estimated from maximum log$K$ values determined by titration of model systems

The % of total Pd held in the more complex species increases in Figure 27 at the expense of simpler species like **100** and **111** although the dominant species Figure 25 and Figure 27 remain the same over the pH range modelled. The same is true for comparisons between Figure 26 and Figure 28. A small change in the Pden:bipy ratio from 1:1 to 1:4 has an obvious effect on the speciation which is apparent by comparing Figure 25 and Figure 27. A large shift in the speciation is also observed when Figure 27 and Figure 28 are compared. If the results summarized by Figure 25 through Figure 28 are considered within the context of the objective in this chapter, the impact of small differences in estimated log$K$ values is minor compared to other factors such as Pden:bipy ratio and pH.

2.7 Conclusions

The results of this chapter are based on a general approach for the determination of solution speciation. The method was used to model a solution that contained Pden and bipy. This work explores the effect of pH and Pden:bipy ratio on the speciation and identifies the conditions that would be most favourable for the formation of **440**. The solution was simulated based on estimated values of $\log\beta_{pbh}$ for the species in the solution.

Stepwise formation constants used to calculate $\log\beta'_{pbh}$ were estimated using model systems that approximate the interactions between Pden+bipy, (Pden)(bipy)+bipy, (Pden)(bipy)+OH, (Pden)(bipy)+H and (Pden)(bipy)+Pden. Values for $\log K_{m1}$, $\log K_{m2}$, $\log K_{mb}$, $\log K_{mH}$ and $\log K_{mOH}$ were determined by potentiometric titration. Values for $\log\beta'_{pbh}$ were corrected by a symmetry factor to give $\log\beta_{pbh}$. Additional species corresponding to the monometallic species, free Pden and free bipy were also added to complete the model. The final model included 56 species. The speciation as a function of pH and Pden:bipy molar ratio was determined. This data was used to make a contour plot which showed that **110** and **440** and, **210** and **100** were in direct equilibrium. The equilibrium constants between these pairs were calculated from concentrations computed from the model. The results from the speciation model revealed that the maximum amount of the square is obtained between pH = 4-7 and at Pden:bipy ratios of 0.4-6.

The component species in equilibrium with a product can be identified by deconstructing the product in a stepwise fashion such that each equilibrium represents a possible pathway towards a particular product. Multiple pathways are possible for product species which consists of more than 3 synthons.

Consider the product species **440** which consists of eight synthons, 4 bipy and 4 Pden. There are six penultimate stepwise equilibria that contribute to the formation of **440** (Table 7). The change in free energy ($\Delta\Delta G$) can be calculated by (2-38). The greatest change in free energy is -61 kJ/mol, observed for the equilibrium in entry 3, Table 7. The average value for $\Delta\Delta G$ is -58 kJ/mol. The difference in $\Delta\Delta G$ between any two equilibria that contribute to the formation of **440** is no greater than ~5 kJ/mol which is about the amount of energy that is required for a C-C bond rotation at room temperature. The similarity in the values for $\Delta\Delta G$ illustrate that the energetic differences between the starting components in **440** is small. Therefore, the solution at equilibrium consists of a relatively flat energy landscape with a deeper well for **440**.

Table 7 Summary of the stepwise equilibrium constants and the changes in free energy observed for equilibria that contribute to the formation of 440

Entry	Equilibrium	ΔΔG at 298.15K, kJ/mol	Relative rates
1	**110+330 ⇆ 440**	-56	40
2	2 * **220 ⇆ 440**	-56	50
3	**010+430 ⇆ 440**	-61	1
4	**100+340 ⇆ 440**	-56	1
5	**210+230 ⇆ 440**	-60	10
6	**120+320 ⇆ 440**	-60	13

$$\Delta\Delta G = -RT \ln \beta(\textbf{product}) + RT \ln \beta(\textbf{reactant}) \qquad \textbf{(2-38)}$$

The Hammond postulate states[90]:

> *If two states, as for example a transition state and an unstable intermediate, occur consecutively during a reaction process and have nearly the same energy content, their interconversion will only involve a small reorganisation of molecular structure.*

The postulate infers that the energy of the transition state is similar to the reactants in an equilibrium process. If this postulate is applied to a set of equilibria in which the energy of the starting components are similar, such as the

equilibria which describe the formation of **440**, then it can be assumed that the energies of the transition states will also be similar. This implies that the activation energies, E_a, will be comparable for equilibria that have energetically similar reagents and transition states. The activation energy is related to the rate constant, k, by the Arrhenius equation:

$$\ln k = \ln A - E_a/RT$$

where, A is the Arrhenius factor, E_a is the activation energy, R is the gas constant and T is the temperature.

For the equilibria which contribute to the formation of **440**, the rate of the forward reaction is generalized as

$$\text{Rate} = k[\mathbf{pbh}]_1[\mathbf{pbh}]_2 \qquad \textbf{(2-39)}$$

where, k is the rate constant, and $[\mathbf{pbh}]_1$ and $[\mathbf{pbh}]_2$ are concentration of the starting species. Because E_a are similar for all the equilibria, then k will also be similar. This means that pathways which include species with low concentrations will proceed slowly relative to pathways in which the reactive components are more abundant. Thus, low concentrations of the starting species present a kinetic barrier to the formation of **440**. Equilibria with **440** will be dominated by the kinetic factors because the differences in $\Delta\Delta G$ between stepwise reaction pathways are small.

The concentrations for the species in equilibrium with **440** are computed from the model at a total Pd concentration of 1×10^{-5} M, Pden:bipy = 1:1 and pH = 7. These values are used to calculate the relative rates of the forward reactions (*i.e.* formation of **440**) for the equilibria in Table 7. Entries 1 and 2 in Table 7 have rates that are 40 and 50 times faster than equilibria in entries 3 and 4 and 10 and 13 times faster than the equilibria in entries 5 and 6. Therefore the major species

that contribute to the formation of **440** are **220** and **110** and **330**. This method of analysis can be extended to the rest of the species in equilibrium assuming that the energetic differences between the starting species are always small.

2.8 Experimental procedures used for titrations

2.8.1 Preparation of stock solutions

All reagents were obtained from commercial sources and were used without further purification unless noted otherwise. All solutions were prepared with boiled Millipore water. Concentration is used in place of activity throughout the titration experiments and modeling calculations.

All synthesis in this thesis were carried out using commercially sourced reagents were used without purification. Dry solvents were obtained from commercial sources in bottles fitted with rubber septa. ^{1}H and ^{13}C NMR spectra were recorded on a Bruker AMX-300 MHz instrument. FT-IR spectra were recorded on a Perkin-Elmer Spectrum One FT-IR spectrometer. Elemental analysis was performed by Canadian Microanalytical Services Ltd, Delta, BC, Canada. Mass spectra were obtained on a Finnigan 3300 or a Kratos Concept H instrument using either fast atom bombardment or electron ionization.

The titrations were carried out using a Mettler DL21 automatic titrimeter. The operation of the titrimeter and data collection was managed using a Microsoft Excel macro. The sample solutions were added to a closed jacketed glass cell kept at 25 ± 0.2 °C, under a nitrogen atmosphere and fitted with a magnetic stir bar. The electrode circuit was set up as follows: Ag/AgCl|4M KCl|0.1 M KNO_3 or

0.1 M $NaClO_4$ (the electrolyte was chosen to match test solution) | glass frit | | test solution | | proton selective glass electrode.

Stock solutions of $NaClO_4$, KNO_3, HNO_3, $HClO_4$, NaOH, bipy, py, 3ppy, and 4ppy were prepared using boiled and cooled water in volumetric glassware. $NaClO_4$ or $NaNO_3$ was added to the NaOH solution as an electrolyte such that the final concentration of electrolyte was 0.1 M. Standardized 0.2 M acid (in either HNO_3 or $HClO_4$) was added using a microlitre syringe to protonate all the basic sites in the bipy and pyR (R = 3-phenyl, 4-phenyl or H) solutions. NaOH was standardized using potassium hydrogen phthalate which was then used to standardize the HNO_3 and $HClO_4$ solutions.

Procedure used to prepare stock solutions of $Pden(NO_3)_2$

$PdenCl_2$ and $Pden(NO_3)_2$ was prepared and characterized according to a published procedure[91]. To prepare the $Pden(NO_3)_2$ stock solution, $PdenCl_2$ (0.1487 g, 0.6277 mmol) was suspended in ~2ml water in a test tube fitted with a magnetic stir bar. To the suspension was added 0.4991 M $AgNO_3$ (2.50 ml) while stirring. A white solid precipitated immediately. The mixture was left to stir for at least 4 hours then vacuum filtered to recover a lemon yellow solution. The solution was transferred quantitatively through a 0.45 µm syringe filter and diluted in a 25ml volumetric flask with water.

Procedure used to prepare stock solutions of $Pddien(ClO_4)_2$

$PddienBr_2$ was prepared and characterized according to a published procedure[92-94] (^1H NMR (D_2O): δ 2.46-3.09(m) ppm. MS (FAB) m/z: 207.9 [53%], 245 [100%]). To prepare the $Pddien(ClO_4)_2$ stock solution, $PddienBr_2$ (0.2570 g, 0.5837 mmol) was dissolved in ~2ml water in a test tube outfitted with a magnetic stir bar. To

the yellow solution was added $AgClO_4$ (0.2631 g, 1.167 mmol) dissolved in ~1ml water while stirring. A white solid precipitated immediately. The mixture was left to stir for at least 6 hours at 40°C then vacuum filtered to recover a light yellow solution. The solution was transferred quantitatively through a 0.45 µm syringe filter into a 25 ml volumetric flask. The solution was diluted to the mark with water. $Pddien(ClO_4)_2$ cannot be made from the chloride derivative because the metathesis with $AgClO_4$ was not complete.

Synthesis of $PdaapCl_2$

The synthesis of $PdaapCl_2$ proceeded according to the following synthetic scheme:

Scheme 1 Synthesis of $PdaapCl_2$

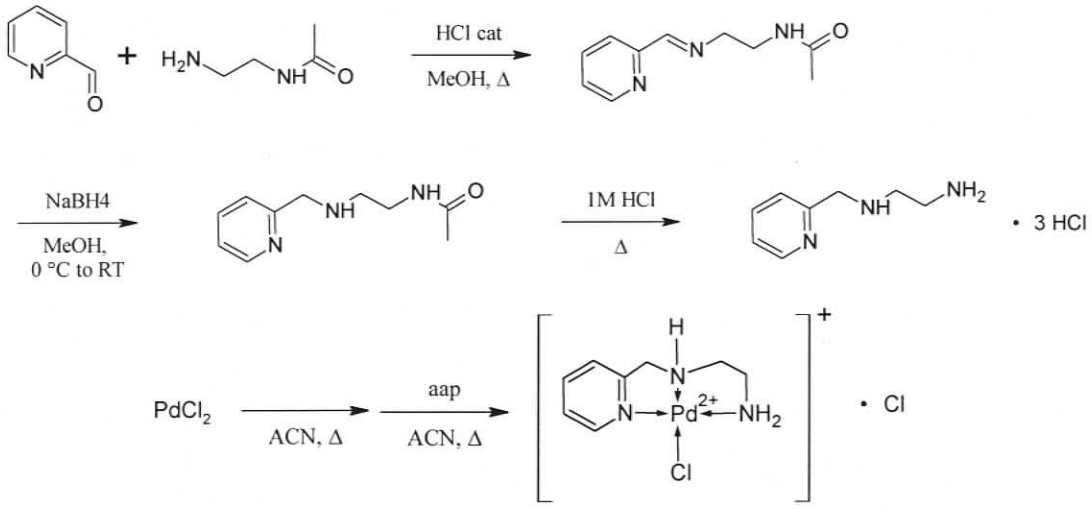

To a round bottom flask fitted with a magnetic stir bar was added pyridine-2-carbaldehyde (2.5 ml, 26.3 mmol, 1.08), N-(2-amino ethyl)-acetamide (2.489g, 24.4 mmol, 1 eq), HCl (3 drops) and MeOH (50 ml). The mixture was heated to reflux for 3 hours then cooled to 0 °C. To the cooled solutions was added $NaBH_4$ (1.077g, 29.1 mmol, 1.04 eq) in two aliquots. The solution was allowed to stir for 30 min at 0 °C then warmed to room temperature and allowed to stir for another

1.5 hours. The solvent was removed to isolate orange oil. This material was dissolved in water (25 ml) and acidified with ~6 M HCl (20 ml) to resulting solution was brown-black in color. A second aliquot of HCl (1M, 25 ml) was added and the solution was heated to reflux for 2 days. The reaction was cooled to room temperature and made basic by adding NaOH (7g) dissolved in water (40 ml). The final pH of the reaction mixture was ~ 12. The solvent was removed to recover viscous brown oil which separated into white solid and brown supernatant after adding MeOH. The solvent was removed from the brown supernatant to recover brown oil which was dissolved in i-PrOH (75 ml). The solution was cooled in an ice bath while concentrated HCl was added dropwise until the pH ~ 5. A beige precipitate was recovered from the acidified solution and purified by suspending the solid in 4% v/v HCl and warming the mixture to 50 °C. The purified solid was beige. The overall yield was 17%. Although app is a known compound, the procedure described is a new synthetic route[95-98]. The salt was transformed to the free base by stirring the solid with K_2CO_3 in $CHCl_3$. (^{1}H NMR (D_2O): δ3.32(s, 0.3 H), 3.45(t, 2H, J = 7 Hz), 3.62(t, 2H, J = 7 Hz), 4.76(s, 2H), 8.05-8.10(m, 1H), 8.19(d, 1H, J = 8 Hz), 8.61(dt, 1H, J = 1.4, 8 Hz) , 8.85(d, 1H, J = 3 Hz) ppm. ^{13}C NMR(D_2O): δ 35.6, 44.9, 47.8, 128.2, 128.4, 143.6, 144.3, 147.7 ppm. FT-IR (KBr): 3436 (s, br), 3048 (sh, m), 2757 (sh, m), 1628 (m), 762 (s), 744 (m) cm^{-1}. Anal Calc for $C_8H_{16}N_3Cl_3$: C, 36.9; H, 6.19.; N, 16.1. Found: C, 36.20; H, 6.23; N, 16.15.

$PdCl_2$ (0.265g, 1.5 mmol, 1 eq) was heated in ACN (10 ml) until a deep red-orange solution was formed. A solution of app (0.251 g, 1.66 mmol, 1.1 eq) in ACN (5 ml) with a few drops of water is added drop wise to the hot filtrate while stirring. A yellow precipitate was formed. The mixture was heated at reflux for 5-10 min after the addition of app solution was complete. The solid was recovered and recrystallized in ACN and water. An orange microcrystalline solid was recovered in 27% yield. (^{1}H NMR (D_2O): δ2.78-3.05(m, 1H), 3.08-3.26(m, 2H),

4.08(d, 1H, J = 16 Hz), 4.58(d, 1H, J = 16 Hz), 7.25-7.41(m, 2H), 7.87(m, 1H), 8.23(d, 1H, J = 6 Hz) ppm. ^{13}C NMR(D_2O): δ 49.7, 54.9, 57.9, 107.1, 122.3, 124.7, 140.9, 149.4, 164.8 ppm. MS (FAB) m/z: 255.9 [35%], 293.9 [100%].

Procedure used to prepare stock solutions of Pdaap(ClO_4)$_2$

To prepare the Pdaap(ClO_4)$_2$ stock solution, $PdaapCl_2$ (0.1918 g, 0.5837 mmol) was dissolved in ~2ml water in a test tube fitted with a magnetic stir bar. To the yellow solution was added $AgClO_4$ (0.2631 g, 1.167 mmol) dissolved in ~1ml water while stirring. A white solid precipitated immediately. The mixture was left to stir for at least 6 hours at 40°C then vacuum filtered to recover a light yellow solution. The solution was transferred quantitatively through a 0.45 µm syringe filter into a 25 ml volumetric flask. The solution was diluted to the mark with water.

Calibration of the electrodes

The electrodes were calibrated daily by adding 100ul of ~0.1M standardized HNO_3 or $HClO_4$ measured using a microlitre syringe and 4 ml of electrolyte (either 0.1M KNO_3 or 0.1M $NaClO_4$) into the cell. The calibration titration was performed by adding 5ul aliquots every 10 seconds. A simple calculation will convert the volume of base added into the concentration of H^+ in the cell after each addition which was plotted against the electrode potential observed. The data was treated by removing the 3 or 4 data points nearest the endpoint and fitting the curve using a linear least squares method. The line obtained can be correlated to a modified form of the Nernst equation ($E = E^0 + f(RT/F)(\log [H^+])$. The intercept determines the standard electrode potential, E^0, and the slope determines the slope factor, f. These terms are used to standardize the data obtained for the test solutions. Records of E_0 and f were kept for the over the

duration of the experiments to monitor the quality of the performance of the electrodes and ensure that the data obtained was reliable.

Preparation of sample solutions

Sample solutions were prepared from stock solutions in 10 ml volumetric flasks. Stock solutions were measured using microlitre syringes for volumes less than 1ml and volumetric pipettes for volumes more than 1 ml. In order to ensure that all basic sites were protonated, 100 µl of standardized 0.2 M acid was added to the solutions. Solutions with at least three different Pden to pyR (or Pddien to bipy) molar ratios were prepared and titrated for each model system. Each titration was usually carried out in duplicate with at least 52 points per titration curve. At least 15 of these points were useful in determining the unknown logβ values. Standardized NaOH was added in 2 or 5 µl aliquots every 5, 10 or 20 seconds. Variation in the volume of the aliquots added and time intervals did not seem to make a difference in the titration curve obtained for Pden titrations. This implies that equilibrium was reached quickly in these systems. The titrant was added in 20 seconds for the Pddien species because survey titrations showed that the kinetics were a bit slower, so that a longer time interval was needed between additions in order to reach equilibrium.

Fitting titration curves to determine the logβ

The titration curves from each model system were fitted using the program HyperQuad which simulates a curve using logβ for the species predicted to be in the solution. Because the model systems were simple, the species in solution are easily predicted and the logβ corresponding to a particular species can be determined from previous experiments or literature[76, 83]. Only the species that

were required to fit the experimental data were included to calculate the curve. The unknown logβ values were allowed to vary until the calculated curve fitted the experimental data with greater than 95% confidence. The differences between appropriate logβ values determined from curve fitting were used to determine log$K$ for the model equilibria. The error in log$K$ determined for a single species in equilibrium with H^+ was ± 0.04. The error in log$K$ calculated for equilibria involving more than one species was ±0.15.

3 Syntheses of lipophilic 1, 2-diaminoethane palladium complexes

3.1 Introduction

The merits of the proposed ion channel design, **14**, were discussed in the Chapter 1. The following chapter will focus on the synthesis of the palladium complexes of 1,2-diamino-3-(decanoxy)propane, **15a**, and 1,2-diamino-3-(hexadecanoxy)propane, **15b**, which are synthons used to form the corners of **14**.

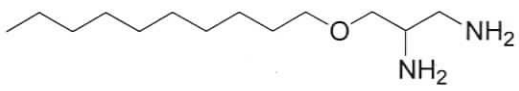

15a

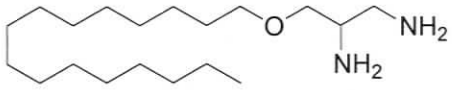

15b

3.2 Synthesis of ligands 15a and 15b

The simplest way to make the square sufficiently lipophilic to partition into a bilayer was to derivatize the ethylenediamine moiety with long alkyl chains. Derivatives with 10 and 16 carbon alkyl chains were synthesized according to the procedure outlined in Scheme 2.

Scheme 2 Synthesis of 15

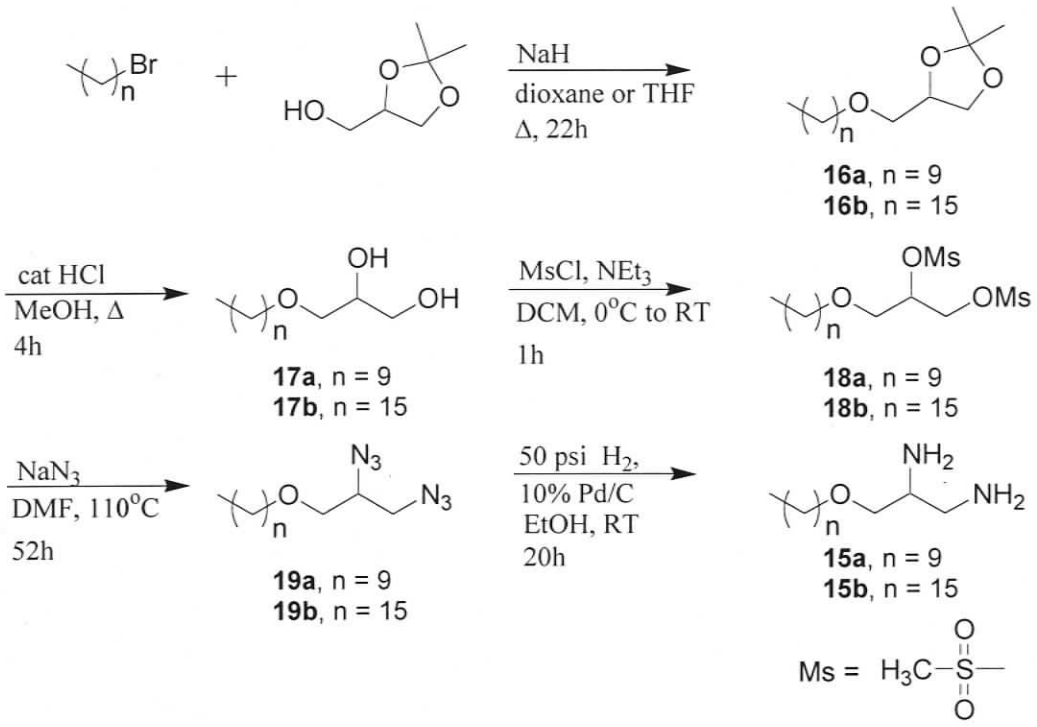

Starting from the protected glycerol solketal, the primary alcohol was transformed into decyl or hexadecyl ethers by way of a Williamson ether reaction. The decyl derivative, **16a**, was made by reacting solketal with 1-bromodecane and the hexadecyl derivative, **16b**, was made by reacting solketal with 1-bromohexadecane. Although the synthesis may be carried out in dry tetrahydrofuran, greater yields are obtained with 1,4-dioxane as the solvent. For **16a** the yield after purification was improved from 41% to 69% when the solvent was changed from THF to 1,4-dioxane. The yield after purification for **16b** was 66% when 1,4-dioxane was used.

The diol was obtained after heating **16a** and **16b** in MeOH at reflux for 4h with catalytic amounts of concentrated hydrochloric acid and water. Because the solketal used was racemic, products in this reaction sequence will be a mixture of stereoisomers. The implications of this on the isomers of **14** will be discussed in a later section.

A molecular formula of $C_{19}H_{40}O_3$ for **17b** was supported by mass ion peak at m/z = 316 in the EI-MS and the purity of the compound was established by elemental analysis. A strong, broad band at 3369 cm^{-1} and a sharp band at 1123 cm^{-1} in the IR spectrum confirmed the presence of alcohol and aliphatic ether groups, respectively.

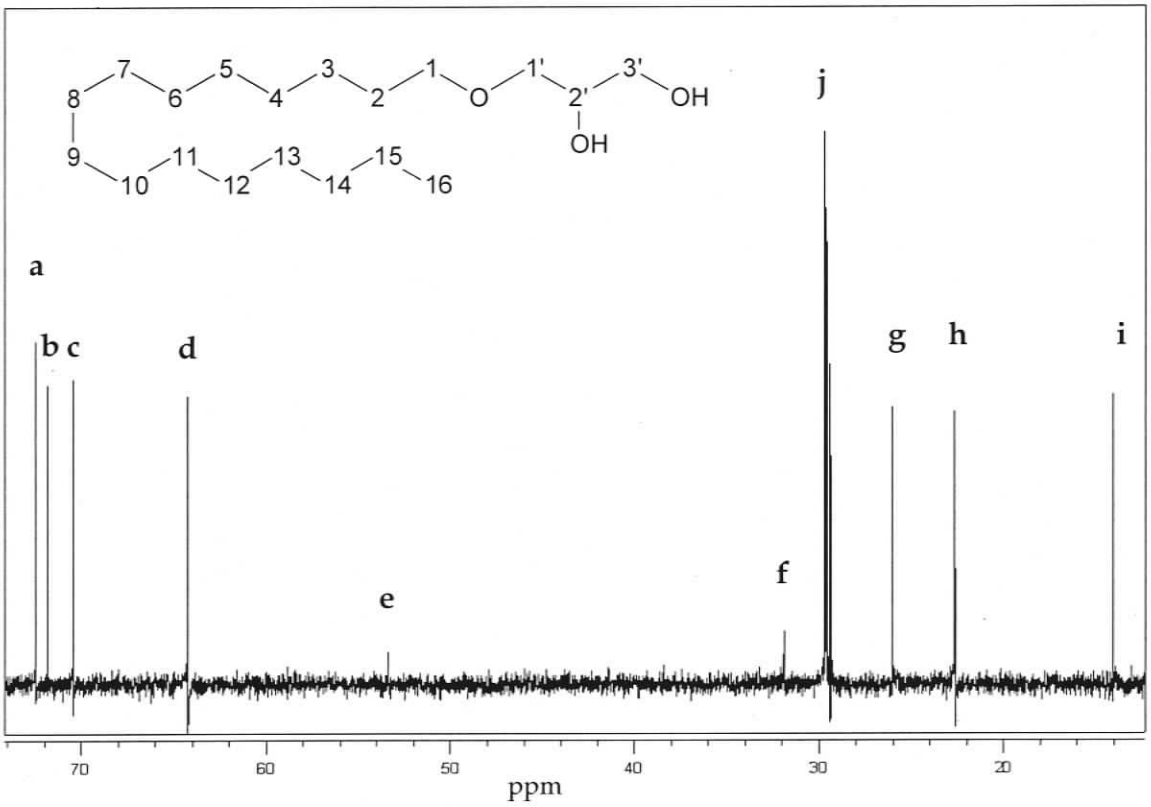

Figure 29 ^{13}C NMR spectrum for 17b in $CDCl_3$

Peaks a and b in the ^{13}C NMR spectrum (Figure 29) have chemical shifts consistent with aliphatic carbons adjacent to ether groups, C-1' and C-1. The chemical shifts of peaks c and d are assigned to C-2' and C-3', respectively, by DEPT-45. Peaks g, h, i and j confirm the presence of an aliphatic alkyl chain. The CH_2Br peak for 1-bromohexadecane and methyl peaks corresponding to the ketal were lost in the ^1H NMR spectrum of **17b** (Figure 30). The concurrent appearance of peaks A, B, C and D in the 3-4 ppm region of the ^1H NMR spectrum supports

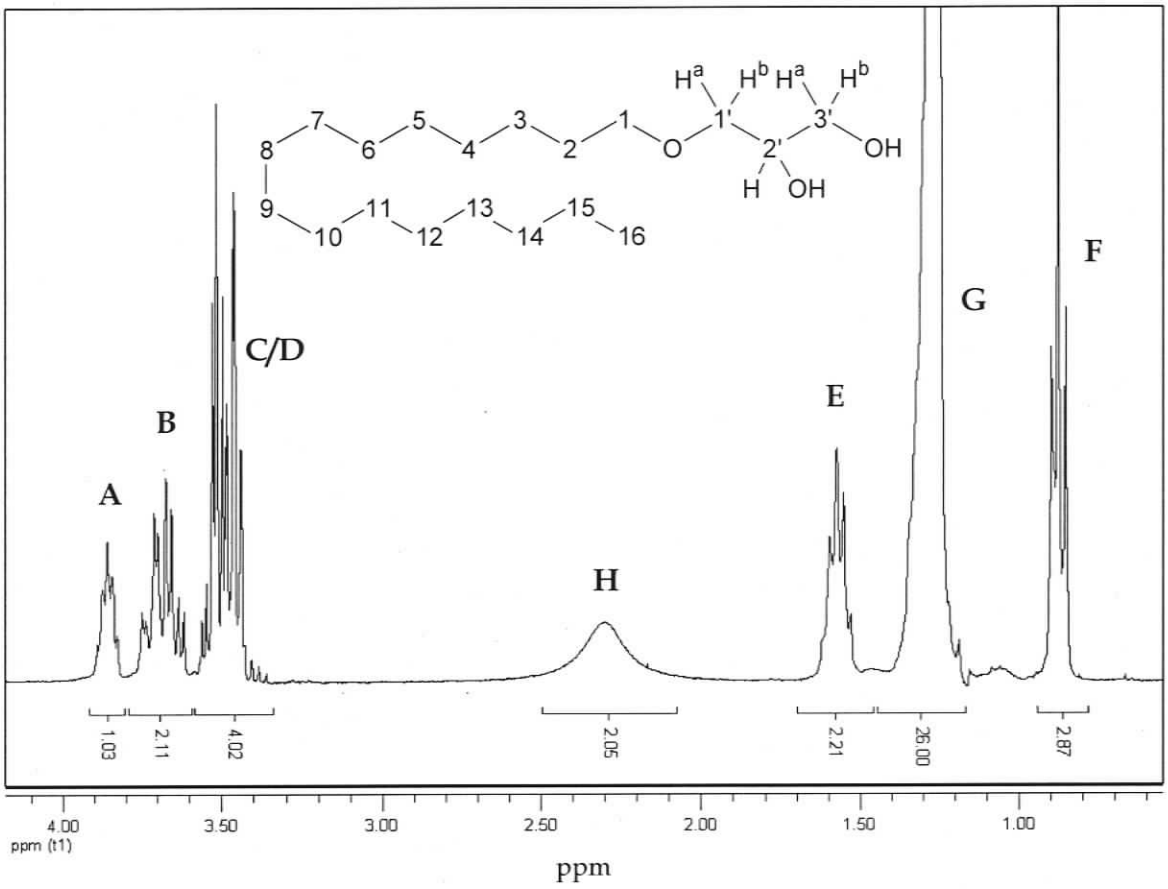

Figure 30 ^{1}H NMR spectrum for 17b in $CDCl_3$

the formation of ether and/or alcohols. Peaks C/D could not be resolved in the ^{1}H NMR spectrum, but have been assigned to H-1, H-1'a and H-1'b on the basis of their chemical shift values and their correlation to Peaks A and E in the COSY (Appendix 3). The integration for peaks C/D is 4H, which is consistent with this assignment. Peak B integrates to two protons and is correlated only to Peak A in the COSY, therefore it was assigned as H-3'a and H-3'b. Peak A is assigned to H-2' because it was correlated to peaks B and C/D in the COSY spectrum and because it integrates to 1 proton. Peak E is assigned to H-2 on the basis of its correlation with the methylene peak G in the COSY spectrum, its chemical shift, integration and multiplicity in the proton spectrum. Peak D was assigned to H-1 because it was correlated to peak D in the COSY spectrum and had a chemical shift consistent with CH_2OR. Peak G and F integrate to 26H and 3H, respectively.

Peak G has a chemical shift and multiple resonance patterns consistent with aliphatic methylene protons and is assigned to H-3 to 15. Peak F has a chemical shift and multiplicity consistent with H-16. All the preceding spectroscopic data is consistent with the structure for **17b**.

The diol group in **17b** was transformed into the *bis*-methanesulfonyl derivative in order to facilitate its substitution by NaN_3. The transformation was carried out by reacting **17b** with MsCl at 0°C in DCM containing triethylamine. The reaction mixture was quenched with water and washed with aqueous $NaHCO_3$ and HCl to remove NEt_3 and unreacted MsCl. The product, **18b**, was isolated from the organic phase by solvent evaporation. Sodium azide was reacted with **18b**, without purification, at 110°C for 52h in DMF. Normally, the azide ion is an extremely efficient nucleophile; however, more forcing conditions and longer reaction times than usual were necessary in order to achieve acceptable yields. This may be attributed to the steric congestion around the reaction sites. The reaction mixture was extracted with diethyl ether and water and the organic fraction was dried with $MgSO_4$. The ether solution was concentrated and used in the subsequent step without any further manipulation. Complete removal of the ether yielded yellowish oil. Amounts greater than ~50 mg were never isolated for **19b** due to the potential explosion hazard associated with azides[99].

A solution of **19b** in ether was diluted with ethanol and hydrogenated at 50 psi in the presence of Pd/C for 20h. A white solid, **15b**, was isolated as the product after removing the solvent and could be used without purification. The product was characterized by EI-MS, ^1H and ^{13}C NMR spectrometry and IR spectrometry. The peak at m/z = 313 was observed in the EI-MS was consistent with the [**15b** - H] ion for **15b**. Although a peak for the molecular ion was not observed, fragments consistent with **15b**, such as [**15b** – $CH_2NH_2]^+$, $[CHCH_2NH_2]^+$, and $(CHNH_2)CH_2NH_2]^+$ are observed by EI-MS.

A peak at 1123 cm^{-1} which is coincident with the peak assigned to the ether group in **17b** was observed in the IR spectrum for **15b**. A broad peak at 3369 cm^{-1} previously assigned to the alcohol groups in **17b** disappeared while new peaks, consistent with amine groups, at 3361 and 3301 cm^{-1} appeared. Additional evidence of the presence of amine groups is given by the peak observed at 1645 cm^{-1}, which is consistent with NH_2 scissoring.

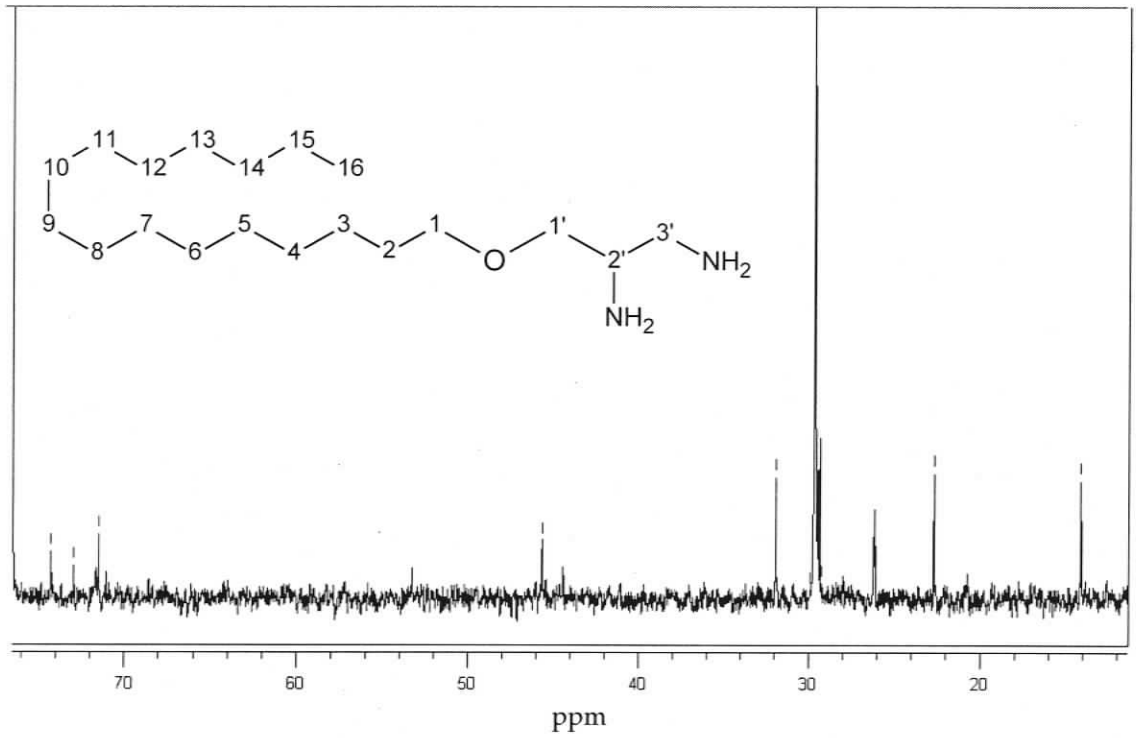

Figure 31 ^{13}C NMR spectrum for 15b in $CDCl_3$

Five peaks in the ^{13}C NMR spectrum for **15b** (Figure 31) appear at the same chemical shifts as peaks assigned to C-2 to C-15 in **17b**, confirming the presence of an aliphatic moiety in **15b**. Peaks at 72.7 and 72.1 ppm assigned to C-1 and C-1′ in **17b** have shifted slightly to 74.5 and 71.7 ppm in **15b**. These chemical shifts are still within the expected range for methylene units adjacent to aliphatic ethers. Peaks at 70.8 and 64.5 ppm previously assigned to C-2′ and C-3′ in **17b**

are shifted to 45.6 and 44.4 ppm in **15b**, as expected for the transformation of a diol to a diamine.

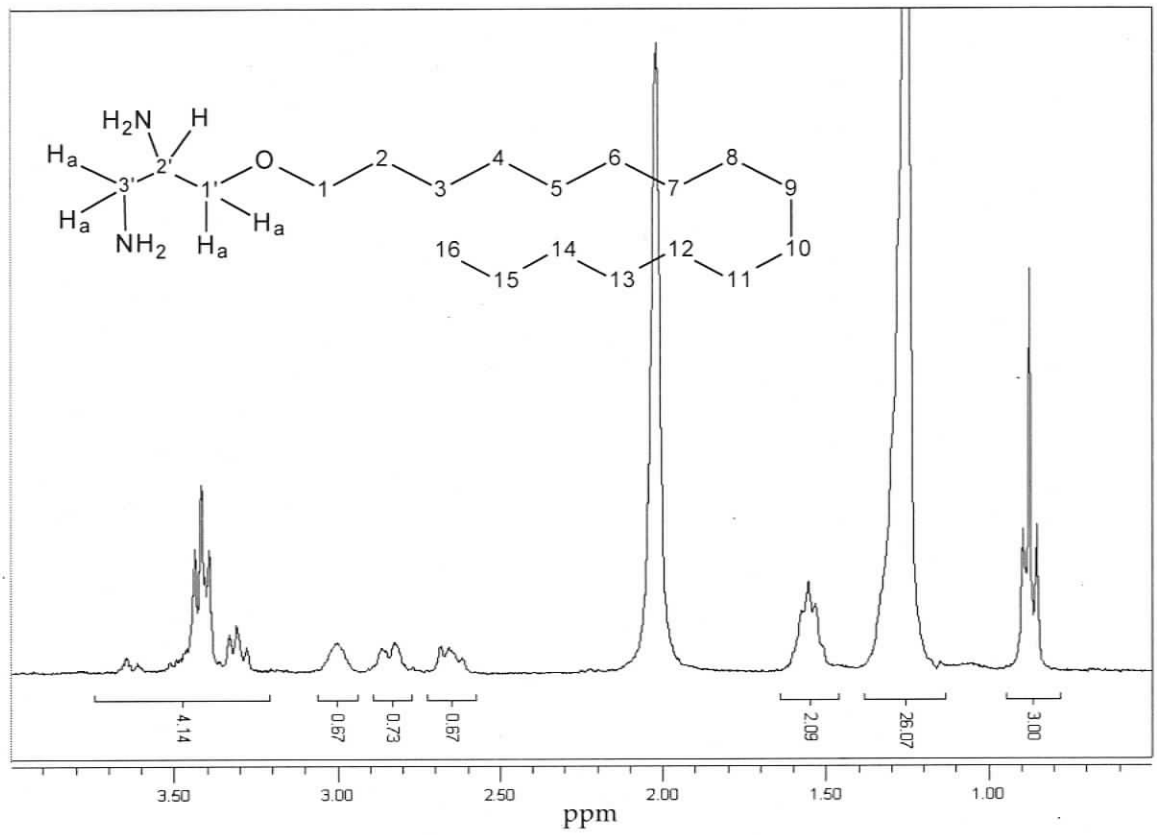

Figure 32 ^{1}H NMR spectrum for 15b in $CDCl_3$

Peaks at 0.88, 1.25 and 1.55 ppm in ^{1}H NMR spectrum for **15b** integrate to 3H, 26H and 2H, respectively (Figure 32). These chemical shifts and integrations support a structure with a 16 carbon alkyl ether group. The peak at 3.41 ppm is assigned to H-1 in **15b** using the COSY spectrum. The peak at 3.30 ppm is assigned to H-1' in **15b** on the basis of chemical shift. The two peaks at 3.41 and 3.30 ppm integrates to a total of 4H, which is consistent with the assignments. Peaks at 2.66 and 3.00 ppm integrate to 1H each and are assigned to H-3'a and H-3'b using the COSY spectrum and chemical shifts. The peak at 2.84 ppm integrates to 1H and is assigned to H-2' in **15b**.

Compound **15a**, which is an analog of **15b**, was prepared according to Scheme 2 in 40 % yield over 5 steps. The compounds **15a** and **15b**, and their precursors **17a** and **17b**, are structurally similar in every respect except for the number of methylene units in the alkyl chain. Therefore, the NMR and IR spectra can be assigned by comparison.

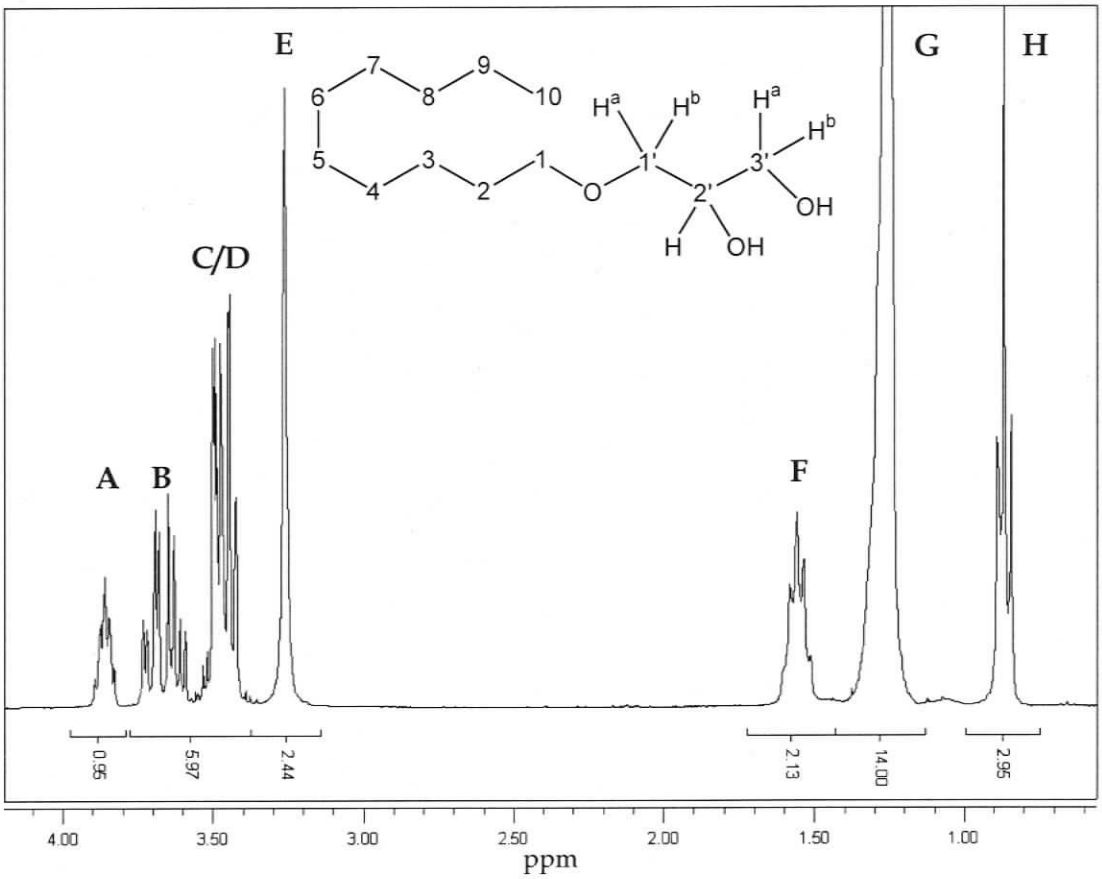

Figure 33 ^{1}H NMR spectrum for 17a in $CDCl_3$

The high resolution mass spectrum of **15a** shows a peak at m/z = 255.1930 which is consistent with the ion [**17a**+Na]$^+$ and the low resolution EI-MS spectrum shows a peak at m/z = 232 which is consistent with the molecular ion. The IR spectrum for **17a** shows peaks at 3390 cm^{-1} and 1124 cm^{-1} which are consistent with the alcohol and ether stretches observed in the IR spectrum for **17b**, respectively. The ^{1}H NMR spectrum for **17a** (Figure 33) and **17b** are expected to have similar chemical shifts and splitting patterns but differ in the relative

integration. Peaks A and B in Figure 33 are assigned to H-2′ and H-3′ in **17a** by comparing the chemical shift and integration to the assigned spectrum for **17b**. The peaks C/D for **17a** have a splitting pattern, integration and chemical shift similar to peaks C/D in Figure 30 and so are assigned to H-1′ and H-1 by comparison. The peaks F, G and H are assigned to H-2, H-3 to H-15 and H-16, respectively, by comparison to Figure 30. The chemical shifts of the 9 peaks observed in the ^{13}C NMR spectrum of **17a** (Figure 34) match the peaks observed in the ^{13}C NMR spectrum for **17b** (Figure 29).

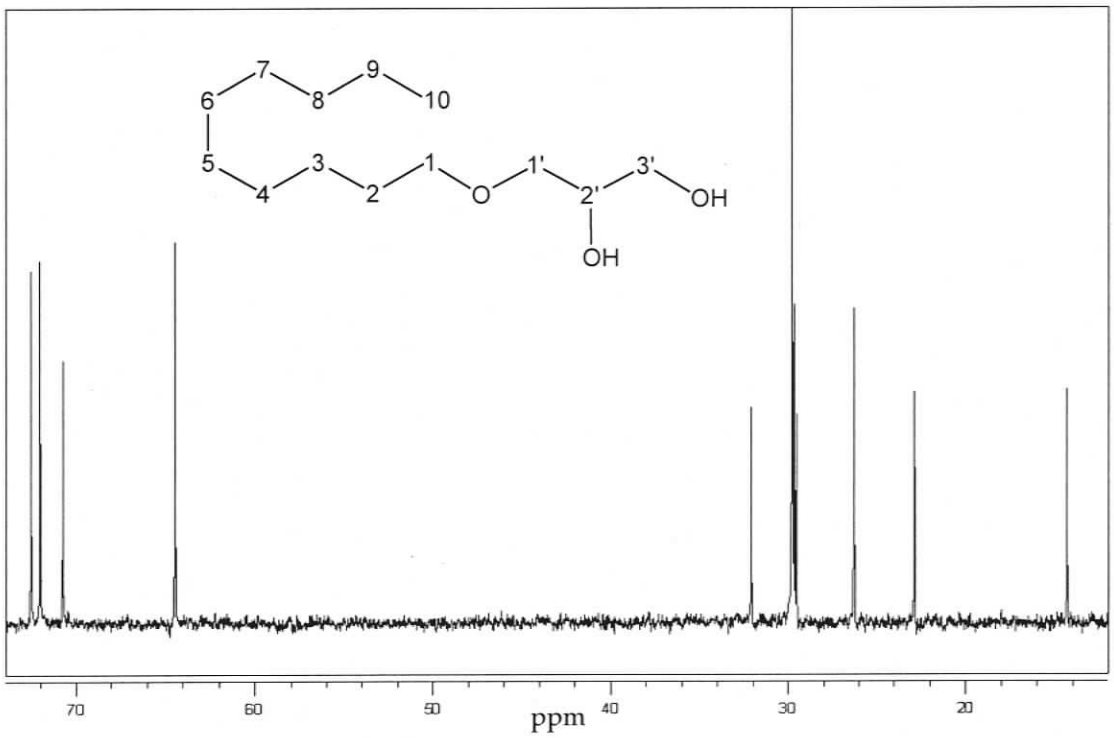

Figure 34 ^{13}C NMR spectrum for 17a in $CDCl_3$

Compound **15a** is prepared from **17a** in 63% yield. The high resolution mass spectrum for **15a** shows a peak at m/z = 231.2434 which is consistent with the chemical formula for the product. Peaks at 3360 and 3294 cm^{-1} in the IR spectrum for **15a** are consistent with the peaks assigned to the amine groups in **15b**. A peak at 1115 cm^{-1}, which supports the presence of an ether group, is also observed in the IR spectrum. Because the functional groups in **15a** and **15b** are

identical except for the length of the alky chain, the chemical shifts in the ^{13}C NMR spectrum and the chemical shifts and splitting patterns in the ^{1}H NMR spectrum should be the same. The ^{13}C NMR spectrum for **15a** supports the structure because it consists of nine peaks that have chemical shifts which match the chemical shifts observed in **15b**. The ^{1}H NMR spectrum for **15a** is similar to Figure 32 in chemical shift and splitting pattern and could be assigned by comparison. The relative integration in the ^{1}H NMR spectrum for **15a** between the peaks at 2.5 to 4 ppm and the aliphatic peaks was 11H to 19H which agrees with the proposed structure. ^{1}H and ^{13}C NMR spectra for these compounds are documented in the experimental section.

3.3 Synthesis of palladium complexes using ligands 15a and 15b

The compound $Pd(COD)Cl_2$ (COD = 1,5-cyclooctadiene) was reacted with **15b** in $CHCl_3$ at reflux to make **20b** in 47% yield (Scheme 3). Elemental analysis of the product was consistent with the theoretical composition of **20b** and the base peak at m/z=419 is consistent with the [**20b** – 2Cl]$^{+}$ fragment. A peak at 1123 cm^{-1} in the IR spectrum that previously was assigned to the ether group in **15b** is still evident. Peaks observed at 3193 and 3276 cm^{-1}, which are consistent with the amine groups, appear sharper in the palladium coordinated species than in **14b**, probably due to the loss of hydrogen bonding between the amine groups. Direct characterization of **20b** by NMR spectroscopy was not possible due to the poor solubility of the product.

Scheme 3 Synthesis of 21

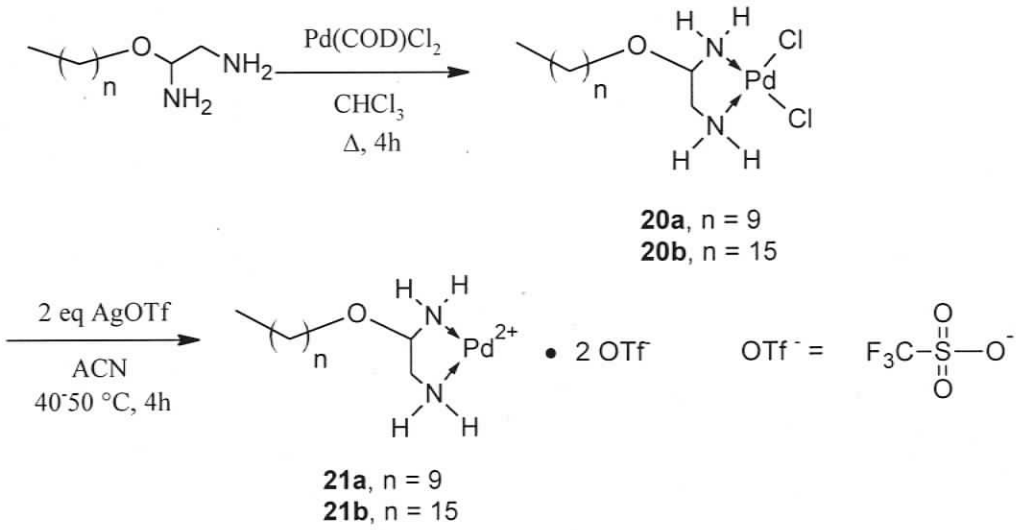

Metathesis of **20b** with 2 equivalents of AgOTf in d_3-ACN (Scheme 3) resulted in a soluble species that was characterized by NMR spectroscopy. A white precipitate corresponding to AgCl formed within minutes of adding AgOTf to a suspension of **20b** in d_3-ACN. The resulting product, **21b**, is the triflate salt of **20b**. The ^{1}H NMR spectrum of the **21b** solution (Figure 35) is similar to **15b** in that the peaks assigned to the aliphatic protons (H-2 to H-14) and the methylene protons adjacent to CH_2OR group (H-1 and H-1′) are still present and have retained their multiplicity and chemical shifts. The peaks assigned to H-2′ and H-3′ in **15b** shift downfield, as expected, for a ligand complexed to Pd. Unfortunately, **27b** was not soluble enough in d_3-ACN to obtain a good quality ^{13}C NMR spectrum. The procedure outlined in Scheme 3 was also used to synthesize **20a** and **21a**. Compounds **20a** and **21a** were identified by comparing the NMR, IR and MS spectra similar to **20b** and **21b**.

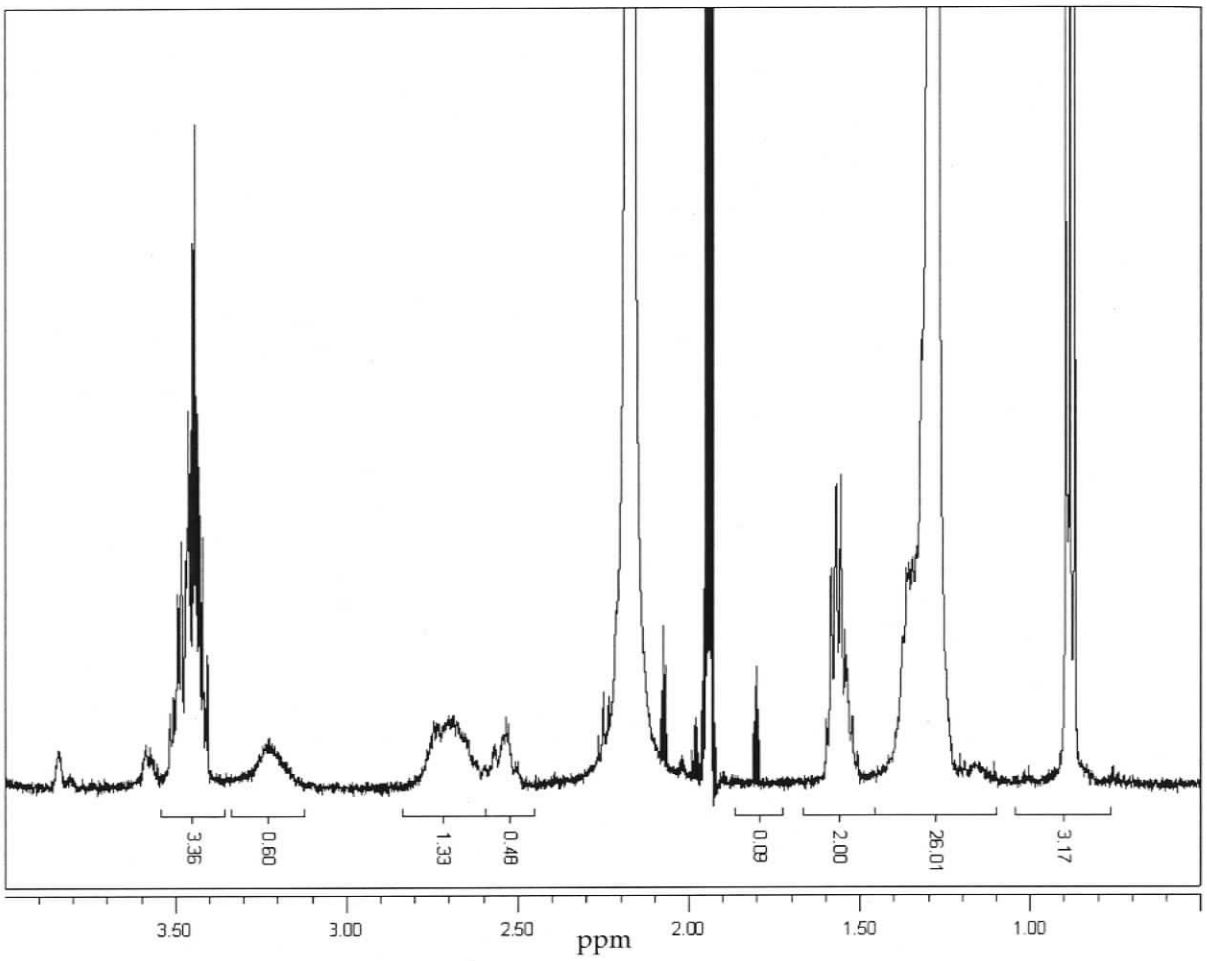

Figure 35 ^{1}H NMR spectrum for 21b in d_3-ACN

3.4 Synthesis of 14a and 14b

The ^{1}H NMR spectrum for **13** reported by Fujita consists of three main peaks at 8.64, 7.64 and 2.70 ppm[66]. The two peaks at 8.64 and 7.64 are assigned to protons on the bipy and the peak at 2.70 ppm is assigned to the protons on the en ligand. Similar chemical shifts and splitting patterns should be observed for **14a** and **14b**. Figure 36 shows the spectrum for a solution prepared by mixing **21b** with one equivalent of bipy in d_3-ACN at ~15 mM. This mixture is expected to react to form **14b**. Some precipitation occurred when bipy was added to the solution of **21b**. The ^{1}H NMR spectrum of the reaction mixture showed two peaks at 7.9 and

8.9 ppm (Figure 36) which is indicative of coordination with Pd. The chemical shifts observed for **14b** are slightly higher than the values reported for **13** probably due to differences in the solvent[66]. The chemical shifts and splitting patterns observed for peaks assigned to the alkyl chain and the methylene units adjacent to the ether group in **21b** are too far from the Pd to be affected by complexation with bipy so the chemical shifts and multiplicity of these protons in **14b** remain unchanged. Peaks assigned to H-2′ and H-3′ in **27b** shift to higher chemical shift, which may be rationalized by through space interaction with the bipy. Similar observations were made when **21a** was mixed with one equivalent of bipy in d_3-ACN at 10^{-1} to 10^{-2} M.

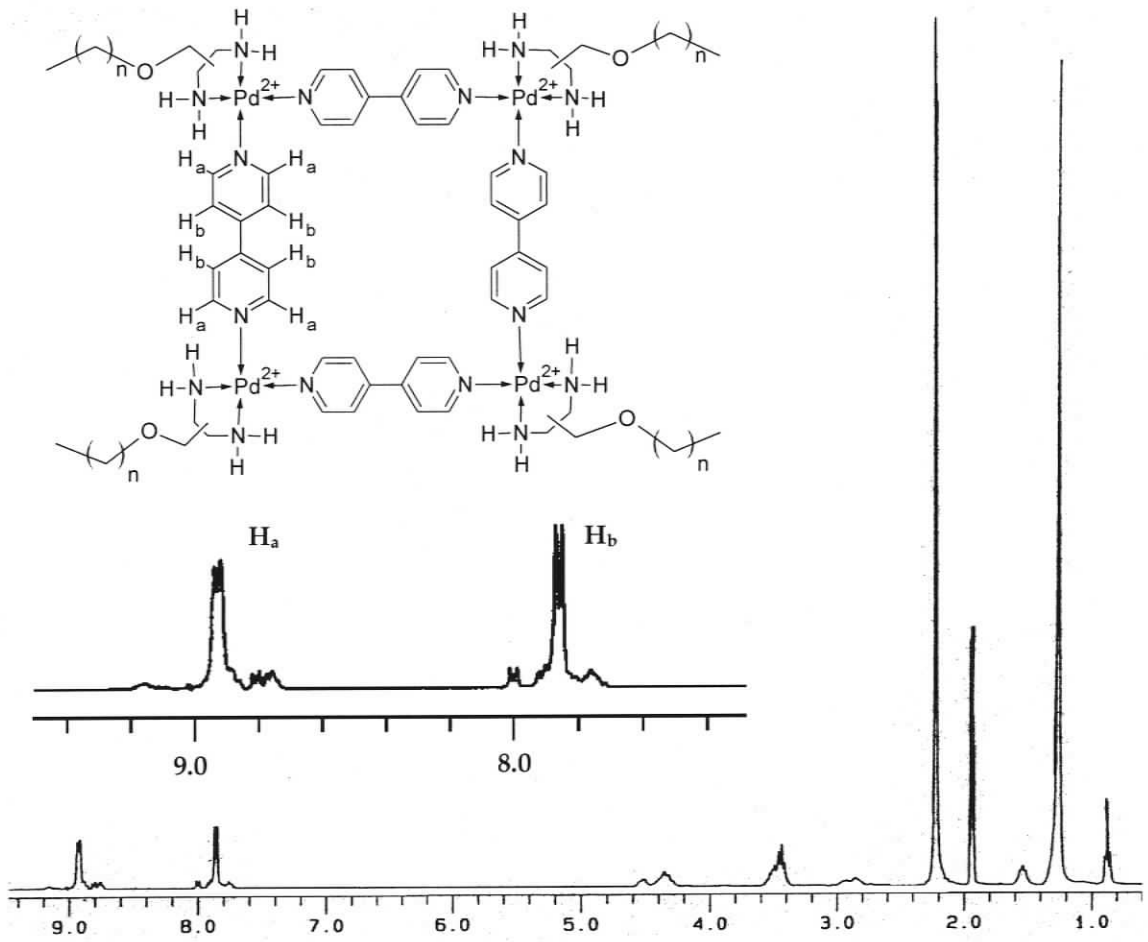

Figure 36 ^{1}H NMR spectrum of 14b in d_3-ACN

We view equilibrium self-assembly in a holistic fashion such that individual species must be considered within the context of the reaction mixture. If the ^1H NMR spectrum reported by Fujita is considered as a system then the spectrum should be interpreted as characteristic of a solution rather than a specific species. Each peak observed at a particular chemical shift represents the weighted average chemical shift for multiple species in fast exchange with respect to the NMR time scale. Species that are in slow exchange contribute to peaks with different chemical shifts.

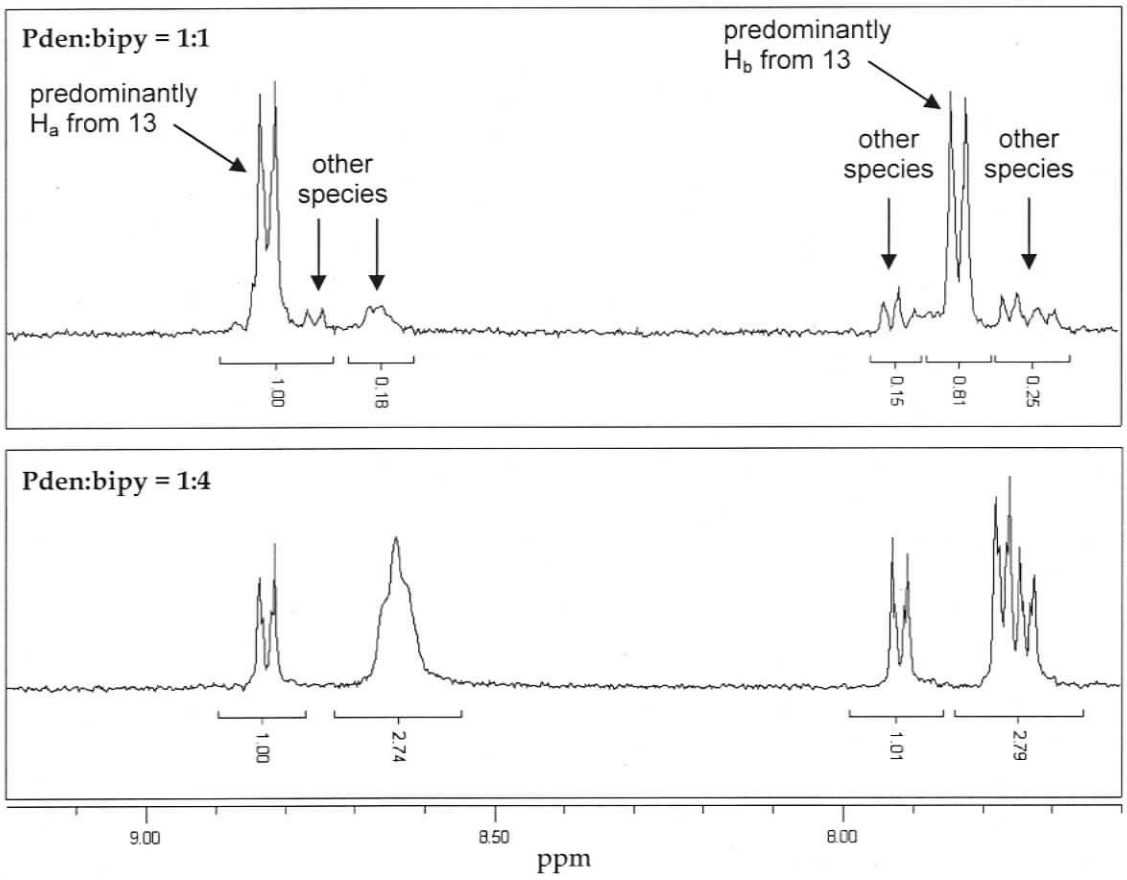

Figure 37 ^1H NMR spectra for 13 in D_2O at Pden:bipy = 1:1 and 1:4

The ^1H NMR spectrum for the solution prepared with Pden:bipy = 1:1 at pH = 6-7 for [Pd] = 10^{-5} M is shown in Figure 37. The chemical shifts observed in Figure 37 are slightly different than the values reported by Fujita, possibly because of

small differences in pH. We interpret the peaks at 8.8 and 7.8 ppm as the chemical shift that arises predominantly from **13** averaged with other species that are in fast exchange. The peaks at 6.65 and 6.75 ppm are also averaged chemical shift values of other species. Because these peaks have different chemical shifts, the species that contribute to a particular peak must be in slow exchange with species that contribute to the other peaks. Increasing the Pden:bipy ratio to 1:4 changes the speciation, and as a result the weighted average chemical shift is redistributed and a change in the spectrum is observed (Figure 37). Similar changes are observed for peaks consistent with en as well. Because Figure 36 and Figure 37 are similar in the down field region, the small peaks near the base of the major peaks in Figure 36 can be attributed to isomers in slow equilibrium with **14b**.

3.5 The implications of stereoisomeric (or racemic) ligands on the lipophilic square

The ligands **15a** and **15b** are a mixture of enantiomers, labelled R and S in Figure 38. Ligands that occupy the corners of the square can be oriented with either the alkyl chain above or below the plane of the square. Because there are four corners in a square and two possible ligand orientations for each corner (above or below the plane of the square), there are 16 (= 2^4) possible arrangements of the alkyl chains with respect to the plane of the square. Four of the 16 arrangements are unique, that is they cannot be related to another arrangement by symmetry. These unique arrangements are labelled M1-M4 in Figure 39. The axis of symmetry for each arrangement is indicated with the dotted lines.

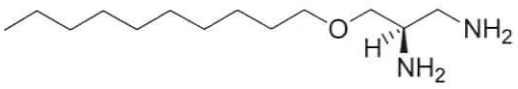

R -1, 2-diamino-3-(decanoxy)propane

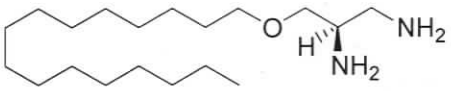

R - 1,2-diamino-3-(hexadecanoxy)propane

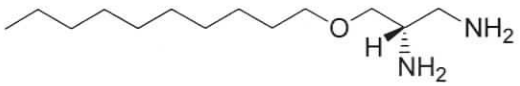

S -1, 2-diamino-3-(decanoxy)propane

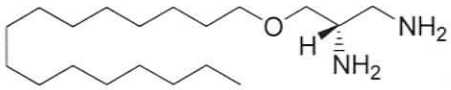

S - 1,2-diamino-3-(hexadecanoxy)propane

Figure 38 Enantiomers of 15a and 15b

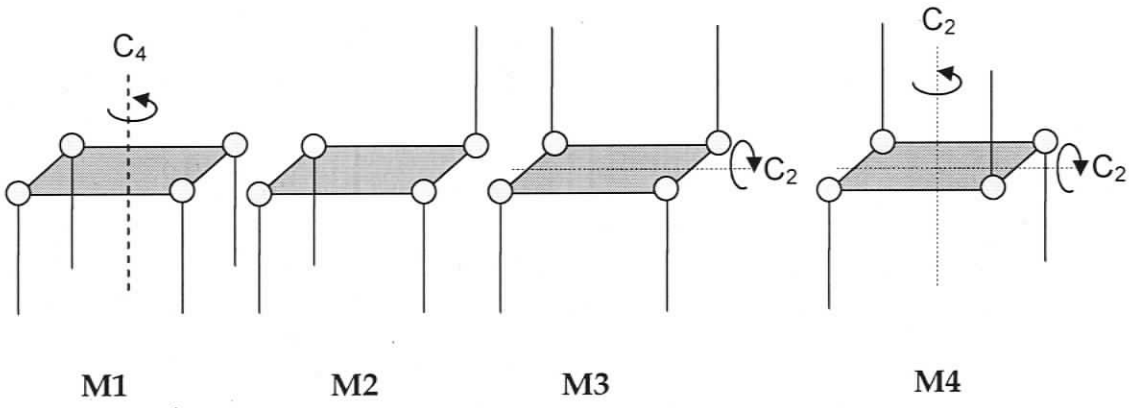

Figure 39 All possible orientations of the aliphatic chain with respect to the plane of the square in 14

The ligands that occupy the corners of the square are either R or S enantiomers. Statistically, there are 2^4 (=16) ways to organize the enantiomers around the square, assuming that all the corners are occupied. All the possible permutations for M1 are shown in Figure 40; six of these are unique. The equivalent molecules are labelled using the same letter. A total of 64 (= 4 · 16) permutations are possible for M1-M4, of which only 41 are unique.

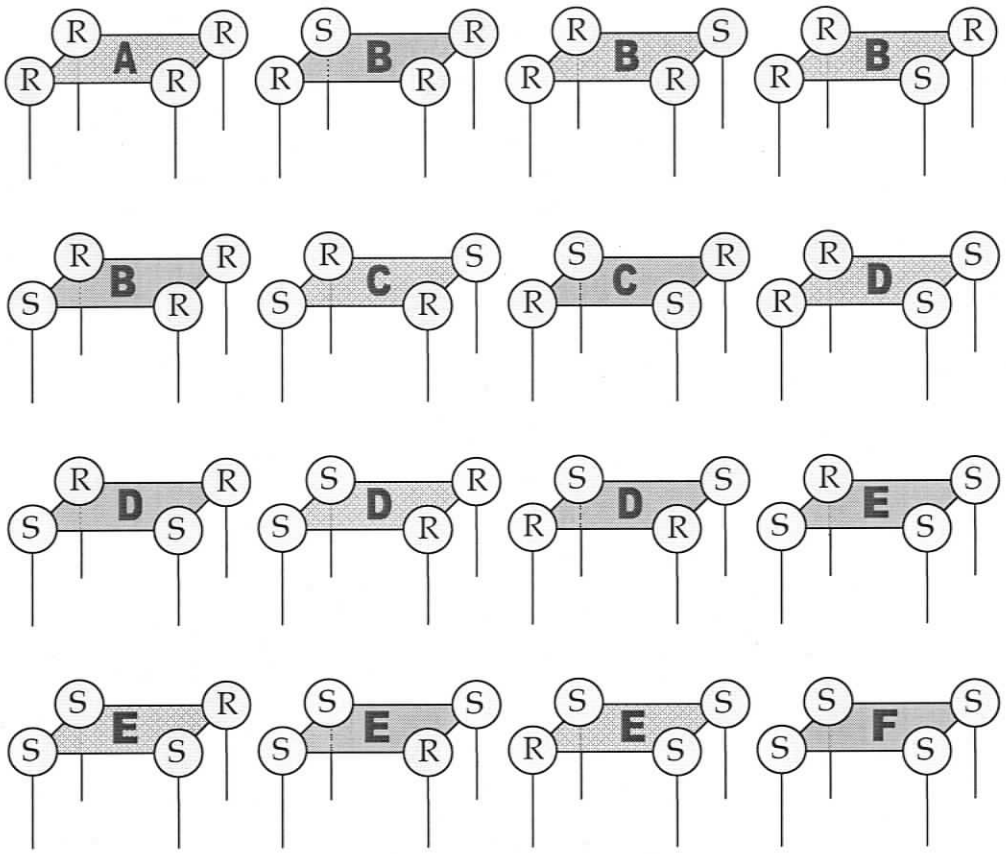

Figure 40 All possible permutations for M1. The six unique isomers are labelled A through F.

The ion channel design relies on the lipophilicity of the alkyl groups to anchor the square in the bilayer. If all the lipophilic groups must be on one side of the square in order for channels to form, then only ~15% of the species with **440** stoichiometry in solution will form active channels, assuming that the free energies of the isomers are equal and that the channel is preassembled in solution before partitioning into the bilayer. If enantiomerically pure **15** was synthesized and used to make **14**, isomers M1-M4 would still be present in solution. This means that only 25% of the isomers in solution would yield active channels for a statistical mixture. However, a strictly statistical analysis over simplifies the problem. Figure 37 demonstrates that the isomers are in fast exchange with other species so if M1 partitions into the bilayer, then the

speciation in solution will shift to accommodate the change in concentration of M1. Alternatively, the channel may be formed by components that have partitioned into the bilayer. If channels form by the latter mechanism, the issue of isomerism becomes irrelevant. The amount of material that is needed to form a channel in the bilayer is miniscule so activity should be observed regardless of the isomers present as long as channel forming species can intercalate into the bilayer.

3.6 Conclusions about synthesis

The ligands **15a** and **15b** were synthesized in 5 steps. The overall yield was ~ 49% from solketal and bromoalkane. Products **20a** and **20b** were made by reacting **15a** and **15b** with $Pd(COD)Cl_2$. The product was isolated in ~40-50 % yield and characterized by IR spectroscopy, MS and elemental analysis but was too insoluble to be characterized by NMR spectroscopy. More soluble palladium species, **21a** and **21b**, were prepared by suspending **20a** and **20b** in ACN and exchanging the Cl^- counter ion with OTf^-. Solutions of **21a** and **21b** were prepared analytically and used for all subsequent self-assembly reactions. The solution was characterized by ^1H NMR spectroscopy. Data collected by MS, IR and NMR spectroscopy were consistent with what is expected for the products.

3.7 Experimental procedure for syntheses

Synthesis for ***17b***

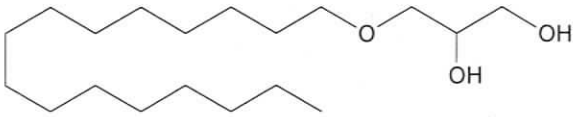

To a dry 100 ml 2-neck flask under N_2 and outfitted with a magnetic stir bar was added 60% NaH dispersed in oil (0.734 g, 18.4 mmol, 1 eq). The NaH was rinsed with two 3-5 ml aliquots of hexanes. To the NaH was added dry 1, 4-dioxane (40 ml) followed by the dropwise addition of solketal (2.588g, 19.58mmol, 1.06eq). The rate of solketal addition was regulated to keep the effervescing under control. Once the solketal addition was complete the cloudy, slightly yellow solution was stirred at RT for a further 10 minutes upon which the solution became clear. 1-bromohexadecane (6.473g, 21.2mmol, 1.16eq) was then added to the solution. The mixture was heated to reflux for 22 h during which a white precipitate formed. The reaction was quenched with 5 ml of ice cold water. The reaction mixture was extracted three times with diethyl ether. The organic extracts were combined and dried with anhydrous $MgSO_4$. Light yellow oil was recovered after the solvent was removed. The crude material was purified by column chromatography on silica gel (5 cm diameter, 600 ml silica), eluted with hexanes at first then increasing polarity to 4:1 hexanes:ethyl acetate. The product was recovered from the second band eluted from the column. The yield was 53% after purification by chromatography. ^1H NMR ($CDCl_3$): δ0.88(t, 3H, J=6.6 Hz), 1.2-1.4 (m, 26H), 1.57(m, 2H), 2.30(broad s), 3.44-3.56 (m, 4H), 3.62-3.75 (m, 2H), 3.86 (m, 1H) ppm. ^{13}C NMR($CDCl_3$): δ 14.1, 22.7, 26.0, 29.3-29.7, 31.9, 64.3, 70.4, 71.8, 72.5 ppm.

This **16b** was added to a 1-neck 100 ml RBF outfitted with a magnetic stir bar. To this was added MeOH (50 ml) and 6 drops concentrated HCl, and 15 drops H_2O. The mixture was heated to reflux for 4 h. After the solvent was then removed by rotary evaporation, a white, slightly waxy solid was recovered in quantitative yield. The product was characterized and used without further purification. ^1H NMR ($CDCl_3$): δ0.87(t, 3H, J=6.6 Hz), 1.2-1.4 (m, 26H), 1.57(m, 2H), 2.30(broad s), 3.41-3.58 (m, 4H), 3.60-3.76 (m, 2H), 3.81-3.90 (m, 1H) ppm. ^{13}C NMR($CDCl_3$): δ 14.1, 22.7, 26.0, 29.3-29.7, 31.9, 64.3, 70.4, 71.8, 72.5 ppm. FT-IR (KBr): 3369 (m, br), 2954 (sh, m), 2919 (m), 2850 (m), 1471 (s), 1328 (m), 1123 (s), 1060 (s) cm^{-1}. MS (EI) m/z: 316 [2%], 285 [22%], 225 [50%] Anal Calc for $C_{19}H_{40}O_3$: C,72.10; H,12.74. Found: C, 72.71; H, 13.16.

Synthesis for ***15b***

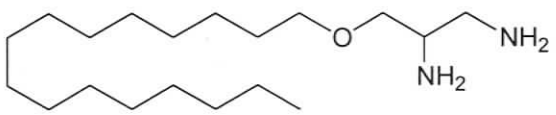

To a dry 3-neck 100ml flask under N_2 outfitted with a stir bar and a pressure equalized dropping funnel was added **17b** (2.726 g, 8.1 mmol, 1 eq), DCM (35 ml) and NEt_3 (9.6 ml, 68.9 mmol, 8 eq). The solution was cooled to 0°C in an ice bath. To the dropping funnel was added DCM (5 ml) and methanesulfonyl chloride (2.963 g, 25.8 mmol, 3 eq). This solution was added dropwise to the reaction mixture at a rate that maintained a constant temperature of 0°C. Once the addition was complete the solution was stirred at 0°C for 30 min then allowed to warm to room temperature and stirred at room temperature for 30 min. The reaction was quenched with a small amount of water, transferred to a separatory funnel and extracted with three 20 ml aliquots of saturated $NaHCO_3$ followed by three 20 ml aliquots of 1 M $HCl_{(aq)}$. The organic phase was dried with anhydrous $MgSO_4$, and then solvent was removed by rotary evaporation.

To this material was added DMF (40 ml) and NaN_3 (2.102 g, 32.3 mmol, 5.5 eq). This solution was heated with stirring to 110°C for 52 h. The mixture was concentrated on the rotary evaporator to about 5-10 ml and extracted with diethyl ether and water. The organic phase was dried with anhydrous $MgSO_4$ and the solvent removed by rotary evaporation. ***(CAUTION: Organic azides are known to be explosive. In small molecule synthesis, diazides are handled only in solution. However, small amounts (< 50 mg) of* 19a *and* 19b *have both been handled as pure materials on several occasions without incident. Larger amounts were handled as solutions only.***[99]) This synthesis was continued by concentrating the diethyl ether solution to about 5-10 ml. The yellow oil was then dissolved in 100% ethanol (25 ml) and added to a low pressure hydrogenation bottle containing 10% Pd on carbon (0.170 g) wetted with 100% EtOH (15 ml). The bottle was purged three times with H_2 and sealed under 50 psi of H_2 and shaken for 20 h. The solution was then filtered through a pad of celite and the solvent was removed from the filtrate by rotary evaporation. The recovered material was then dried under vacuum. The yield for **15b** from **17b** is 92%. The product could be further purified by careful recrystalization from warm DCM. ^{1}H NMR ($CDCl_3$): δ 0.88(t, 3H, J=6.6 Hz), 1.25(m, 26H), 1.55(m, 2H), 2.02(broad s), 2.66(m, 1H), 2.84(m, 1H), 3.00 (m, 1H), 3.25-3.53(m, 4H) ppm. ^{13}C NMR($CDCl_3$): δ 14.1, 22.7, 26.1, 29.3-29.7, 31.9, 44.4, 45.6, 53.2, 71.7, 74.5 ppm. FT-IR (KBr): 3361 (m, br) , 3301 (m, br), 2918 (m), 2850 (m), 1645 (m), 1468 (m), 1123 (s) cm^{-1}. MS (FAB) m/z: 597.6 [18%], 343.3 [16%], 316.3 [100%] Anal Calc for $C_{19}H_{42}N_2O$: C,72.55 ; H,13.46 ; N, 8.91; O, 5.09. Found: C, 67.27; H, 11.80; N, 7.09.

Synthesis of ***20b***

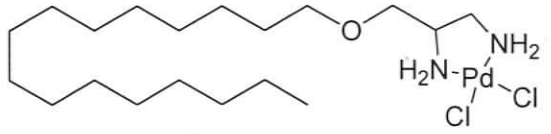

To a 1-neck 10 ml round bottom flask outfitted with a magnetic stir bar was dissolved $Pd(COD)Cl_2$ (0.072 g, 25 mmol) in ~3 ml $CHCl_3$. To the solution was added **15b** (0.080 g, 25 mmol). The reaction mixture was heated to reflux for 3 h. The reaction is cooled to room temperature and filtered to recover a beige solid. The grayish yellow solid was washed with small portions of acetone and ethanol. The yield was 47%. The isolated solid presumed to be **20b** was not soluble enough to be characterized by NMR spectroscopy. FT-IR (KBr): 3276(m), 3193(m), 2917(s), 2850(s), 1557(m), 1468(m), 1124(m) cm^{-1}. MS (EI) m/z: 419.2 [100%] Anal Calc for $C_{19}H_{42}Cl_2N_2OPd$: C, 46.39; H, 8.61; N, 5.70. Found: C, 46.62; H, 8.55; N, 6.00.

Synthesis of ***21b****(OTf)*$_2$

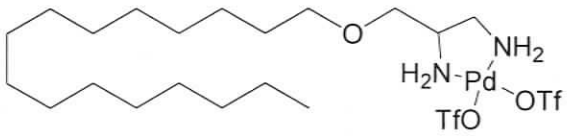

To a test tube was added a magnetic stir bar, **20b** (0.0709 g, 14 mmol) and 5 ml ACN. AgOTf (0.7688 g, 30 mmol) dissolved in 2 ml ACN was added to the suspension. The mixture was warmed at 40-50°C for at least 4 h protected from light. During this time a white precipitate formed and the solution became light yellow. The suspension was cooled to room temperature and filtered to recover a light yellow solution which was transferred to a 10 ml volumetric flask and diluted to the mark with water. The solution was used in experiments without further treatment. This procedure was assumed to be quantitative. The reaction

carried out in d_3-ACN was used to characterize the product. ^{1}H NMR (d_3-ACN): δ 0.88(t, 3H, J = 6.7Hz), 1.2-1.4(m, 28H), 1.57(m, 2H), 2.71(br, 1H), 3.24(broad s), 3.47(m, 4H) ppm.

Synthesis of ***17a***

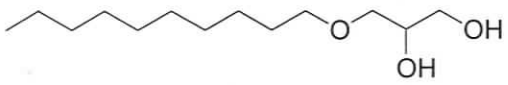

To a dry 100 ml 2-neck flask under N_2 and outfitted with a magnetic stir bar was added 60% NaH dispersed in oil (0.770 g, 19.3 mmol, 1.71 eq). The NaH was rinsed with two 3-5 ml aliquots of hexanes. To the NaH was added dry dioxane (40 ml) followed by the dropwise addition of solketal (2.560 g, 19.4 mmol, 1.72 eq). The rate of solketal addition was regulated to keep the effervescing under control. Once the solketal addition was complete the cloudy, slightly yellow solution was stirred at RT for a further 10 min upon which the solution became clear. 1-bromodecane (2.5 g, 11.3 mmol, 1 eq) was then added to the solution. The mixture was heated to reflux for 22 h during which a white precipitate formed. The reaction was quenched with 5 ml of ice cold water and extracted three 20 ml aliquots of diethyl ether. The organic extracts were combined and dried with anhydrous $MgSO_4$. Light yellow oil was recovered after the solvent was removed on the rotary evaporator. The crude material was purified by column chromatography on silica gel. The column was 5 cm in diameter and packed with 600 ml of silica gel and eluted with hexanes (~1 l) then 4:1 hexanes:ethyl acetate (~1.5 l). The product was recovered from the second band eluted from the column. The yield was 69% after purification by chromatography. ^{1}H NMR ($CDCl_3$): δ0.87(t, 3H, J=6.6 Hz), 1.2-1.4 (m, 26H), 1.56(m, 2H), 2.26(broad s), 3.40-3.55 (m, 4H), 3.64 (m, 2H), 3.86 (m, 1H) ppm. ^{13}C NMR($CDCl_3$): δ 14.3, 22.9, 26.3, 29.4-29.9, 32.1, 64.4, 70.7, 72.1, 72.6 ppm.

The resulting product, **16a**, was added to a 1-neck 100 ml RBF outfitted with a magnetic stir bar. To this was added MeOH (50 ml) and 6 drops concentrated HCl, and 15 drops H_2O. The mixture was heated to reflux for 4 h. After the solvent was then removed by rotary evaporation to recover white, slightly waxy solid in quantitative yield. The product was characterized and used without further purification. ^1H NMR ($CDCl_3$): δ0.88(t, 3H, J=6.6 Hz), 1.2-1.4 (m, 14H), 1.57(quintet, 2H, J= 6.8 Hz), 2.22(broad s), 3.38-3.58 (m, 4H), 3.64 (dd, 1H), 3.72 (dd, 1H), 3.86(m, 1H) ppm. ^{13}C NMR($CDCl_3$): δ 14.1, 22.7, 26.1, 29.2-29.8, 64.3, 70.4, 71.8, 72.5 ppm. FT-IR (KBr): 3390 (s, br) , 2919 (s), 2855 (s), 1729 (w, br), 1470 (s), 1327 (m), 1124 (s), 1061 (s) cm^{-1}. MS (FAB) m/z: 283[100%], 232[30%], 137[13%], 93.0[34%], 57.1[26%] Anal Calc for $C_{13}H_{28}O_3$: C, 67.2; H, 12.15; O, 20.66. Found: C, 69.58; H, 12.78.

Synthesis for ***15a***

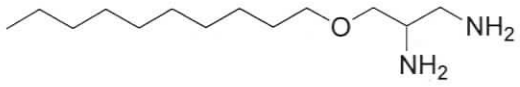

To a dry 3-neck 100ml RBF under N_2 outfitted with a stir bar and a pressure equalized dropping funnel was added **17a** (1.913 g, 8.23 mmol, 1 eq), DCM (40 ml) and NEt_3 (9.0 ml, 64 mmol, 7.8 eq). The solution was cooled to 0°C in an ice bath. To the dropping funnel was added DCM (5 ml) and methanesulfonyl chloride (2.824 g, 2.47 mmol, 3 eq). This solution was added dropwise to the RBF at a rate that maintained a constant temperature of 0°C. Once the addition was complete the solution was stirred at 0°C for 30 min then allowed to warm to room temperature and stirred at room temperature for 30 min. The reaction mixture was transferred to a separatory funnel and extracted from the organic phase with saturated $NaHCO_3$ and 1M HCl(aq). The organic phase was dried

with anhydrous $MgSO_4$ and the solvent was removed by rotary evaporation. The crude yield for **18a** was 91%. The synthesis was continued without further purification.

To **18a** (2.825 g, 7.28 mmol, 1eq) was added a magnetic stir bar, DMF (40 ml) and NaN_3 (2.620 g, 40.3 mmol, 5.5 eq). This solution was heated to 110°C for 52 h. The mixture was concentrated on the rotary evaporator to about 5-10 ml and extracted with diethyl ether and water. The organic phase was dried with anhydrous $MgSO_4$ and the solvent removed by rotary evaporation. The yellow oil was then dissolved in 100% ethanol (25 ml) and added to a low pressure hydrogenation bottle containing 10% Pd on carbon (0.2 g) wetted with 100% EtOH (15 ml). The bottle was purged three times with H_2 sealed under 50 psi of H_2 and shaken for 20 h. The solution was then filtered through a pad of celite and the solvent was removed from the filterate by rotary evaporation. The recovered material with then dried under vacuum. The yield for this final step is 62%. The product could be further purified by careful recrystalization from warm DCM. ^1H NMR ($CDCl_3$): δ 0.85(t), 1.2-1.4(m), 1.55(m) 2.4(br s), 2.75(m), 2.9(m), 3.4 (m), 3.8(m) ppm. ^{13}C NMR($CDCl_3$): δ 14.1, 22.9, 26.3, 29.5-29.8, 32.1, 44.4, 64.4, 70.8, 71.8, 73.2 ppm. FT-IR (KBr): 3360 (m, br) , 3294 (m, br), 2923 (m), 2853 (m), 1653 (w), 1598(w), 1464 (m), 1115 (s) cm^{-1}. MS (EI) m/z: 321[M^+,2%], 285[22%], 200[52%], 85[32%], 71[32%], 60[80%], 42[100%]

Synthesis of **20a**

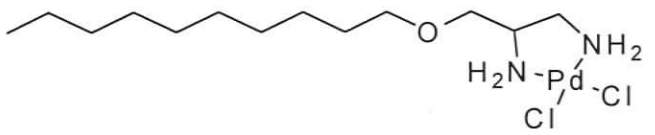

To a 1-neck 10 ml round bottom flask outfitted with a magnetic stir bar was dissolved $Pd(COD)Cl_2$ (0.279g, 1.21 mmol) in ~3ml $CHCl_3$. To the solution was added **15a** (0.355g, 1.24 mmol). The reaction mixture was heated to reflux for 3 hours. The reaction is cooled to room temperature and filtered to recover a beige solid. The grayish yellow solid was washed with small portions of acetone and ethanol. The yield was 46%. The isolated solid presumed to be **20a** was not soluble enough to be characterized by NMR spectroscopy.

Synthesis of **21a**$(OTf)_2$

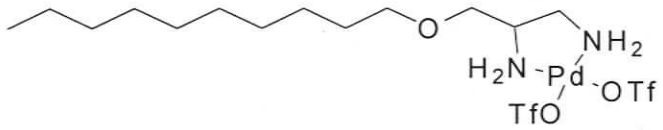

To a test tube was added a magnetic stir bar, **20a** (0.059g, 0.19mmol) and 5 ml ACN. AgOTf (0.0.067g, 0.39 mmol) dissolved in 2 ml ACN was added to the suspension. The mixture was warmed at 40-50°C for at least 4 h protected from light. During this time a white precipitated formed and the solution became light yellow. The suspension was cooled to room temperature and filtered to recover a light yellow solution which was transferred to a 10 ml volumetric flask and diluted to the mark with water. The solution was used in experiments without further treatment. This procedure was assumed to be quantitative.

4 Ion channel activity from solutions of 14b

4.1 Introduction

The design of self-assembled ion channels that utilize **15** and 4, 4'-bipyridine as coordinating species was discussed in the introduction. This chapter will focus on the results and interpretation of the ion channel activity observed for solutions of **14** in a planar bilayer. However, **14a** solutions failed to show any sign of pore formation under a wide range of experimental conditions and will not be discussed further. Although **14b** refers to a specific complex, **14b** in solution should be understood as mixtures in which **14b** is the dominant species.

4.1.1 Bilayer clamp experiment

The bilayer clamp experiment is a standard technique used to characterize ion channel function. It utilizes the fundamental relationship between voltage, conductance and current described by Ohm's law. Figure 41 shows the general set-up for the experiment. It consists of two electrolyte filled chambers connected by a hole 250 μm in diameter. An electrode separated by a salt bridge is immersed into each chamber. A potential applied between the electrodes results in an observable current when the hole separating the chambers is open. When the hole is spanned by a lipid bilayer, the two chambers are separated by an insulator and no current is observed for applied potentials as long as the bilayer is intact. If an ion channel is present in the bilayer then the two sides become connected and ions can flow between the two chambers. In this case, current is observed when potential is applied. The data collected using this set-up reports the current as a function of time.

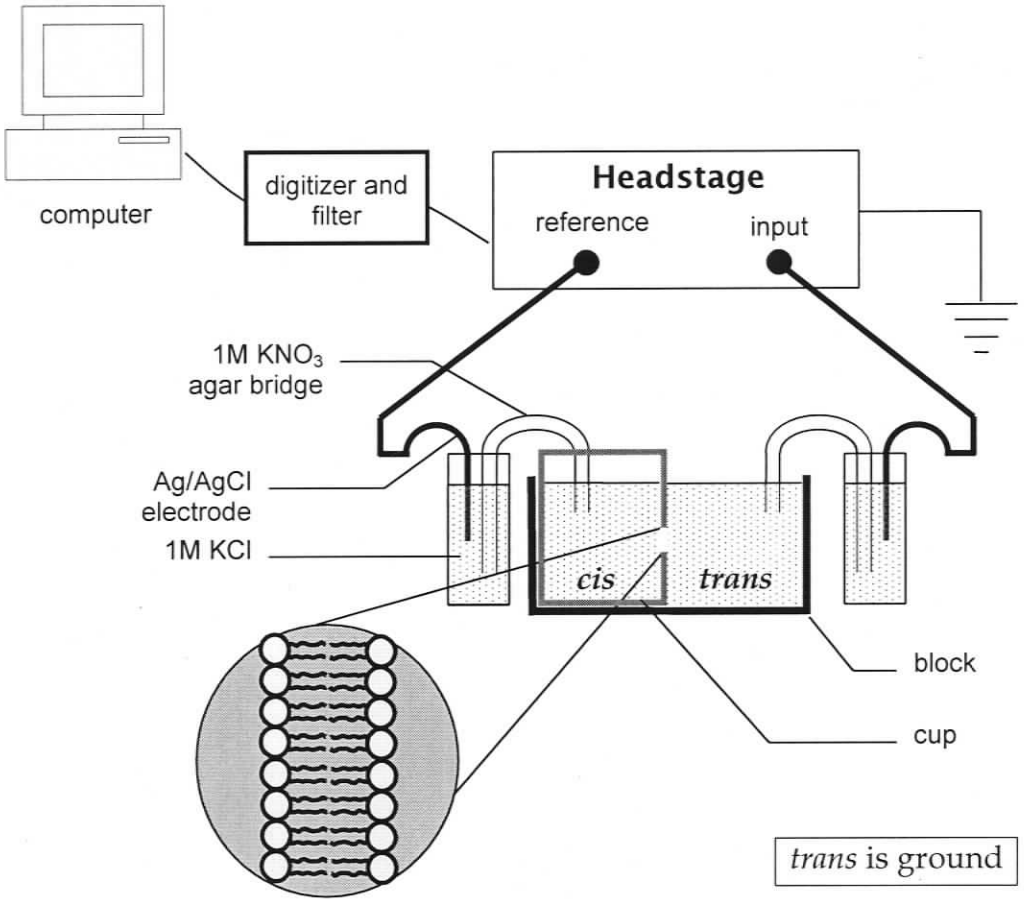

Figure 41 Bilayer clamp experimental set up

Figure 42 shows observations made at -120 mV in a bilayer containing gramicidin which is a channel forming peptide. There are three levels in this recording. The current is zero during the 'off' state and indicates that all the channels in the bilayer are closed. At t_1, a single channel opens suddenly and the two chambers are temporarily connected so that ions can flow between the two chambers. This is observed as a non-zero current at level one. Current continues to pass at a constant value while the ion channel remains open. At t_2 a second channel opens which results in an increase in current up to level two. The first closing event is observed at t_3 when one of the channels closes and the current returns back to level one. At t_4 a second channel closes and the system returns to the off state. The opening and closing of the channel creates a feature know as a

square top which is typical for ion channels. Several square tops are usually observed during a single recording.

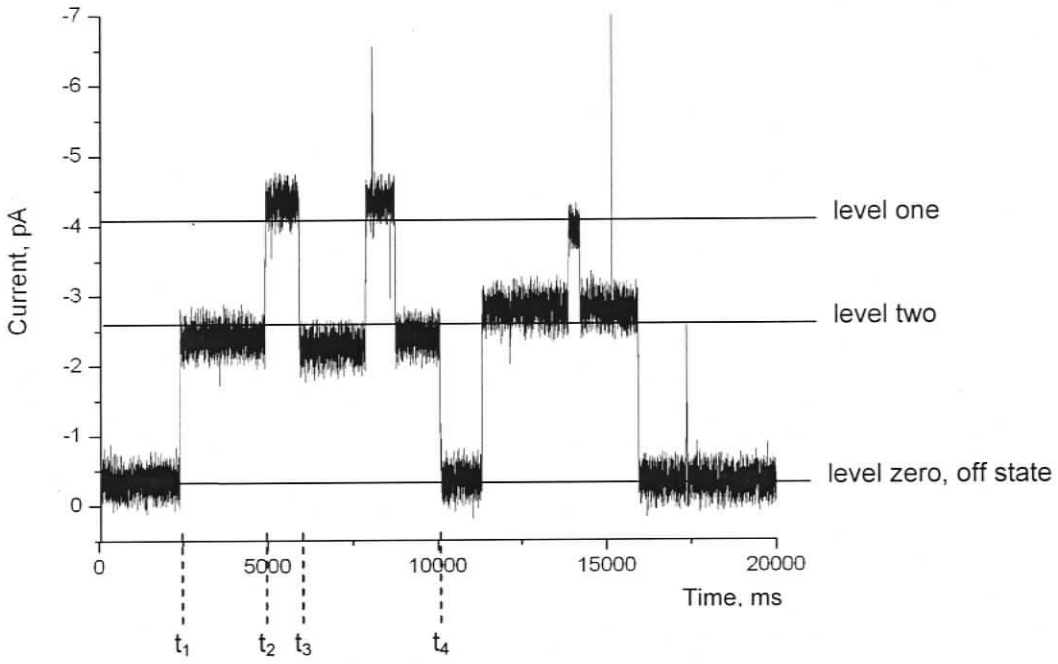

Figure 42 Current-time recording at -120 mV for a bilayer with gramicidin in 1M KNO_3

Multiple levels are often observed in the current-time recordings. The open channels can be either the same or different species. A simple way to distinguish between the two situations is to examine the current at a constant potential. If the current passed at the different levels are integral multiples of one another then they are most likely the same species of channel, if the values are different then they are most likely different species. A number of experiments are possible once activity is observed. These will be described later in this chapter.

4.2 Results from bilayer experiments on 14b solutions

Ion channels are normally characterized by their probability of opening, lifetime, selectivity and conductance observed using the bilayer clamp technique. The

channel activity for **14b** in solution was tested; but despite collecting a broad set of observations over a variety of conditions, full characterization using the usual parameters was not possible. As a result, some of the activity observed remains poorly understood. Three types of activity were observed: erratic openings, short openings and long openings. Erratic openings were frequently observed but difficult to study; therefore only a simple account of their behaviour is presented. Short openings were extremely rare. However, their behaviour was more conventional and could be interpreted to give estimates of the channel radii. Studies on long openings gave insight into the selectivity as well as channel radii. The following section is an account of the types of activity observed in diphyPC bilayers.

"Dipping" is a term used to describe the action of sliding the cup in and out of the block. It was used to help re-establish or thin the bilayer. The integrity of the bilayer was checked and deemed satisfactory before continuing with the experiment. Bilayer integrity was also checked throughout the experiment to ensure that the activity was due to ion channels and not changes in the bilayer. Criteria for a satisfactory bilayer are described in the experimental section. The methods used to prepare the bilayer and introduce solutions of **14b** to the bilayer clamp were the same for all the experiments. Complex **14b** was formed in ACN at [Pd] ≈ 14 mM. The most consistent results were obtained when solutions of **14b** were used at full strength. Activity was observed when a brush dampened with **14b** solution and lipid solution was passed over a broken bilayer until the bilayer was reformed. Although activity occurs readily, there is no way to reliably predict the type of activity that would be observed in a given experiment.

Attempts to prepare bilayers from lipid solutions in which **14b** (and the corresponding equilibrium species) were dissolved were unsuccessful because

stable bilayers that exhibited channel activity could not be formed. The ratio of Pd to lipid was 1:4 in these lipid solutions. Efforts directed towards introducing **14b** solutions into the bilayer (by adding small aliquots of **14b** solution into the block and cup) were also unproductive due to precipitation.

4.2.1 Erratic openings

Erratic openings are characterized by the random passage of current which leads to the spikey current-time trace in Figure 43. This type of behaviour was observed in a number of different electrolytes. Continuous erratic activity can be

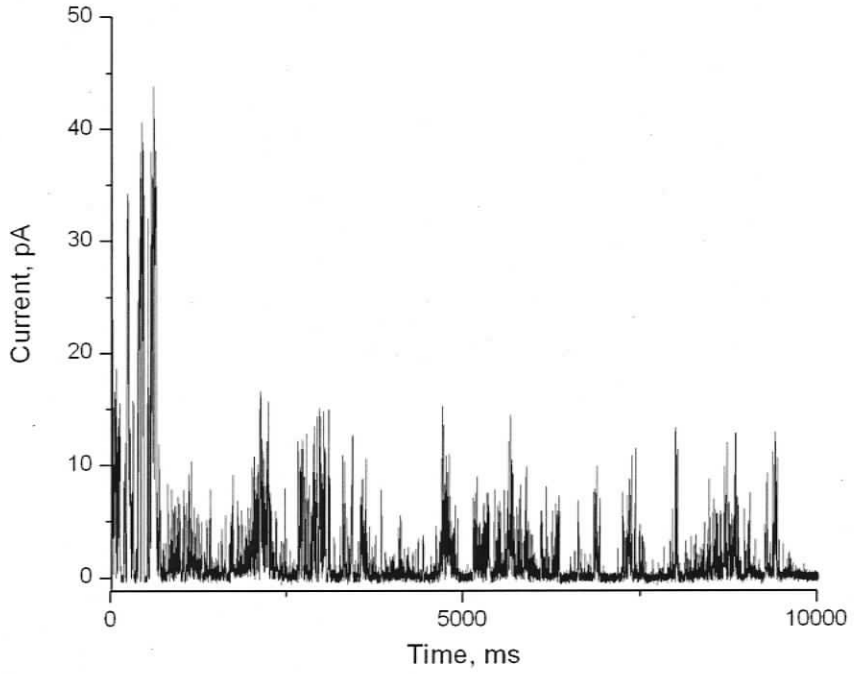

Figure 43 Current-time recording of erratic behaviour observed for 14b solutions in a diphyPC bilayer and 1 M KCl at +80 mV

observed on the order of seconds to minutes. The amount of current passed during these events can vary between <5 pA to >200 pA which is the maximum current that our instrument can observe. The amount of current observed is affected by changes in potential during a single erratic opening event but

separate bursts of erratic activity will not respond in the same way, even during a single experiment. Erratic activity is usually observed as transitions from zero current but not always.

Erratic behaviour can be ascribed to the passage of ions through the bilayer membrane in a non-uniform fashion. It is difficult to draw conclusions regarding channel structures from the observations because the behaviour is random. Erratic activity has also been observed in other systems[100].

Current is expected to flow across the membrane according to the potential gradient applied; for example, if a positive potential is applied, a positive current should be observed. Current that flows opposite the direction of the applied potential is sometimes observed during an experiment (Figure 44). This anti-potential current lasts between 0.01 to 2 seconds. The bilayer integrity remains

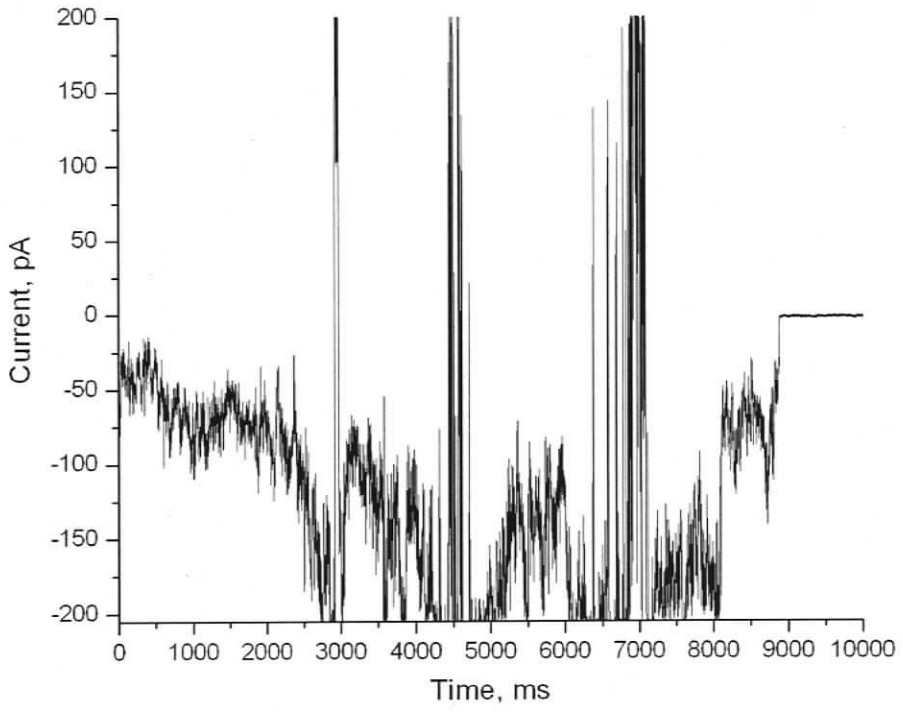

Figure 44 Observation of current which runs opposite the applied potential at -160 mV in 0.1 M Cs_2SO_4 for diphyPC bilayer with 14b solutions

unchanged after these events and current that flows in the expected directions may be observed. Anti-potential currents are observed in conjunction with erratic openings only and are never observed on their own. They tend to appear after a period of applied potential of various magnitudes. Although anti-potential currents may be an artifact of the channels, the events are too infrequent to be recognized as a type of channel activity. There is no clear explanation for this type of behaviour.

4.2.2 Short openings

Short opening activity resembles square top activity but has large variations in the current passed while the channel is opened. Short openings (Figure 45) were observed in seven of thirty experiments and lasted for no more than a couple of

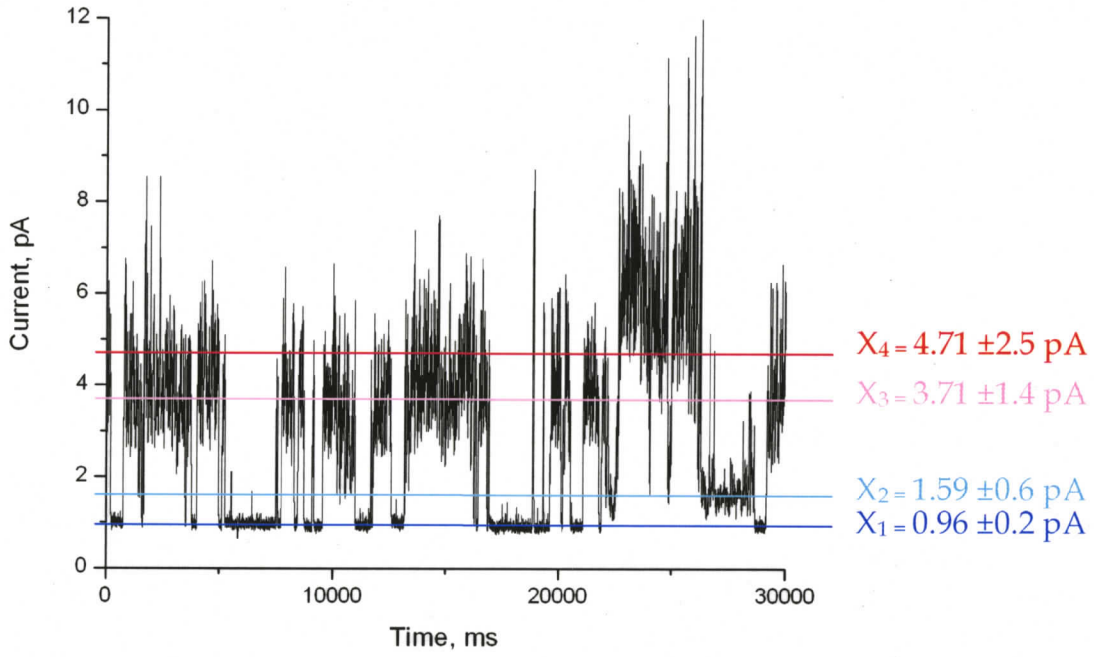

Figure 45 Current-time recording of short openings observed for 14b solutions in a diphyPC bilayer and 1 M KCl at +100 mV

minutes in each case. The lifetime of these channels were between 0.5 and 5 seconds. The probability of opening and selectivity could not be reliably determined due to the infrequency of short opening activity.

For channels that show consistent square top behaviour with a good probability of opening, a series of current-time curves are collected at varying potentials during a single experiment. Square top behaviour is normally analyzed by deconstructing current-time traces recorded at different potentials into histograms which are fitted using a Gaussian function. The average current and deviations are obtained from the Gaussian fit. The peak maximum is the average current and width of the peak at half height represents the deviation in the activity observed. Normally, the variation in current during an open state is no more than what would be observed in the baseline thus the peak widths should be narrow. The number of peaks observed in the histogram is the number of levels in the current-time trace. A similar approach can be used to interpret the short openings observed for **14b** solutions.

Four levels are identified in the histogram (Figure 46) for the current-time trace shown in Figure 45. The average current (X_n) and their deviations are summarized in Table 8. The deviation from the average current is large compared to deviations expected in ideal systems which suggest that the pore is unstable. The levels identified by the histogram are indicated on Figure 45. Peaks X_3 and X_4 are fairly broad as the result of large variation in current observed at those levels.

Table 8 Average current observed for short openings

Level	Average Current, pA	Width at half height, pA
1	0.96	0.2
2	1.59	0.5
3	3.71	1.4
4	4.71	2.5

The average current-voltage plot for simple, non-rectified channels such as gramicidin A varies linearly according to Ohm's law (V = IR, where V is the potential, I is the current and R is the resistance) given that the electrolyte on both sides of a bilayer is the same. Conductance (g) is the inverse of resistance and is determined from the slope of the current-potential plot in Siemens (S). The conductances observed for short openings due to **14b** solutions are determined using a single average current-voltage relationship. This method is less reliable than the conventional method that uses the slope of average current-voltage plots; however, it is the only alternative given the low probability of opening.

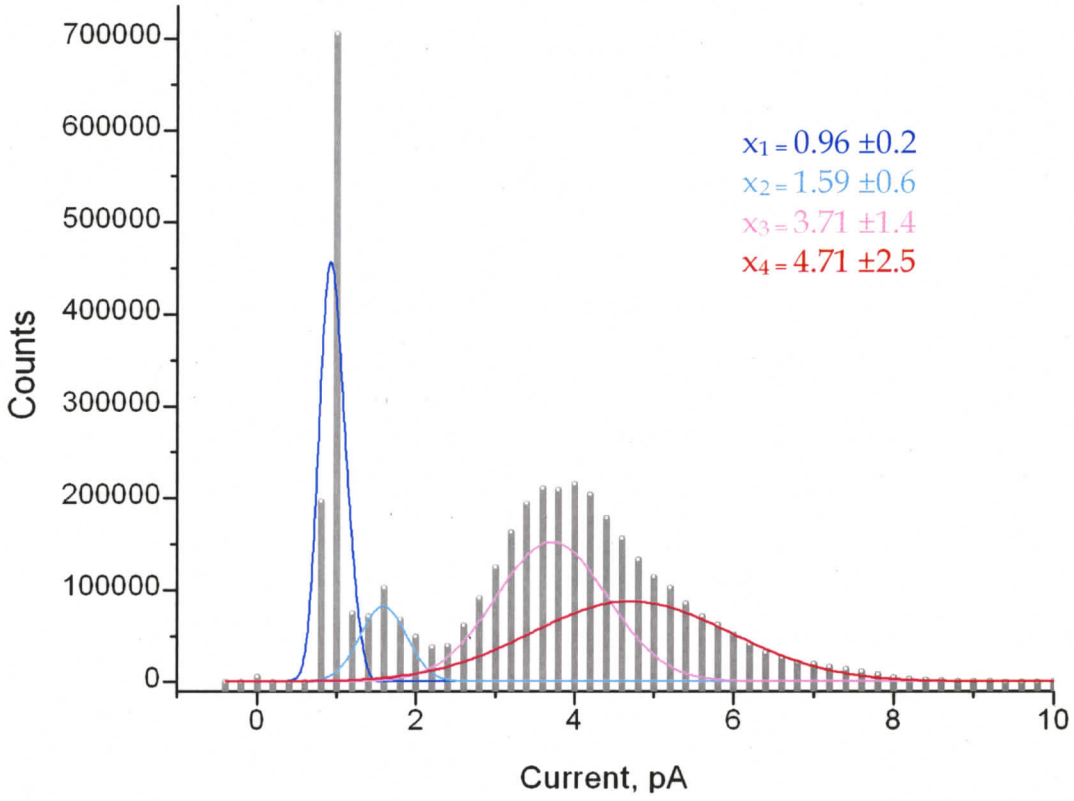

Figure 46 Histogram and Gaussian fit for openings observed at 100 mV in 1 M KCl, bin size = 0.05 pA

Conductance is dependent on the resistivity of the electrolyte. A method that would correct for ionic conductivity was needed so that rare openings observed with different electrolytes could be compared. Hille radii[2], which are calculated

from conductance, resistivity and length of the channel, are used as a means of comparing observations obtained under different conditions. The equation used to calculate the Hille radius is shown in (4-1) where R is the resistance, l is the length of the channel, r is the radius and ρ is the resistivity of the electrolyte. Resistivity was calculated from specific conductance values found in the literature[101]. Details regarding the calculations are in the experimental section.

$$R = \left(l + \frac{\pi r}{2}\right)\left(\frac{\rho}{\pi r^2}\right) \qquad \textbf{(4-1)}$$

Hille treats ion channels as simple tunnels that allow ions to travel across the lipid bilayer membrane in derivation of (4-1). This treatment assumes that there are no interactions between the channel and the ions that the flow of ions is neither facilitated nor impeded by interactions with other ions or water. Accepting these parameters means that macroscopic principles, such as Ohm's law, can be used to describe their behaviour.

Equation (4-1) is derived by considering the resistance of a cylindrical tube capped with two hemispheres of equal radius (Figure 47). In this model, the ion channel is represented by the cylindrical portion and the hemispheres account for the resistance of the electrolyte around the mouth of the channel. Bulk resistivity of the electrolyte is used to calculate R.

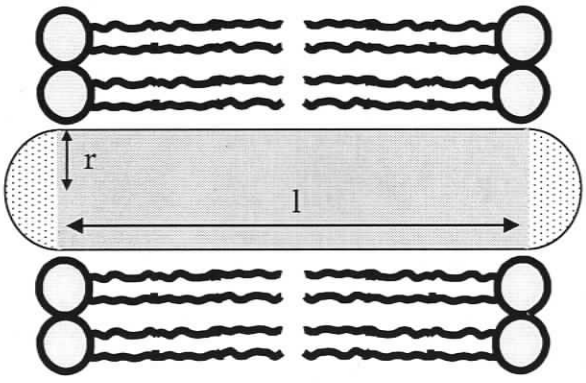

Figure 47 Idealized channel used to derive the Hille equation

The temperature was not regulated during the experiments. Hille radii were calculated at 22 and 26°C to accommodate changes in the resistivity as a result of temperature differences. This gave high and low estimates for pore radii. In practice the variation in radii between the two temperatures is less than 5% difference so the estimates are reasonable as a first approximation. Figure 48 shows all the radii plotted in increasing magnitude for short openings. A detailed table summarizing the short openings data is in the experimental section. Hille radii were calculated assuming the channel length was 34 Å[102].

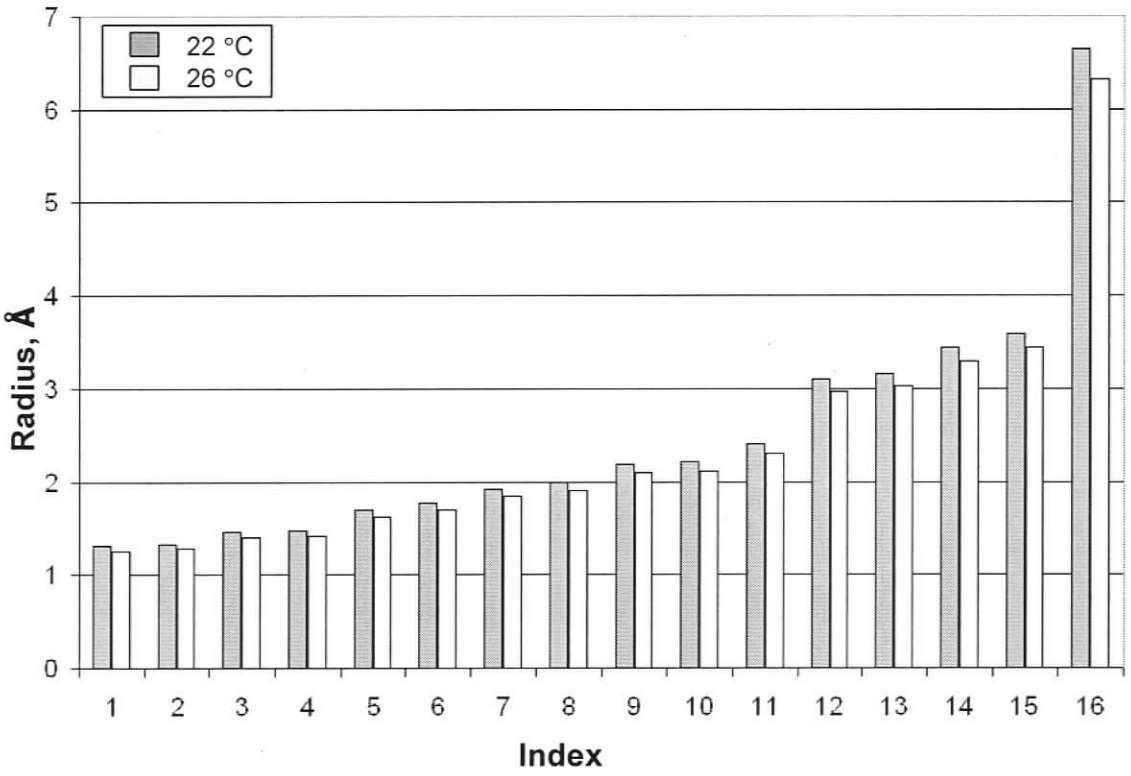

Figure 48 Hille radii calculated from conductances observed at 22 and 26 °C

The crystal structure of **13** shows that the interior of the square is about 7.8 Å in diameter so a channel formed with the square as the portal is expected to have a radius ~ 4-5 Å. The radius of the channel should also be constant if the square is the portal for the channel.

Figure 48 shows that the calculated radii range from approximately 1 to 6 Å. Channels with a radius of ~ 6.5 Å are far too large to be attributed to channels with squares as portals. The large variation in size suggests that the channels observed are not well defined hence cannot be attributed to channels with squares as the portal. The rarity of the short openings observations prevents further analysis and study.

4.2.3 Long openings

Long openings are the second most common type of activity observed for **14b** solutions. Long openings appear after a 30-90 min quiet period where occasional bursts of erratic openings are observed. A potential of ±100 mV is applied for 2-3 min durations during the quiet period to check for activity. Long openings appear like elevated baselines except that the current varies with changes in potential. No current would be observed at any potential applied if channels were absent in the bilayer. Of the three types of activity observed for ion channels, long openings are the most well studied because they have regular behaviour and are active for a long time. Lifetime, probability of opening, conductance and selectivity were used to characterized long openings.

Long openings are similar to square tops except that the closing events are so infrequent that the probability of opening is 1. A long opening can continue to pass current for up to an hour without the appearance of a closing event. The lifetimes for these channels vary between experiments but were commonly between 10-45 minutes which is unusual because most type 2b synthetic ion channels have lifetimes in the milliseconds to seconds range[29, 48, 59, 103].

The conductance was determined by changing the potential applied while the channel was open (Figure 49). Except for some tiny spikes and the occasional

small step (Figure 49 at +35 mV), the current is generally constant at a given potential. These fluctuations may indicate a dynamic component associated with the channel or activity from other channels superimposed on very flat long openings. There is no way to distinguish between the two scenarios from the data.

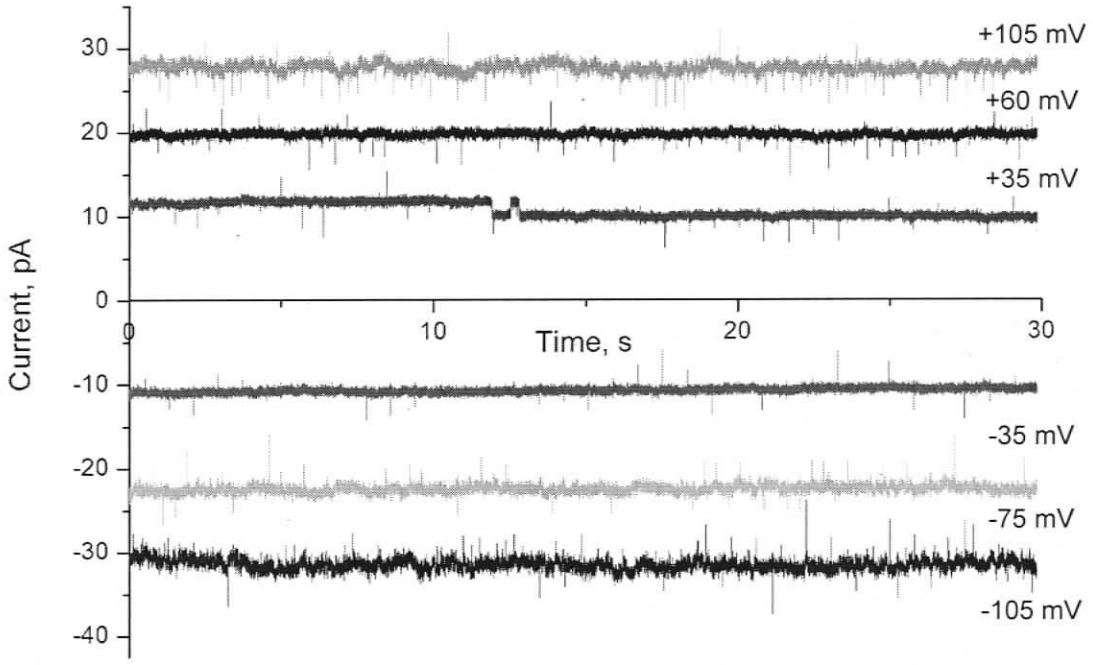

Figure 49 Current-time recordings at different potentials for 14b solutions in diphyPC bilayers and 0.1 M CsCl

The current observed is plotted against the voltage applied so that the conductance of the channel can be determined from the slope of a best fit line. If the relationship is linear then it follows Ohm's law and the pore behaves in an ideal manner (Figure 50). The conductances in various electrolytes and the corresponding Hille radii are summarized in Table 9.

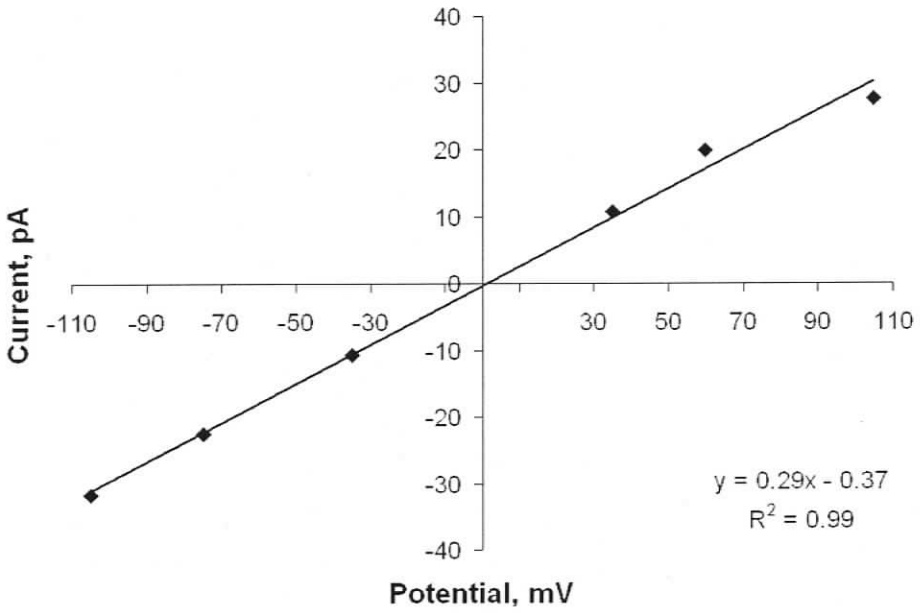

Figure 50 Current-voltage plot for a long opening observed for 14b solutions in diphyPC bilayers and 0.1 M CsCl. The conductance for this channel was 0.29 nS as determined from the slope of the curve.

Table 9 Conductance measured using bilayer clamp for solutions of 14b

Entry	Electrolyte, concentration (M)	Conductance, nS	Radius at 22 °C, Å	Radius at 26 °C, Å	Average Radius, Å
1	Cs_2SO_4, 0.5	0.12	1.3	1.3	1.3
2[a]	KNO_3, 1	0.251 +/- .003	1.9	1.8	1.9
3[a]	KNO_3, 1	0.26	2.0	1.9	1.9
4	CsBr, 0.1	0.066	2.5	2.5	2.5
5	CsCl, 0.1	0.29	5.2	5.0	5.1
6	Cs_2SO_4, 0.1	0.8[c]	7.4	7.1	7.3
7	NaCl, 0.1	0.52	8.4	7.9	8.1
8	Cs_2SO_4, 0.1	1.3	9.9	9.4	9.6
9	KNO3, 1	7.21	13	12	12.5
10	Cs_2SO_4, 0.1	2.1	13	13	13.0
11	CsCl, 0.1	1.7	15	14	14.5

(a) **21b** only

Channel radii were calculated from the conductances by the same method used for square tops assuming that the channel was 34 Å in length.

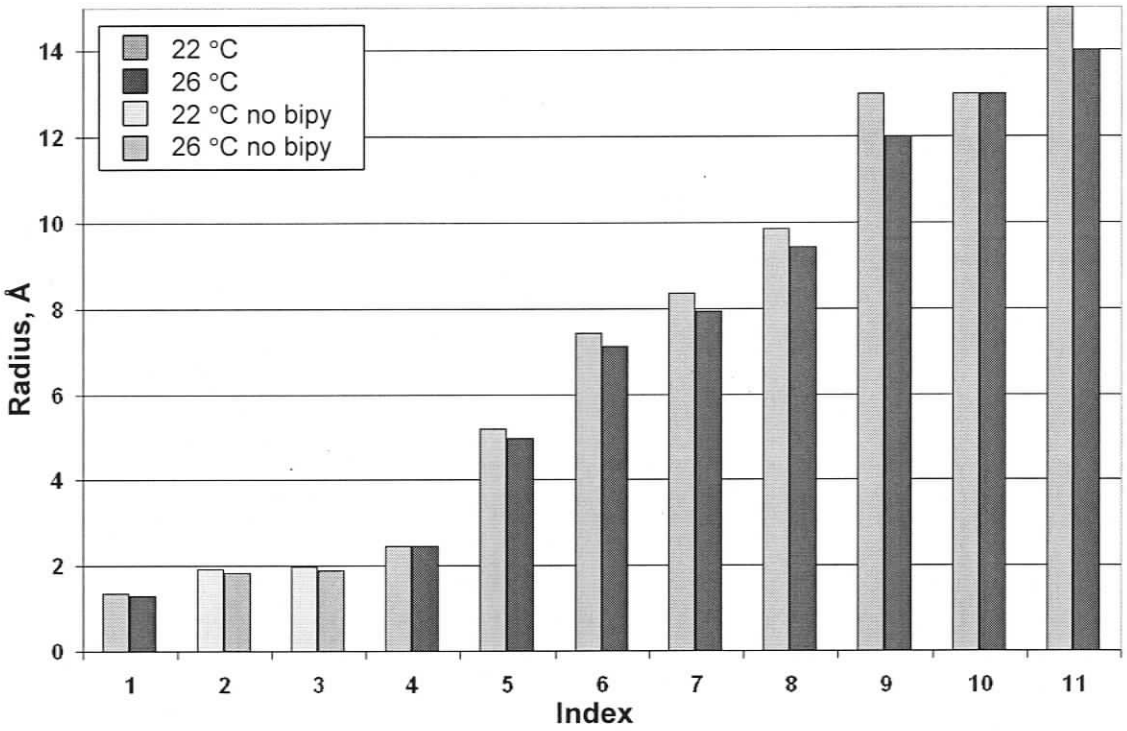

Figure 51 Hille radii for long openings calculated at 22 and 26 °C

The calculated radii for 22 and 26 °C are plotted in ascending order in Figure 51. Details regarding the calculations for Hille radii are presented in the experimental section. Radii indexed 1 to 5 in Figure 51 are less than 4 Å which is in the range expected for channels with Pd-bipy square portals. All other channels have radii which are much larger than what would be expected for the square. If the dimensions of the channels are recalculated assuming that the radius of the channel is 4 Å then the length of the channel becomes unreasonably short and is inconsistent with the channel design. For example the conductance observed for index 8 was 0.52 nS, so the length estimated by the Hille equation is 4.1 Å if a pore radius of 4 Å is assumed.

As well, long openings were observed for experiments with solutions of only **21b**. As with long openings observed when using **14b** solutions, erratic activity was also observed prior to the formation of long openings. The channels that opened during these experiments had radii ~1.9 Å which is consistent with other values observed for long openings (Table 9, entries 2 and 3). Under the conditions of the control experiments, it is possible to form stable long openings and erratic openings without bipy.

4.2.3.1 Relationship between bipy, long openings and short openings

The idea that long openings and short openings could be related by an equilibrium pathway was investigated by changing the concentration of bipy in the electrolyte. If long and short openings were related, they would be expected to interconvert and the channel activity observed would depend on the concentration of bipy in the electrolyte. Examples of the effect of changes in speciation due to variations in Pden:bipy ratios were observed for **13** by ^{1}H NMR spectroscopy in chapter 3 and were studied by modelling in chapter 2.

Once a channel was established in the bilayer, the amount of bipy in the electrolyte was increased by addition of bipy solution in aliquots, each of which corresponded to a 100-fold increase in the Pd:bipy ratio assuming that the concentration of Pd in the system is ~ 2×10^{-8} M. The volume of the aliquot added was adjusted so that the concentration of bipy would be equal on both sides of the bilayer (Figure 41). The bipy solution was prepared in methanol so that sufficiently high concentrations could be obtained. The conductance was determined to be 7.6 nS before any bipy was added (Table 10). This corresponds to a radius of 12 Å for a pore 34 Å in length. The first aliquot of bipy increased the conductance of the channel to 12 nS and a second aliquot of bipy increased

the conductance to 23 nS (Table 10). An additional increase in conductance to 62 nS was observed when 250 µl and 150 µl of MeOH were added to the block and cup, respectively (Table 10). The control experiment must be carried out during the course of the actual experiment because the channels with the same dimensions cannot be reliably reproduced for this system. Because conversion from long openings to short openings was not observed, these results suggest that the short openings and long openings are not related by an equilibrium pathway.

The activity of a channel is dependent on the properties of the bilayer[44]. Changes in the ionic strength alters the interaction energy between the lipids in the bilayer which affects the function of certain types of ion channels[41]. The increase in conductance of the long openings observed upon addition of bipy and MeOH might be attributed to a similar phenomenon.

Table 10 Effect of addition of bipy on the conductance of long channels

Addition	Additive	Conductance, nS	Radius at 34 Å
0	none	7.6	13
1	bipy in MeOH	12	17
2	bipy in MeOH	23	26
3	MeOH	62	54

4.2.3.2 Shape parameter and long openings

The molecule **21b** has no special features that would allow it to self-associate into discrete supramolecular structures (type 2b) so how are channels formed from **21b** alone?

Toroidal ion channels can be formed by molecules or aggregates of molecules that stabilize curvature in the membrane bilayer. Melittin is an example of this

type of molecule (chapter 1). The shape of the membrane, whether spherical or planar, depends on the shape parameter of the constituent lipids (Table 11).

Table 11 Shape parameters and structures formed[2]

Shape parameter, P	Shape of lipid	Lipid structure formed
P ≈ 1	cylinder	planar bilayers
0.5 ≤ P < 1	truncated cone	cylindrical micelles
P < 0.5	cone	spherical micelles

The shape parameter (P) is calculated by

$$P = \frac{v}{a_0 l_c}$$

where v is the volume occupied by the lipid chain, a_o is the surface area occupied by the headgroup and l_c is the critical chain length. The optimum surface area occupied by the headgroup is not easily determined without empirical data[42]. The maximum distance observed between the headgroup and the terminal carbon is known as the critical chain length and is calculated using (4-2). The critical chain length is shorter than the fully extended chain length in fluid bilayers. The volume of the lipid chain is determined by (4-3).

$$l(\text{in nm}) \approx 0.154 + 0.1265n \qquad \textbf{(4-2)}$$

$$v(\text{in nm}^3) \approx (27.4 + 26.9n)(0.01\,\text{nm}^3) \qquad \textbf{(4-3)}$$

where, n is the number of carbons in the saturated chain. The upper limit for v/l_c is 0.21 nm^2 and will remain constant for lipids with long chains[42]. Toroidal channels might be formed if P > 1 for **21b**. The term v/l_c is equal to 0.21 nm^2 for molecule **21b**.

The distance between the Pd and H on the amino group is used as a conservative estimate for the size of the headgroup. It is assumed that thermally induced bond rotations will sweep out an area with a radius equal to the size of the headgroup. The distance from Pd to N on the amino group, determined from the crystal

structure[69], is 0.207 nm and a typical N-H bond[104] is 0.101 nm so the total distance between Pd to the H on the amino group is 0.317 nm. Therefore, a_0 would be estimated to be about 0.32 nm^2. With this value, the shape parameter for **21b** would be 0.66 which means that it is a truncated cone. The size of the headgroup is likely to be larger because groups coordinated to the empty sites on Pd have not been included; in this case, the molecule **21b** would still be "conical" because the headgroup radius will be larger therefore the packing parameter would still be less than 1. This rough calculation demonstrates that the shape of **21b** is a truncated cone and would be able to stabilize curvature in the lipid bilayer thereby allowing ion channel formation[42].

It is not clear from the data whether channels formed by **21b** are the result of single species or as aggregates of molecules. A 30-90 min induction period was necessary before any activity was observed; it is possible that this period is required for the formation of small aggregates which are instrumental in pore formation. Pd carries a +2 charge so electrostatic repulsion between the headgroups would prevent direct aggregation between **21b** molecules; aggregates that contain both **21b** and zwitterionic diphyPC lipid are more likely.

The Pden headgroup may also interact with anions, such as OH^-, in the electrolyte. Coordination of Pden with anions would reduce the charge on the headgroup without significantly changing the shape. Titration experiments from chapter 2 and literature data show that $(Pden)_2(OH)_2$ forms at pH greater than 5[84]. The pH of the electrolyte is near neutral therefore $(\mathbf{21b})_2(OH)_2$ may also be possible in the bilayer. Aggregates of **21b** coordinated to anions or hydroxo are more likely because the electrostatic repulsion is reduced. Any aggregates or complexes of **21b** will have $a_0 > 0.57$ nm^2 therefore $P < 1$ which implies that the shape is still a truncated cone and should stabilize curvature in a planar bilayer. Ceramide and helical peptides are examples that demonstrate curvature

stabilization as a mechanism for ion channel formation[44, 45]. The idea that **21b** is coordinated by either lipid or OH^- is supported by the activity observed in the presence of coordinating electrolytes such as Cl^-.

4.2.3.3 Superposition of long openings and erratic behaviors

Sometimes more than one type of channel is observed simultaneously. The current-time recordings are more complicated as the result of the superposition of the activity from the channels being observed (Figure 52). A common scenario is the simultaneous observation of long openings and erratic openings. The behaviour is thought to be from separate types of channels because the activity can be observed separately. Erratic openings are always observed when short openings and long openings are observed. However, the converse has not been observed so it is not clear if the erratic openings and long openings are correlated or coincidental.

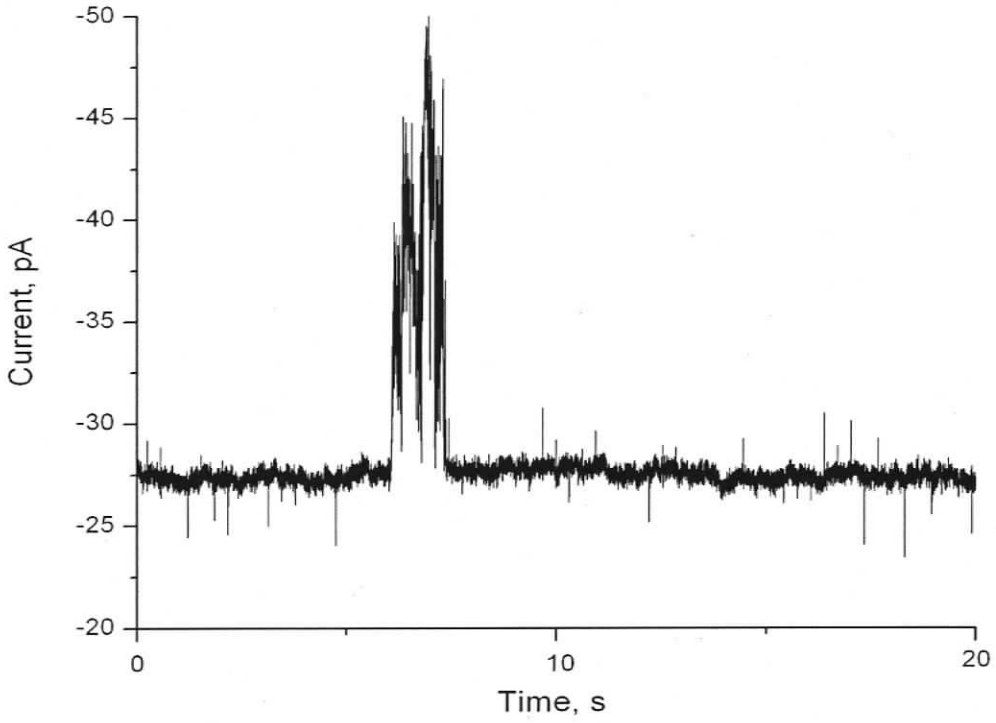

Figure 52 Long opening with erratic activity superimposed. Observed for 14b solution at -100 mV in 0.1M KCl (*cis*) and 0.1 M CsCl (*trans*).

4.2.3.4 Enlargement of pores corresponding to long openings

Sharp transitions between levels are commonly observed in current-time records for ion channels and are usually interpreted as channel openings and closings. The zero level is defined by zero current which means that no channels are open. An increase from the zero level to the first level is interpreted as a channel opening. Subsequent openings from the first level to higher levels may also be observed. Channel openings and closing were seldom observed for long openings. Current-time traces that capture channel openings and closing are even rarer.

Channel openings and closings were observed in one notable experiment. An abrupt transition between the first and second level was observed while the current-voltage relationship for the first level was being tested. The channel was open at the first level for 8 min. A second transition from the second level to the zero level was recorded. The current-voltage relationship of the second level was well characterized before the transition to the zero level. The second level remained open for 15 min before the transition to the zero level was observed.

The conductance for each current-time recording at levels 1 and 2 were determined from the average current and the potential applied and plotted against the time axis (Figure 53). Opening events from the first level to the second level is usually interpreted as the opening of a second channel.

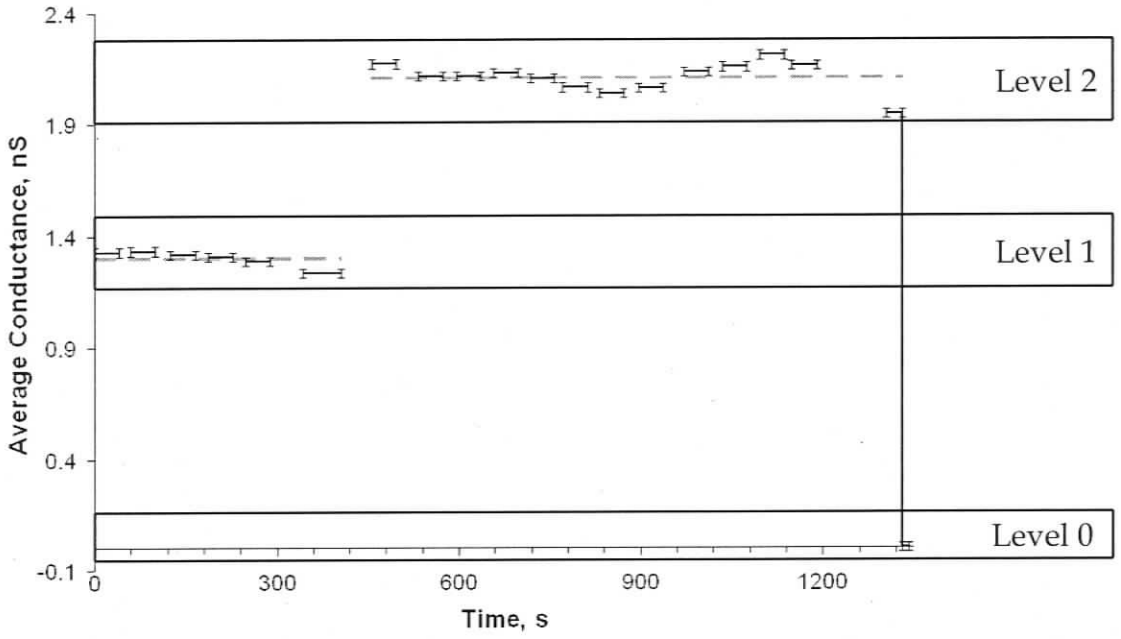

Figure 53 Changes in conductance observed during a single long opening event. The conductance for each recording (solid lines) was calculated from the average current over the 40 second recording. The time resolution of the current-time recording was 100 us. The average conductance for each level (dashed lines) was calculated from the average of all the recordings made at that level.

If the channels are of the same variety, then the conductance observed for the second level should be twice that of the first level. The average conductances observed were 1.3 and 2.1 nS for the first and second levels, respectively. This implies that the channels observed are not the same. The usual interpretation in this case would be that there are two different types of active channels in the bilayer. However, the channel closing observed from the second level to the zero level makes this conclusion unlikely because two channels would have to close simultaneously to give the observed transition. Given the sharpness of the transition, this would be highly improbable. A more likely interpretation of the change in conductance from the first to second level represents an enlargement of an existing channel and the transition from the second level to the zero level is the enlarged channel closing[60].

4.2.3.5 Selectivity of channels corresponding to long openings

The bilayer clamp experiment can also be used to determine the permeability ratio between two ions if different electrolytes are used in each chamber. A channel is said to be selective for an ion if it is more permeable to that ion. The experiment is set-up as shown in Figure 41. It is important to note that *cis* is the cup side, *trans* is the block side and that the *trans* is ground, so the potential is set with respect to the *trans* side. The electrolyte used in the block and cup depend on the permeability ratio being determined. A concentration gradient (and possibly an electric gradient), created by having different electrolytes in the cup and block, drives the ions across the bilayer which gives rise to an observable current. The potential required to negate the ion flux across the bilayer is known as the reversal potential, E_{rev}. Values for E_{rev} are determined by plotting the current-voltage relationship and finding the x-intercept on the I-V plot. Positive values for E_{rev} would be expected if the ion channel was selective for ion A using the experimental set-up described.

The Goldman-Hodgkin-Katz (GHK) voltage equation (4-4) formed the theoretical basis for determining the permeability ratio, P_A/P_B, using the experimental set-up described[105]. The variables R, T and F are the ideal gas constant, temperature in Kelvin and Faraday constant, respectively. The term RT/F is 25.5 mV at 23°C. P_K, P_{Na} and P_{Cl} are the membrane permeability of the ion K^+, Na^+ and Cl^-, respectively. Activity should be used in calculations instead of concentration even though concentration terms are used in the equation for simplicity.

$$V = \frac{RT}{F} \ln \frac{P_{Na}\gamma_{Na}[Na^+]_{trans} + P_{Cs}\gamma_{Cs}[Cs^+]_{trans} + P_{Cl}\gamma_{Cl}[Cl^-]_{trans}}{P_{Na}\gamma_{Na}[Na^+]_{cis} + P_{Cs}\gamma_{Cs}[Cs^+]_{cis} + P_{Cl}\gamma_{Cl}[Cl^-]_{cis}} \qquad (4\text{-}4)$$

This equation is derived under the assumption that a membrane with ion channels can be modelled by a uniform slab in which the electric field gradient and concentration gradient drive ions across the membrane. It also assumes that ions diffuse spontaneously from the solution into the slab and that ions can behave independently. These assumptions restrict the application of the GHK voltage equation to systems that compare ions with the same charge and systems in which ions respond to concentration and inhomogeneties in diffusion coefficient in the bilayer and water-membrane partition coefficient in the same way. The GHK equation is derived specifically for Na^+, K^+ and Cl^- ions but can be expressed more generally as (4-5)[106]. Table 12 presents the general equation in more practical forms that are tailored for use in the scenarios specified. Cases 1-3 are used to determine the permeability ratio for ions with the same polarity. Case 4 is used to determine the permeability ratio for cations and anions with the same valence but opposite charge, for example P_K/P_{Cl}.

$$\frac{P_a}{P_b} = \frac{z_b^2\left(b_{cis} - b_{trans}\exp(-z_b V_r / M)\right)}{z_a^2\left(a_{cis} - a_{trans}\exp(-z_a V_r / M)\right)} \bullet \frac{1-\exp(-z_a V_r / M)}{1-\exp(-z_b V_r / M)} \qquad (4\text{-}5)$$

Table 12 Equations used to calculate permeability ratios for various ions

Case	*Cis* electrolyte	*Trans* electrolyte	Equation
1	$A^{+1\ (or\ -1)}$	$B^{+1\ (or\ -1)}$	$\frac{P_A}{P_B} = \frac{B^+_{cis}}{A^+_{trans}}\exp\left(\frac{FV_r}{RT}\right)$
2	A^{2+}	B^{2+}	$\frac{P_A}{P_B} = \frac{B^{2+}_{cis}}{A^{2+}_{trans}}\exp\left(\frac{2FV_r}{RT}\right)$
3	A^{1+}	B^{2+}	$\frac{P_A}{P_B} = \frac{B^+_{cis}\left\{\exp\left(\frac{FV_r}{RT}\right)\right\}\left\{\exp\left(\frac{FV_r}{RT}\right)+1\right\}}{4A^{2+}_{trans}}$
4	A^{1+}	B^{1-}	$\frac{P_{A^+}}{P_{B^-}} = \frac{B^-_{cis} - QB^-_{trans}}{QA^+_{cis} - A^+_{trans}}$ where, $Q = \exp\left(\frac{V_r F}{RT}\right)$

The diameter of an ion channel restricts the species that can pass through the channel. For many ion channels, the ions must shed some of the water molecules located in the hydration sphere before it can pass through the channel. Selectivity in these channels is governed by the dehydration energies of particular ions. The dehydration energies of group 1 cations in weak field binding sites are summarized by the Eisenmann I series $Cs^+ > Rb^+ > K^+ > Na^+ > Li^+$ in which Cs^+ is dehydrated most easily[2].

The selectivity of channels responsible for long openings was examined to gain insight into the structure of the channel. Channels that contain a number of Pd cations would carry a high positive charge and would be expected to be anion selective. Our experiments showed there was little selectivity between Cs/Cl, Cl/Br or K/Cs (Table 13). Channels with good selectivity have permeability ratios < 0.2, very selective channels such as gramicidin have ratios < 0.007[2]. Poor ion selectivity is consistent with ion channels that have large pores and diffuse charge. The selectivity of long openings is consistent with channels formed by **21b** complexed with anionic ligands because the charge on the Pd centre would be neutralized. Therefore, electrostatic interactions would not influence ion selectivity.

Table 13 Permeability ratios for channels observed using 14b solutions

Ion a	Ion b	P_a/P_b	Reversal potential, mV
Cs	Cl	1.1	1.74, 1.79
Cl	Br	0.63	-11.8
K	Cs	0.66	-10.5

4.3 Conclusions

The original design of the channel assumed that the square would form a portal through which ions could pass. The radii of channels such as these would be expected to be of uniform radius because the structure would have well defined stoichiometry. The channel radius was expected to be ~ 4-5 Å. It was assumed that the channels would in equilibrium with other $(\mathbf{21b})_p(bipy)_b(H)_h$ species in the bilayer so channel openings and closings would also be observed.

Erratic, short and long openings were observed when solutions of **14b** were added to the bilayer. Erratic activity was observed for each experiment that showed activity. The nature of the activity did not allow it to be studied in detail. Short openings were rarely observed so estimates of channel radii were made using single current-voltage relationships. The estimated radii ranged between 1 and 7 Å. Unfortunately, short openings occur too infrequently to study in more detail. Long channels in contrast were amenable to characterization using a range of methods. The long channels occur regularly and are always preceded by a 30 min period of sporadic erratic activity. Channel radii for long openings varied between 1 and 15 Å. The idea that **21b** is strongly coordinated to a ligating species in the channel is supported by the lack of ion selectivity observed for long openings and lack of sensitivity in the activity observed when coordinating electrolytes are used. Control experiments demonstrate that erratic and long opening behaviour can be also observed in the presence of **21b** alone.

An observation in which a level one long opening increases to a level two opening followed by a closing event from level two to level zero is strong evidence that long channels can undergo a growth mechanism. How growth occurs cannot be determined without more structure-function studies.

Channels are formed by solutions of **21b** in the absence of bipy therefore erratic and long openings are not the result of channels formed by **14b**. Short channels have channel radii and lifetimes that are appropriate for channels formed using the square as portals, however the radii varied, which is not expected for channels that have fixed stoichiometry. The variation in radii observed for both the short and long openings is indicative of channels without fixed stoichiometry.

4.4 Experimental section

4.4.1 Experimental for bilayer work

Water purified using a Millipore filtration system was used for all parts of the experiment. Electrolytes were prepared from reagent grade salts from a commercial source without purification. Decane was purchased from a commercial source and used without purification.

Agar solution was prepared by mixing 10 g of KNO_3, 1 g of agar and 100 ml of water then heating the mixture while stirring until the contents made a colourless solution. The bridges were prepared by immersing 8.5 cm lengths of glass tubing bent into a hook shape with an outer diameter of 3 mm and an inner diameter of 2 mm in the prepared agar solution. The bridges were cut out of the agar and rinsed with some deionized water before they were used.

The lipid diphyPC was purchased from Avanti and was used to prepare the planar lipid membrane. The lipid was purchased as a solution in chloroform and

divided into crimp sealed glass vials in 5mg aliquots of lipid and stored in the freezer.

The general experimental set-up is pictured in Figure 41. The cups have 250 μm apertures and were made of polystyrene (Warner Instruments). The blocks were made out of polytetrafluoroethylene. The set up pictured in Figure 41 is enclosed in a Faraday cage suspended on a floating platform in order to dampen the environmental noise. The bilayer clamp instrument used is model BC-525A from Warner Instruments. The signal was manipulated by filtering it through a 1 kHz analog filter and 0.05 kHz digital filter before being recorded. A salt bridged connected each chamber with two shell vials containing 1 M KCl. A silver wire coated in AgCl was immersed in the each of the shell vials and connected to the headstage. The headstage was electrically grounded. The junction potential was adjusted to zero before the bilayer was formed. Measurements were made with respect to the *trans* side, which is ground (Figure 41).

Planar lipid membrane preparation

The chloroform was removed from 5 mg of diphyPC in a crimp sealed vial by a stream of nitrogen through the vial for at least 30 minutes. The lipid was redissolved in 200 μl of decane to give a clear colourless solution. The area around the aperture in the cup was painted with a small amount of the lipid solution. The solvent was evaporated from the area under a stream of nitrogen. The *cis* and *trans* chambers (as defined in Figure 41) were filled with 5 ml and 3 ml of electrolyte, respectively. A 0/5 or 0/10 paint brush wetted with the lipid solution was drawn over the aperture to form the bilayer. The bilayer was formed by dipping the cup in and out of the block.

The quality of the bilayer is judged by the bilayer thickness and how well the bilayer insulates the two chambers. The thickness of the bilayer is assessed by testing the capacitance of the bilayer using the capacitance test function. The instrument applied a 100 Hz triangle wave across the bilayer. A good bilayer is a good capacitor and will charge and discharge with the same frequency. The output is observed as square wave and the instrument is calibrated such that a good bilayer will have a peak height of at least 10 mV. Dipping the cup or drawing a paint brush over the annulus is often necessary to achieve an acceptable thickness. The insulating properties can be accessed in a qualitative manner using the shape of the square wave. A good bilayer should form a seal around the annulus and is therefore an effective insulator between the *cis* and *trans* chambers. The square wave observed for a good bilayer will have flat peaks with zero slope. A leaky bilayer will have sloped peaks. The insulating ability of the bilayer can also be tested quantitatively by applying ± 100 mV across the two chambers for at least 40 s. If the current is less than 1 pA then the bilayer is accepted.

Once a bilayer was established it was generally robust. In cases where the bilayer was broken during the course of an experiment, it could be reformed by dipping or drawing a wetted brush over the annulus. The capacitance and the ability to form a square wave were checked to ensure that the bilayer was of acceptable quality. Capacitance was checked periodically over the course of an experiment, occasionally the capacitance would decrease indicating that the bilayer had thickened. The cup was re-dipped until bilayer of more acceptable capacitance was re-established.

Cleaning procedure

The block and cup were rinsed with water and then sonicated for 1 hour in 95% ethanol. Syringes and brushes were rinsed with hexane and ethanol then sonicated for 1 hour in 95% ethanol. Fresh agar bridges were used for each experiment.

Introducing the channel forming compound

The complex **14b** is formed with limited solubility in acetonitrile by mixing **21b** and bipy in a 1:1 ratio in a test tube outfitted with a stir bar. A small amount of precipitate was formed after the addition of bipy. ^{1}H NMR spectrum of the solution showed that the aromatic region had shifted in a way that was consistent with **13**. Solutions of **14b** were prepared so that the final [Pd] ≈ 10 mM.

Method A – brushing

A paint brush is wetted with **14b** solution is drawn over the lipid membrane.

Method B – mixing with lipid

50ul of **14b** solution is mixed with 5 mg of lipid dissolved in chloroform. The solvents are removed under a stream of nitrogen and the residue is reconstituted in 200 µl of decane. The solution is used to make the lipid bilayer. This method did not lead to reliable channel formation.

Resistivity determination

Resistivity was required to calculate the ion channel radius from the conductance data collected. Values for resistivity in S/m were determined from equivalent

conductivity in ohm/cm^2 mol or specific conductivity in ohm·m from the literature. Specific conductivity was plotted as a function of concentration for a given temperature and interpolated or extrapolated to relevant concentration. The resistivity is then plotted against temperature and interpolated or extrapolated to 22 and 26 °C. These values were used to calculate the channel radii.

5 Conclusions and future work

The object of this thesis was to identify parameters that are important to self-assembly in a bilayer membrane through the complex **14** which was expected to form an ion channel. A model for the self-assembly **13** was developed in order to determine the pH and Pden:bipy ratios that would produce optimum amounts of **440**. The method used to make this model is general and improves upon current models for supramolecular self-assembled systems because it is able to incorporate more than two components and will apply to non-stoichiometric conditions.

Erratic, short and long opening activity was observed for solutions of **14b** using the bilayer clamp technique. Square top behaviour with conductances which correspond to pores of uniform size was never observed. Although erratic and short openings were too random or too infrequent to study, long opening activity was studied in detail. The discovery of long channel activity was an interesting but unexpected outcome of the bilayer experiments. The variation in channel radii, the stepwise increase in radius of a single channel, and the lack of selectivity observed are curious characteristics for synthetic ion channels but control experiments suggest that long openings are the result of **21b** or aggregates of **21b.** Future work aimed towards understanding the structure of large and stable pores could be pursued by changing the lipid used to form the bilayer and varying the coordination geometry of the metal centre.

The molecule **21b** has a shape parameter consistent with a truncated cone which may result in the long opening activity observed by stabilizing curvature in the bilayer membrane. To test this proposal, molecules with different shape parameters could be examined. The lipid part of the channel could also be

changed to try to match the size of the headgroup, in which case the molecule would be cylindrical and should not make channels. The size of the headgroup could also be changed so that the conical shape would be more pronounced which should stabilize greater curvature.

The species included in the model were based on equilibria in solution and did not include species with lipid interactions. The lipid used to make the bilayer is zwitterionic and was not expected to interact with **21b**, bipy or complexes that involved either of these components; if **21b** was coordinated by lipid, then a new species would be introduced to the equilibrium which would affect the speciation in the bilayer such that **14b** is not formed in appreciable amounts. The model could be modified to include species that are complexed by lipid if log*K* for these interactions were known.

The model for Pden+bipy shows that the **440** species is favoured in slightly acidic solution but when the pH > 7 the prevalence of **440** diminishes quickly while the concentration of Pd species containing OH^- increase. For [Pd] = 1×10^{-5} M, Pden:bipy = 1:1 and pH = 8, the relative ratio of $[OH^-]_{total}$:$[Pd]_{total}$ is about 1:9 and the species **440** holds less than 5% of the total Pd. It would be reasonable to assume that lipid and **21b** form complexes through the phosphate oxygens; thus can be roughly approximated by Pden species containing OH^- in the solution model. Because the [bipy]:[lipid] is << 1:9 in the headgroup region, bipy will not be able to compete with the lipid for coordination sites on **21b** at the bilayer surface, so this design under the conditions used is ultimately doomed. Even the addition of bipy to the electrolyte in 200 fold excess did not change the type of activity observed.

In order to make a self-assembled complex in the bilayer headgroup region, either the local concentration has to be high enough to keep the complex together

or the bond between the components has to be energetic enough to compete with the interactions with the bilayer. The present design based on **14b** might work if the competition between bilayer lipid and bipy for coordination with **21b** can be minimized by using neutral, non-coordinating bilayers. In addition, the local concentration of bipy could be improved by derivatizing bipy with using long aliphatic chains so that bipy partitions into the bilayer headgroup region more efficiently. These changes in the design would facilitate Pden-bipy self-assembly by making Pden-bipy interactions more favourable in the bilayer environment.

The major difference noted when the proposed design is compared to other type 2 channel designs is that successful designs have multiple intermolecular bonding interactions between the molecules that make up the channel. The proposed design uses only one Pd-bipy bond to hold the structure together. Comparing the square design with other type 2 designs shows that multiple intermolecular bonds may be more important than the strength of individual bonds. Future designs for metallosupramolecular channels should take this into consideration. The present design can be augmented using Pt(diPPh$_2$) derivatives as the corners instead of **21b** because the Pt-bipy bonds are slightly more robust than Pd-bipy bonds[107]; however, the self-assembly process would be irreversible at room temperature so would be formed by the pathway K_{a1} followed by K_{2AB} as outlined in Figure 1. Although this pathway has been established as a successful strategy, it does not make use of the pathway K_{2a} and K_{2b} followed by K_{1b}, which has been under utilized in synthetic ion channel designs thus far.

Future designs for self-assembled ion channels should consider the thermodynamic and kinetic stability of the channel. Greater thermodynamic stability would help to keep the molecule together in an environment where there are competing ligands such as bilayer lipids. Thermodynamic stability of a self-assembled complex can be improved using stronger intermolecular

interactions or multiple interactions. Intramolecular reactions happen faster than intermolecular reactions so multidentate ligands also have a greater chance of reforming should a metal ligand bond break. Reactions with competing species are minimized by the enhanced kinetic and thermodynamic stability of multiple points of attachment between the components in the channel. Future designs should increase the number of attachment points between the components in the self-assembled structure.

Currently, type 2 channel designs reported in the literature utilize at least three intermolecular bonds between components of the channel. One important outcome of this thesis is that one bond worth ~ 29 kJ/mol is insufficient to stabilize **14b** in a diphyPC bilayer. The minimum energy required to form a supramolecular complex in a bilayer might be determined by derivatizing a self-assembled system so that the number and strength of the intermolecular bonds can be changed until a stable self-assembled channel is observed. Models like the one presented for **13** would be useful in determining the energetics and speciation of these self-assembled system both in solution and in the bilayer. This question would also be greatly simplified if the lipid in the bilayer was non-coordinating.

As supramolecular science continues to advance, methods of visualizing the equilibrium self-assembly process will become more important. Models that describe self-assembly will enable the field to move towards more rational design approaches. The model described in this thesis is a general method that can be applied to any equilibrium self-assembly process provided that formation constants are known.

6 Appendices

Appendix 1 Summary of logβ, log$Y$, log$K$ and logK' values obtained from model titrations at 25 °C in 0.1 M KNO_3 or 0.1 M $NaClO_4$

Synthon 1	Synthon 2	logβ	logβ	Average logβ	Y	log$Y$	log β'	logK'	Average logK'	Ref
Pden	py	5.44		5.44	4	0.60	4.84	4.84		
Pden	3ppy	5.54		5.54	2	0.30	5.24	5.24		
Pden	4ppy	5.95		5.95	4	0.60	5.35	5.35		
Pden	pyR								5.14	
Pdenpy	py	11.37	11.24	11.31	4	0.60	10.77	5.93		
Pden3ppy	3ppy	10.80		10.80	1	0.00	10.80	5.56		
Pden4ppy	4ppy	12.09		12.09	4	0.60	11.49	6.14		
Pddien	bipy	6.07		6.07	2	0.30	5.77	5.77		
Pdenpy	pyR								5.85	
Pdenpy	OH	-0.89	-1.03	-0.96	4	0.60	-1.49	-6.33		
Pden3ppy	OH	-1.18		-1.18	2	0.30	-1.48	-6.73		
Pden4ppy	OH	-0.15		-0.15	4	0.60	-0.75	-6.10		
PdenpyR	OH								-6.39	
Pddien	bipy	6.07		6.07	2	0.30	5.77			
									5.77	
Pddienbipy	H	10.71		10.71	2	0.30	10.41	4.64		
									4.64	
Pddien	OH	-7.21	-7.97	-7.59	1	0.00	-7.59			
									-7.59	
Pddienbipy	Pddien	11.26		11.26	4	0.60	10.66	4.89		
									4.89	
PdenOH	OH	-14.71		-14.71	1	0.00	-14.71			
									-14.71	84
PdenOH	PdenOH	-8.10		-8.10	2	0.30	-8.40			
									-8.40	84
bipy	H	4.73	4.68	4.71	2	0.30	4.40			
									4.40	76
bipyH	H	7.62	7.33	7.48	1	0.00	7.48	3.07		
									3.07	76

Appendix 2 Estimated logβ values used in the HySS simulation of Pden+bipy solutions

pbh	logβ	pbh	logβ	pbh	logβ
10-2	-14.7	**340**	34.1	**661**	66.8
20-2	-8.4	**341**	39.0	**670**	68.0
011	4.4	**342**	43.3	**671**	72.9
012	7.5	**43-2**	20.4	**672**	77.2
00-1	-13.8	**43-1**	27.1		
110	5.70	**430**	33.2		
120	11.50	**44-1**	33.2		
11-1	-0.70	**440**	43.9		
111	10.30	**441**	44.2		
122	20.70	**450**	45.4		
121	16.40	**451**	50.3		
21-2	-2.2	**452**	54.6		
21-1	4.5	**54-2**	31.7		
210	10.6	**54-1**	38.4		
22-1	10.6	**540**	44.5		
220	17.0	**55-1**	44.5		
221	21.6	**550**	50.9		
230	22.8	**551**	55.5		
231	27.7	**560**	56.7		
232	32.0	**561**	61.6		
32-2	9.1	**562**	65.9		
32-1	15.8	**65-2**	43.0		
320	21.9	**65-1**	49.7		
33-1	21.9	**650**	56.1		
330	28.3	**66-1**	55.8		
331	32.9	**660**	61.9		

Appendix 3 COSY spectrum for 17b

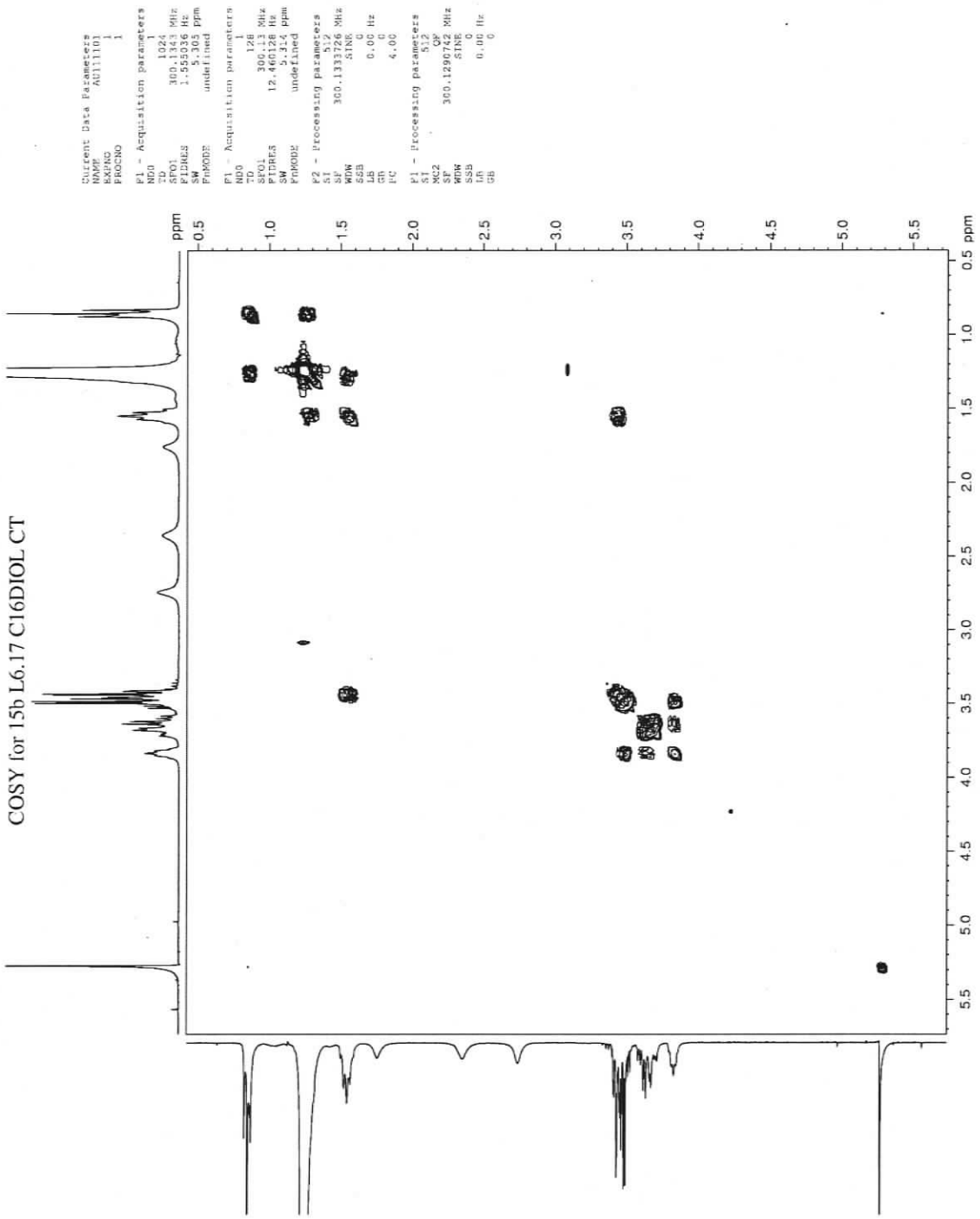

7 References

1. Saier Jr., M. H. M., G.P.; Kotyk, A., Membrane Transport Proteins. In Nomenclature Committee of the International Union of Biochemistry and Molecular Biology (NC-IUBMB): 2002.
2. Hille, B., *Ionic Channels of Excitable Membranes*. Sinauer Associates, Inc.: Sunderland, 1984.
3. Amberg, G. C.; Koh, S. D.; Imaizumi, Y. J.; Ohya, S.; Sanders, K. M., A-type potassium currents in smooth muscle. *American Journal Of Physiology-Cell Physiology* 2003, 284, (3), C583-C595.
4. Tsien, R. W.; Ellinor, P. T.; Horne, W. A., Molecular Diversity Of Voltage-Dependent Ca2+ Channels. *Trends In Pharmacological Sciences* 1991, 12, (9), 349-&.
5. Jentsch, T. J.; Stein, V.; Weinreich, F.; Zdebik, A. A., Molecular structure and physiological function of chloride channels. *Physiological Reviews* 2002, 82, (2), 503-568.
6. Mandegar, M.; Remillard, C. V.; Yuan, J. X. J., Ion channels in pulmonary arterial hypertension. *Progress In Cardiovascular Diseases* 2002, 45, (2), 81-114.
7. Siegelbaum, S. A.; Koester, J., Ion Channels. In *Principles of neural science*, Kandel, E. R.; Scharrtz, J. H.; Jessel, T. M., Eds. McGraw–Hill: New York, 2000; p 105–125.
8. Woolley, G. A.; Lougheed, T., Modeling ion channel regulation. *Current Opinion in Chemical Biology* 2003, 7, (6), 710-714.
9. Bezanilla, F., The voltage sensor in voltage-dependent ion channels. *Physiological Reviews* 2000, 80, (2), 555-592.
10. McNaughton, P. A., Light Response Of Vertebrate Photoreceptors. *Physiological Reviews* 1990, 70, (3), 847-883.
11. Gillespie, P. G.; Walker, R. G., Molecular basis of mechanosensory transduction. *Nature* 2001, 413, (6852), 194-202.
12. Hamill, O. P.; Martinac, B., Molecular basis of mechanotransduction in living cells. *Physiological Reviews* 2001, 81, (2), 685-740.
13. Jiang, Y. X.; Lee, A.; Chen, J. Y.; Ruta, V.; Cadene, M.; Chait, B. T.; MacKinnon, R., X-ray structure of a voltage-dependent K+ channel. *Nature* 2003, 423, (6935), 33-41.
14. Koert, U., Synthetic ion channels: Functional analysis and structural studies. *Physical Chemistry Chemical Physics* 2005, 7, (7), 1501-1506.
15. Bayley, H.; Cremer, P. S., Stochastic sensors inspired by biology. *Nature* 2001, 413, (6852), 226-230.
16. Hector, R. S.; Gin, M. S., Signal-triggered transmembrane ion transport through synthetic channels. *Supramolecular Chemistry* 2005, 17, (1-2), 129-134.
17. Sakai, N.; Mareda, J.; Matile, S., Rigid-rod molecules in biomembrane models: From hydrogen-bonded chains to synthetic multifunctional pores. *Accounts of Chemical Research* 2005, 38, (2), 79-87.

18. Sakai, N.; Matile, S., Synthetic multifunctional pores: lessons from rigid-rod beta-barrels. *Chemical Communications* 2003, (20), 2514-2523.
19. Matile, S., En route to supramolecular functional plasticity: artificial beta-barrels, the barrel-stave motif, and related approaches. *Chemical Society Reviews* 2001, 30, (3), 158-167.
20. Leevy, W. M.; Gokel, M. R.; Hughes-Strange, G. B.; Schlesinger, P. H.; Gokel, G. W., Structure and medium effects on hydraphile synthetic ion channel toxicity to the bacterium E-coli. *New Journal Of Chemistry* 2005, 29, (1), 205-209.
21. Fernandez-Lopez, S.; Kim, H. S.; Choi, E. C.; Delgado, M.; Granja, J. R.; Khasanov, A.; Kraehenbuehl, K.; Long, G.; Weinberger, D. A.; Wilcoxen, K. M.; Ghadiri, M. R., Antibacterial agents based on the cyclic D,L-alpha-peptide architecture. *Nature* 2001, 412, (6845), 452-455.
22. Matile, S.; Som, A.; Sorde, N., Recent synthetic ion channels and pores. *Tetrahedron* 2004, 60, (31), 6405-6435.
23. Chen, W. H.; Shao, X. B.; Regen, S. L., Poly(choloyl)-based amphiphiles as pore-forming agents: Transport-active monomers by design. *Journal Of The American Chemical Society* 2005, 127, (36), 12727-12735.
24. Gokel, G. W.; Mukhopadhyay, A., Synthetic models of cation-conducting channels. *Chemical Society Reviews* 2001, 30, (5), 274-286.
25. Horne, W. S.; Ashkenasy, N.; Ghadiri, M. R., Modulating charge transfer through cyclic D,L-alpha-peptide self-assembly. *Chemistry-A European Journal* 2005, 11, (4), 1137-1144.
26. Lehn, J.-M., *Supramolecular Chemistry: Concepts and Perspectives*. Wiley-VCH: Weinheim, 1995.
27. Atwood, J. L.; Lehn, J.-M., *Comprehensive supramolecular chemistry*. Pergamon: New York, 1996.
28. Pfeifer, J. R.; Reiss, P.; Koert, U., Crown ether-gramicidin hybrid ion channels: Dehydration-assisted ion selectivity. *Angewandte Chemie-International Edition* 2006, 45, (3), 501-504.
29. Eggers, P. K.; Fyles, T. M.; Mitchell, K. D. D.; Sutherland, T., Ion channels from linear and branched bola-amphiphiles. *Journal Of Organic Chemistry* 2003, 68, (3), 1050-1058.
30. van Maarseveen, J. H.; Horne, W. S.; Ghadiri, M. R., Efficient route to C-2 symmetric heterocyclic backbone modified cyclic peptides. *Organic Letters* 2005, 7, (20), 4503-4506.
31. Piguet, C.; Borkovec, M.; Hamacek, J.; Zeckert, K., Strict self-assembly of polymetallic helicates: the concepts behind the semantics. *Coordination Chemistry Reviews* 2005, 249, (5-6), 705-726.
32. Piguet, C.; Borkovec, M.; Hamacek, J., Simple thermodynamics for unravelling sophisticated self-assembly processes. *Dalton Transactions* 2006, (12), 1473-1490.

33. Fujita, M.; Tominaga, M.; Hori, A.; Therrien, B., Coordination assemblies from a Pd(II)-cornered square complex. *Accounts of Chemical Research* 2005, 38, (4), 369-378.
34. Wilkinson, G.; Gillard, R. D.; McCleverty, J. A., *Comprehensive coordination chemistry: the synthesis, reactions, properties & applications of coordination compounds.* Pergamon Press: Oxford, 2004.
35. Tominaga, M.; Suzuki, K.; Kawano, M.; Kusukawa, T.; Ozeki, T.; Sakamoto, S.; Yamaguchi, K.; Fujita, M., Finite, spherical coordination networks that self-organize from 36 small components. *Angewandte Chemie-International Edition* 2004, 43, (42), 5621-5625.
36. Kusukawa, T.; Fujita, M., Self-assembled M6L4-type coordination nanocage with 2,2 '-bipyridine ancillary ligands. Facile crystallization and X-ray analysis of shape-selective enclathration of neutral guests in the cage. *Journal Of The American Chemical Society* 2002, 124, (45), 13576-13582.
37. Kusukawa, T.; Yoshizawa, M.; Fujita, M., Probing guest geometry and dynamics through host-guest interactions. *Angewandte Chemie-International Edition* 2001, 40, (10), 1879-1884.
38. Kusukawa, T.; Fujita, M., "Ship-in-a-bottle" formation of stable hydrophobic dimers of cis-azobenzene and -stilbene derivatives in a self-assembled coordination nanocage. *Journal Of The American Chemical Society* 1999, 121, (6), 1397-1398.
39. Kusukawa, T.; Fujita, M., Encapsulation of large, neutral molecules in a self-assembled nanocage incorporating six palladium(II) ions. *Angewandte Chemie-International Edition* 1998, 37, (22), 3142-3144.
40. Ito, H.; Kusukawa, T.; Fujita, M., Wacker oxidation in an aqueous phase through the reverse phase-transfer catalysis of a self-assembled nanocage. *Chemistry Letters* 2000, (6), 598-599.
41. White, S. H., The Physical Nature of Planar Bilayer Membranes. In *Ion Channel Reconstitution*, Miller, C., Ed. Plenum Press: New York, 1986; pp 3-35.
42. Israelachvili, J., *Intermolecular and surface forces*. 2nd ed.; Academic Press: London, 1992.
43. Huang, H. W.; Chen, F. Y.; Lee, M. T., Molecular mechanism of peptide-induced pores in membranes. *Physical Review Letters* 2004, 92, (19).
44. Lee, M. T.; Chen, F. Y.; Huang, H. W., Energetics of pore formation induced by membrane active peptides. *Biochemistry* 2004, 43, (12), 3590-3599.
45. Zemel, A.; Fattal, D. R.; Ben-Shaul, A., Energetics and self-assembly of amphipathic peptide pores in lipid membranes. *Biophysical Journal* 2003, 84, (4), 2242-2255.
46. Gokel, G. W., Hydraphiles: design, synthesis and analysis of a family of synthetic, cation-conducting channels. *Chemical Communications* 2000, (1), 1-9.
47. Bong, D. T.; Clark, T. D.; Granja, J. R.; Ghadiri, M. R., Self-assembling organic nanotubes. *Angewandte Chemie-International Edition* 2001, 40, (6), 988-1011.

48. Fyles, T. M.; Hu, C. W.; Knoy, R., Transmembrane ion conductance by an acyclic bolaamphiphile. *Organic Letters* 2001, 3, (9), 1335-1337.
49. Riddell, F. G.; Hayer, M. K., The Monensin-Mediated Transport Of Sodium-Ions Through Phospholipid-Bilayers Studied By Na-23-Nmr Spectroscopy. *Biochimica Et Biophysica Acta* 1985, 817, (2), 313-317.
50. Riddell, F. G.; Arumugam, S.; Brophy, P. J.; Cox, B. G.; Payne, M. C. H.; Southon, T. E., The Nigericin-Mediated Transport Of Sodium And Potassium-Ions Through Phospholipid-Bilayers Studied By Na-23 And K-39 Nmr-Spectroscopy. *Journal Of The American Chemical Society* 1988, 110, (3), 734-738.
51. Gokel, G. W.; Ferdani, R.; Liu, J.; Pajewski, R.; Shabany, H.; Uetrecht, P., Hydraphile channels: Models for transmembrane, cation-conducting transporters. *Chemistry-A European Journal* 2001, 7, (1), 33-39.
52. Weber, M. E.; Schlesinger, P. H.; Gokel, G. W., Dynamic assessment of bilayer thickness by varying phospholipid and hydraphile synthetic channel chain lengths. *Journal Of The American Chemical Society* 2005, 127, (2), 636-642.
53. Leevy, W. M.; Donato, G. M.; Ferdani, R.; Goldman, W. E.; Schlesinger, P. H.; Gokel, G. W., Synthetic hydraphile channels of appropriate length kill Escherichia coli. *Journal Of The American Chemical Society* 2002, 124, (31), 9022-9023.
54. Murray, C. L.; Shabany, H.; Gokel, G. W., The central 'relay' unit in hydraphile channels as a model for the water-and-ion 'capsule' of channel proteins. *Chemical Communications* 2000, (23), 2371-2372.
55. Shabany, H.; Gokel, G. W., Enhancement of cation transport in synthetic hydraphile channels having covalently-linked headgroups. *Chemical Communications* 2000, (23), 2373-2374.
56. Weber, M. E.; Elliott, E. K.; Gokel, G. W., Activity of synthetic ion channels is influenced by cation-pi interactions with phospholipid headgroups. *Organic & Biomolecular Chemistry* 2006, 4, (1), 83-89.
57. Shabany, H.; Murray, C. L.; Gloeckner, C. A.; Grayson, M. A.; Gross, M. L.; Gokel, G. W., Evidence for multiple alkali metal cation complexation in membrane-spanning ion transporters. *Chemical Communications* 2000, (23), 2375-2376.
58. Bandyopadhyay, P.; Janout, V.; Zhang, L. H.; Sawko, J. A.; Regen, S. L., An ion conductor derived from spermine and cholic acid. *Journal Of The American Chemical Society* 2000, 122, (51), 12888-12889.
59. Fyles, T. M.; Knoy, R.; Mullen, K.; Sieffert, M., Membrane activity of isophthalic acid derivatives: Ion channel formation by a low molecular weight compound. *Langmuir* 2001, 17, (21), 6669-6674.
60. Siskind, L. J.; Davoody, A.; Lewin, N.; Marshall, S.; Colombini, M., Enlargement and contracture of C-2-ceramide channels. *Biophysical Journal* 2003, 85, (3), 1560-1575.

61. Yang, L.; Harroun, T. A.; Weiss, T. M.; Ding, L.; Huang, H. W., Barrel-stave model or toroidal model? A case study on melittin pores. *Biophysical Journal* 2001, 81, (3), 1475-1485.
62. Chen, C. C.; England, S.; Akopian, A. N.; Wood, J. N., A sensory neuron-specific, proton-gated ion channel. *Proceedings Of The National Academy Of Sciences Of The United States Of America* 1998, 95, (17), 10240-10245.
63. Seo, J.; Ionescu-Zanetti, C.; Diamond, J.; Lal, R.; Lee, L. P., Integrated multiple patch-clamp array chip via lateral cell trapping junctions. *Applied Physics Letters* 2004, 84, (11), 1973-1975.
64. Ishida, H.; Qi, Z.; Sokabe, M.; Donowaki, K.; Inoue, Y., Molecular design and synthesis of artificial ion channels based on cyclic peptides containing unnatural amino acids. *Journal Of Organic Chemistry* 2001, 66, (9), 2978-2989.
65. Imoto, K., Ion Channels - Molecular-Basis Of Ion Selectivity. *Febs Letters* 1993, 325, (1-2), 100-103.
66. Fujita, M.; Yazaki, J.; Ogura, K., Preparation of a Macrocyclic Polynuclear Complex, (En)Pd(4,4'-Bpy) 4(No3)8, Which Recognizes an Organic-Molecule in Aqueous-Media. *Journal of the American Chemical Society* 1990, 112, (14), 5645-5647.
67. Bianchi, A.; Bowman-James, K.; Garcia-Espana, E., *Supramolecular Chemistry of Anions*. John Wiley & Sons, Inc.: New York, 1997.
68. Fujita, M.; Yazaki, J.; Ogura, K., Macrocyclic Polynuclear Complexes [(En)M(4,4'-Bpy)]4(No3)8 (M = Pd Or Pt) As Inorganic Cyclophane - Their Ability For Molecular Recognition. *Tetrahedron Letters* 1991, 32, (40), 5589-5592.
69. Fujita, M.; Sasaki, O.; Mitsuhashi, T.; Fujita, T.; Yazaki, J.; Yamaguchi, K.; Ogura, K., On the structure of transition-metal-linked molecular squares. *Chemical Communications* 1996, (13), 1535-1536.
70. Ercolani, G., A model for self-assembly in solution. *Journal of Physical Chemistry B* 2003, 107, (21), 5052-5057.
71. Borkovec, M.; Hamacek, J.; Piguet, C., Statistical mechanical approach to competitive binding of metal ions to multi-center receptors. *Dalton Transactions* 2004, (24), 4096-4105.
72. Zeckert, K.; Hamacek, J.; Rivera, J. P.; Floquet, S.; Pinto, A.; Borkovec, M.; Piguet, C., A simple thermodynamic model for rationalizing the formation of self-assembled multimetallic edifices: Application to triple-stranded helicates. *Journal of the American Chemical Society* 2004, 126, (37), 11589-11601.
73. Bielejewska, A. G.; Marjo, C. E.; Prins, L. J.; Timmerman, P.; de Jong, F.; Reinhoudt, D. N., Thermodynamic stabilities of linear and crinkled tapes and cyclic rosettes in melamine-cyanurate assemblies: A model description. *Journal Of The American Chemical Society* 2001, 123, (31), 7518-7533.
74. McMurry, J.; Fay, R. C., *Chemistry*. 2nd ed.; Prentice-Hall: Upper Saddle River, 1998.
75. Atkins, P. W., *Physical Chemistry*. Oxford University Press: Oxford, 1998.
76. Smith, R. M.; Martel, A. E., *Critical Stability Constants*. Plenum Press: New York, 1976; Vol. 4.

77. Ercolani, G., Assessment of cooperativity in self-assembly. *Journal of the American Chemical Society* 2003, 125, (51), 16097-16103.
78. Chi, X. L.; Guerin, A. J.; Haycock, R. A.; Hunter, C. A.; Sarson, L. D., The thermodynamics of self-assembly. *Journal Of The Chemical Society-Chemical Communications* 1995, (24), 2563-2565.
79. Zerkowski, J. A.; Seto, C. T.; Whitesides, G. M., Solid-State Structures Of Rosette And Crinkled Tape Motifs Derived From The Cyanuric Acid Melamine Lattice. *Journal Of The American Chemical Society* 1992, 114, (13), 5473-5475.
80. Seto, C. T.; Whitesides, G. M., Molecular Self-Assembly Through Hydrogen-Bonding - Supramolecular Aggregates Based On The Cyanuric Acid.Melamine Lattice. *Journal Of The American Chemical Society* 1993, 115, (3), 905-916.
81. Hamacek, J.; Borkovec, M.; Piguet, C., A simple thermodynamic model for quantitatively addressing cooperativity in multicomponent self-assembly processes - Part 1: Theoretical concepts and application to monometallic coordination complexes and bimetallic helicates possessing identical binding sites. *Chemistry-a European Journal* 2005, 11, (18), 5217-5226.
82. Alderighi, L.; Gans, P.; Ienco, A.; Peters, D.; Sabatini, A.; Vacca, A., Hyperquad simulation and speciation (HySS): a utility program for the investigation of equilibria involving soluble and partially soluble species. *Coordination Chemistry Reviews* 1999, 184, 311-318.
83. Anderegg, G., The Stability Of The Palladium(Ii) Complexes With Ethylenediamine, Diethylenetriamine And Tris(Beta-Aminoethyl)-Amine. *Inorganica Chimica Acta* 1986, 111, (1), 25-30.
84. Tercero-Moreno, J. M.; Matilla-Hernandez, A.; Gonzalez-Garcia, S.; Niclos-Gutierrez, J., Hydrolytic species of the ion cis-diaqua(ethylenediamine) palladium(II) complex and of cis-dichloro(ethylenediamine) palladium(II): Fitting its equilibrium models in aqueous media with or without chloride ion. *Inorganica Chimica Acta* 1996, 253, (1), 23-29.
85. Sautter, A.; Schmid, D. G.; Jung, G.; Wurthner, F., A triangle-square equilibrium of metallosupramolecular assemblies based on Pd(II) and Pt(II) corners and diazadibenzoperylene bridging ligands. *Journal of the American Chemical Society* 2001, 123, (23), 5424-5430.
86. Benson, S. W., *Thermochemical kinetics: Methods for the estimation of thermochemical data and rate parameters*. 2nd ed.; John Wiley & Sons: Toronto, 1976.
87. May, P. M.; Murray, K.; Williams, D. R., The Use Of Glass Electrodes For The Determination Of Formation-Constants.2. Simulation Of Titration Data. *Talanta* 1985, 32, (6), 483-489.
88. Cotton, A. F.; Wilkinson, G., *Advance Inorganic Chemistry*. 4 ed.; John Wiley & Sons: Toronto, 1980.

89. Fryer, C. W.; Smith, J. A. S., A Cis-Influence In Square-Planar Palladium And Platinum Complexes. *Journal Of Organometallic Chemistry* 1969, 18, (2), P35-P38.
90. Hammond, G. S., A correlation of reaction rates. *Journal Of The American Chemical Society* 1955, 77, (2), 334-338.
91. Ahlrichs, R.; Ballauff, M.; Eichkorn, K.; Hanemann, O.; Kettenbach, G.; Klufers, P., Polyol metal complex, part 30 - Aqueous ethylenediamine dihydroxo palladium(II): A coordinating agent for low- and high-molecular weight carbohydrates. *Chemistry-A European Journal* 1998, 4, (5), 835-844.
92. Chin, P.-K. F.; Hartley, F. R., Preparation and Some reactions of Diethylenetriaminepalladium(II) Solvento Complexes. *Inorganic Chemistry* 1976, 15, (4), 982-984.
93. Wimmer, F. L.; Wimmer, S.; Castan, P.; Puddephatt, R. J., [N-(2-aminoethyl)-1,2-ethanediamine]-Chloropalladium(II) Chloride. *Inorganic Synthesis* 1992, 29, 185-187.
94. Basolo, F.; Baddley, W. H.; Weidenba.Kj, Intermolecular Isomerization Of A Thiocyanatopalladium(2) Complex To Its Isothiocyanato Linkage Isomer. *Journal Of The American Chemical Society* 1966, 88, (7), 1576-&.
95. Romary, J. K.; Zacharia.Rd; Barger, J. D.; Schiesse.H, New 2-Pyridyl Polyamines. Synthesis Spectra And Proton Dissociation Constants. *Journal Of The Chemical Society C-Organic* 1968, (23), 2884-&.
96. Barger, J. D.; Zachariasen, R. D.; Romary, J. K., Coordination by (2-pyridylmethyl)(2-aminoethyl)amine [2-[(2-aminoethyl)aminomethyl]pyridine]. *Journal of Inorganic and Nuclear Chemistry* 1969, 31, (4), 1019-1022.
97. Lacoste, R. G.; Martel, A. E., New multidentate ligands. I. Coordinating Tendencies of Polyamines Containing a-Pyridyl Groups with Divalent Metal Ions. *Inorganic Chemistry* 1964, 3, 881-884.
98. Hofmann, A.; Jaganyi, D.; Munro, O. Q.; Liehr, G.; van Eldik, R., Electronic tuning of the lability of Pt(II) complexes through pi-acceptor effects. Correlations between thermodynamic, kinetic, and theoretical parameters. *Inorganic Chemistry* 2003, 42, (5), 1688-1700.
99. Lewis, R. J. S. In *Sax's dangerous properties of industrial materials*, 2004; Wiley-Interscience: 2004.
100. Loock, D. Ion Transport Mechanisms of Bola-amphiphiles in Planar Bilayer Membranes. University of Victoria, Victoria, 1997.
101. Lobo, V., *Electrolyte solutions: Literature Data on Thermodynamic and Transport Properties*. Coimbra, 1981; Vol. 2.
102. Litvinchuk, S.; Bollot, G.; Mareda, J.; Som, A.; Ronan, D.; Shah, M. R.; Perrottet, P.; Sakai, N.; Matile, S., Thermodynamic and kinetic stability of synthetic multifunctional rigid-rod beta-barrel pores: Evidence for supramolecular catalysis. *Journal Of The American Chemical Society* 2004, 126, (32), 10067-10075.

103. Cameron, L. M.; Fyles, T. M.; Hu, C. W., Synthesis and membrane activity of a bis(metacyclophane)bolaamphiphile. *Journal Of Organic Chemistry* 2002, 67, (5), 1548-1553.
104. Lide, D. R., *CRC Handbook of Chemistry and Physics*. 81 ed.; CRC Press: New York, 2000.
105. Ashley, R. H., *Ion Channels: A practical approach*. Oxford University Press: Oxford, 1995.
106. Miedema, H., Surface potentials and the calculated selectivity of ion channels. *Biophysical Journal* 2002, 82, (1), 156-159.
107. Stang, P. J.; Cao, D. H., Transition-Metal Based Cationic Molecular Boxes - Self-Assembly Of Macrocyclic Platinum(Ii) And Palladium(Ii) Tetranuclear Complexes. *Journal Of The American Chemical Society* 1994, 116, (11), 4981-4982.